UNIVERSITÀ DEGLI STUDI DI PADOVA

Dipartimento di Fisica e Astronomia "Galileo Galilei"

Master Degree in Physics

Final Dissertation

Common explanations for the Dark Matter and the muon g-2 anomaly

Thesis supervisor

Prof. Paride Paradisi

Candidate

Giorgio Palmieri

Academic Year 2022/2023

Abstract

Recently, the Muon g-2 collaboration at Fermilab measured the muon anomalous magnetic moment, confirming the deviation from the Standard Model prediction already found by the E821 experiment at Brookhaven. In this thesis, we will provide a general classification of beyond Standard Model extensions capable to explain such discrepancy while being compatible with all experimental bounds arising from related observables. Furthermore, we will address the interesting question of whether the observed Dark Matter relic density in the Universe can be naturally connected with the muon g-2 discrepancy. This will bring us to identify specific classes of models providing a viable Dark Matter candidate, a solution to the muon g-2, as well as additional specific signature to be tested experimentally. This thesis work emphasises the intimate connection between Particle Physics and Cosmology to unveil the laws of Nature and their experimental footprints.

Contents

Introduction

The anomalous magnetic moment of the muon, $a_\mu \equiv \frac{(g-2)_\mu}{2}$, plays a crucial role in the establishment of the Standard Model (SM) of elementary particle physics, therefore motivating continuous and enduring efforts from both theoretical and experimental sides. The very recent a_μ measurement by the Muon g-2 collaboration at Fermilab has confirmed the earlier result by the E821 experiment at Brookhaven. The comparison of these results with the SM prediction of the Muon g-2 Theory Initiative leads to an intriguing 5.0σ discrepancy.

This discrepancy can be accommodated in a number of theories beyond the SM (BSM). In this thesis, we aim at classifying the general features of such BSM scenarios focusing on simplified benchmark models contributing to a_μ at the 1-loop level. To further constrain the considered New Physics (NP) models, we require that they must also contain a Dark Matter candidate, i.e. an electromagnetically neutral and color singlet state that is stable on cosmological time scales while being capable of reproducing the observed relic density abundance.

In fact, the final goal of this work is to investigate on the possibility of conceiving a coherent theoretical framework where to accommodate both cosmological and laboratory measurements.

In Chapter 1, we introduce the SM, showing its triumphs as well as its limits, which underscore the need for NP extensions. The muon g-2 anomaly is then discussed in some details in Chapter 2 where we present an overview of the various SM contributions as well as a brief history of its measurements. The chapter ends with general considerations about NP contributions to the muon g-2. Instead, in Chapter 3, we discuss the Dark Matter paradigm, offering evidence for its existence as well as possible production mechanisms. We end the chapter by discussing the direct, indirect, and collider searches of Dark Matter. In Chapter 4, we build NP models assessing their contribution to the muon g-2 and the Dark Matter relic abundance. Finally, we will provide a numerical analysis of our results.

Chapter 1

Standard Model: virtues and shortcomings

Recently, the FNAL Muon $g-2$ experiment measured a deviation of 4.2σ for the muon anomalous magnetic moment from the most recent Standard Model predictions, improving the previous result obtained at BNL. This represents one of the most striking disagreements between theory and experimental results; it is thus interpreted as evidence for the existence of new physics beyond the Standard Model, leading theorists to formulate lots of different models capable of explaining it. Of particular interest are those models that, among the possible new fields introduced, admit a dark matter candidate, thus giving an explanation for another flaw of the Standard Model. It is precisely on these that we will focus in this work.

In this first chapter, we will discuss the Standard Model in general, as well as its strengths and limitations, with a special emphasis on the anomalous magnetic moment of the muon and dark matter.

1.1 The Standard Model Lagrangian

The Standard Model of Particle Physics (SM) is a theory that describes the properties of fundamental particles and how they interact among themselves [1]. It was built during the previous century through the interplay between experimental discoveries and theoretical predictions, and it is currently one of the most successful theories in physics. The SM is based on the formalism of Quantum Field Theory (QFT) that is able to combine Classical Field Theory, Special Relativity and Quantum Mechanics, treating particles as quanta of their underlying quantum fields (from here on, we will consider this implied, so "particles"and "fields"will be used as synonymous). To construct the theory Lagrangian, the field content and the internal symmetries, under which they transform, must be provided, and then two principles are used: Lorentz invariance and Renormalizability. The first one implies that every vector and spinor index must be contracted in order to preserve space-time symmetry, while the second implies that all operators in the Lagrangian have a dimension equal to or less than four, ensuring the ability to reabsorb all loop divergences in a finite number of counterterms. This technique is realized by introducing scale dependent coupling constants and, at least in principle, allowing computation at any order in perturbation theory.

The internal symmetry of the SM is given by the local Gauge group

$$G_{SM} = SU(3)_c \times SU(2)_L \times U(1)_Y \tag{1.1}$$

where $SU(3)_c$ is the color group responsible for the strong force with coupling g_s while $SU(2)_L \times U(1)_Y$ is responsible for the electroweak interaction, $SU(2)_L$ is related to the weak isospin, and $U(1)_Y$ to the hypercharge. The couplings associated with these last two groups are g_2 and g_Y respectively. One of the main features of the SM is that it undergoes a Spontaneous Symmetry Breaking after which the Gauge group is:

$$G_{SM}^{Broken} = SU(3)_c \times U(1)_{EM} \tag{1.2}$$

where $U(1)_{EM}$ is the electromagnetic Gauge group with coupling the electric charge e. As for field content of the theory, it can be divided into three categories: gauge fields, matter fields, and the Higgs multiplet. The gauge fields are

$$G_\mu = G^a_\mu \lambda^a, \quad W_\mu = W^i_\mu \tau^i, \quad B_\mu \tag{1.3}$$

where λ^a are the Gell-Mann matrices and τ^i the Pauli matrices. The first one is associated with eight gluon fields, mediators of the strong force, and since it is associated with a non-Abelian group, its field strength is defined as $G_{\mu\nu} = \partial_\mu G_\nu - \partial_\nu G_\mu + ig_s[G_\mu, G_\nu]$. The second one is associated with the three $SU(2)_L$ fields, and the field strength is given by $W_{\mu\nu} = \partial_\mu W_\nu - \partial_\nu W_\mu + ig_2[W_\mu, W_\nu]$. The last one is the hypercharge field, the only Abelian Gauge boson, its field strength reads $B_{\mu\nu} = \partial_\mu B_\nu - \partial_\nu B_\mu$. After electroweak symmetry breaking, the two fields W and B mix through the Weinberg angle θ_W, giving rise to the vector bosons of the weak and electromagnetic forces, which are:

- The W bosons $W^\pm_\mu = \frac{1}{\sqrt{2}}(W^1_\mu \mp iW^2_\mu)$, mediators of the charged current weak interactions;
- The Z boson $Z_\mu = W^3_\mu cos(\theta_W) - B_\mu sin(\theta_W)$, mediator of the neutral current weak interaction;
- The photon $A_\mu = W^3_\mu sin(\theta_W) + B_\mu cos(\theta_W)$, mediator of the electromagnetic interaction.

The SM matter content is made of fermion fields that can be divided into left-handed $SU(2)_L$ doublets

$$Q^i_L(3, 2, +\frac{1}{6}) = \begin{pmatrix} u^i_L \\ d^i_L \end{pmatrix}, \quad L^i_L(1, 2, -\frac{1}{2}) = \begin{pmatrix} \nu^i_L \\ e^i_L \end{pmatrix} \tag{1.4}$$

and right-handed singlets

$$u^i_R(3, 1, +\frac{2}{3}), \quad d^i_R(3, 1, -\frac{1}{3}), \quad e^i_R(1, 1, -1). \tag{1.5}$$

The numbers in brackets are the quantum numbers under the SM group G_{SM} and the index $i = 1,\ 2,\ 3$ represents the flavor index. Indeed, fermions can be divided into three families called flavors; as far as leptons $(L,\ e)$ are concerned, each one of the three families contains an electrically charged particle: electron (e) the first, muon (μ) the second, and tau (τ) the third, and for each of them there is a neutral particle called neutrino, ν_e, ν_μ, and ν_τ respectively. Regarding the quark fields $(Q,\ u\ d)$, the upper components carry electric charge $+\frac{2}{3}$ and are called up (u), charm (c), and top (t), while the lower components have charge $-\frac{1}{3}$ and are referred to us as down (d), strange (s), and bottom (b). The only thing that distinguishes two fermions of the same kind belonging to different families is their mass, which can assume very different values. Indeed, the fermions mass range spans over lots of orders of magnitude, with the least massive being the electron with $m_e = 0.511\ MeV$, while the heaviest is the top quark with $m_t = 170\ GeV$.

The Higgs multiplet is a scalar $SU(2)_L$ doublet

$$H(1, 2, +\frac{1}{2}) \tag{1.6}$$

It couples both fermions and Gauge bosons and its potential breaks spontaneously G_{SM} as

$$SU(3)_c \times SU(2)_L \times U(1)_Y \longrightarrow SU(3)_c \times U(1)_{EM} \tag{1.7}$$

This Spontaneous Symmetry Breaking is called electroweak symmetry breaking, and it allows to provide a mass to fermions and to the Z and $W^\pm$ gauge bosons in a gauge invariant way.

Once the field content and symmetry are understood, the most general renormalizable Lagrangian is the following

$$\mathcal{L}_{SM} = \mathcal{L}_k + \mathcal{L}_H + \mathcal{L}_Y \tag{1.8}$$

where the first piece contains the kinetic terms for both fermions and gauge bosons

$$\mathcal{L}_k = -\frac{1}{4}G^{\mu\nu,\,a}G^a_{\mu\nu} - 1/4W^{\mu\nu,\,i}W^i_{\mu\nu} - \frac{1}{4}B^{\mu\nu}B_{\mu\nu} + \sum_f \bar{\psi_f} i\gamma^\mu D_\mu \psi_f \tag{1.9}$$

where $D_\mu = \partial_\mu - i\frac{g_s}{2}G^a_\mu\lambda^a - i\frac{g_2}{2}W^i_\mu\tau^i - ig_Y Y_f B_\mu$ is the covariant derivative built through the gauge fields with Y_f the fermion hypercharge.

The second piece is the Higgs Lagrangian

$$\mathcal{L}_H = (D^\mu H)^\dagger (D_\mu H) - \mu^2 H^\dagger H - \lambda (H^\dagger H)^2 \tag{1.10}$$

where μ^2 and λ are real parameters, and $\mu^2 < 0$ in order to realize the electroweak spontaneous symmetry breaking. It is responsible for Higgs-Gauge interactions, Higgs self-interactions and Gauge boson masses when H assumes its vacuum expectation value $H = \begin{pmatrix} 0 \\ \frac{v}{\sqrt{2}} \end{pmatrix}$, with $v = \sqrt{\frac{-\mu^2}{\lambda}}$.

The last term is the Yukawa Lagrangian, responsible for the fermions-Higgs interactions

$$\mathcal{L}_Y = -Y_u^{ij}\bar{Q}_{Li}u_{Rj}\tilde{H} - Y_d^{ij}\bar{Q}_{Li}d_{Rj}H - Y_e^{ij}L_{Li}e_{rj}\tilde{H} + h.c. \tag{1.11}$$

where Y matrices are called Yukawa matrices and $\tilde{H} = i\tau^2 H$ is the conjugate Higgs field. It is responsible for Higgs fermions interactions and, after the electroweak symmetry breaking, fermion masses[1]. This last piece contains the whole flavor structure of the SM.

1.2 Standard Model success

With the discovery at the LHC of a particle that, in all its properties, appears just as the Higgs boson of the SM, the main missing block for the experimental validation of the theory is now in place [2]. The Higgs discovery is the last milestone in the long history, almost 130 years, of the development of a field theory of fundamental interactions. An additional LHC result of great importance is that a large new territory has been explored and no new physics has been found. If one considers that there has been a big step in going from the Tevatron at 2 TeV up to the LHC at 8 TeV (a factor of 4) and that only another factor of 1.75 remains to go up to 14 TeV, the negative result of all searches for new physics is particularly astonishing. In particular, while NP can still appear at any moment, clearly it is now less unconceivable that no new physics will show up at the LHC. As is well known, in addition to the negative searches for new particles, the constraints on new physics from flavor phenomenology are extremely demanding: when adding higher-dimensional effective operators to the SM, flavor constraints generically lead to very large suppression scales Λ in the denominators of the corresponding coefficients. In fact, in the SM there are powerful protections against flavor-changing neutral currents and CP violation effects, in particular through the smallness of quark mixing angles. Powerful constraints also arise from the leptonic sector. In particular, we refer to the recently improved MEG result on the $\mu \to e\gamma$ branching ratio, $Br(\mu \to e\gamma) \leq 4.2 \times 10^{-13}$ at $90\% C.L$ and other similar processes such as $\tau \to \mu\gamma$ or $\tau \to e\gamma$ and to the bound on the electron dipole moment $|d_e| \leq 8.7 \times 10^{-29}\ ecm$ by the ACME Collaboration. In this respect, the SM is very special and, as a consequence, if there is new physics, it must be highly non-generic in order to satisfy the present constraints.

1.3 Standard Models limit

The SM is a very successful theory: its predictions, tested in the last three decades with increasingly high precision, are in excellent agreement with experimental data for a wide range of phenomena, but new-physics signals arise anyway, both from experimental measurements and from conceptual arguments. Let us first of all point out that the SM does not include gravity, and nowadays there are not fully consistent theories able to embed gravity within a QFT context compatible with the SM. Therefore, an extension of the SM or a drastic modification of our way of conceiving fundamental

[1] Since the right-handed neutrino is not included in the SM, neutrinos are considered massless

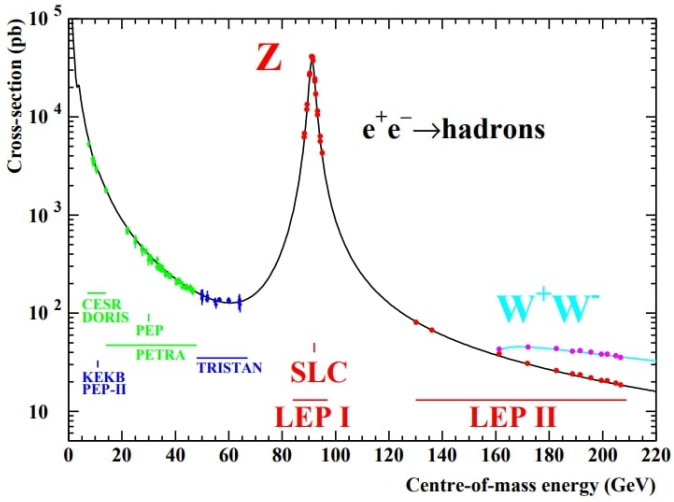

Figure 1.1: Hadronic cross section as a function of the center of mass energy. The solid line represent the theoretical prediction, while the dots are the experimental measuraments. Also indcated are the energy ranges of various e^+e^- accelerators.

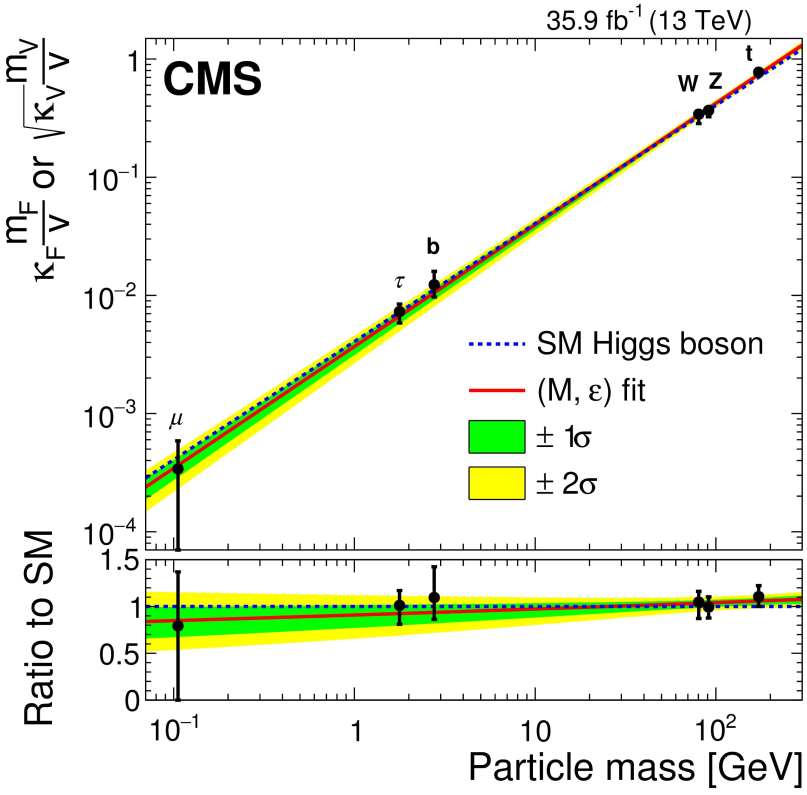

Figure 1.2: Comparison of the SM expectations and the results of the Higgs boson coupling fit from CMS at $\sqrt{s} = 13\ TeV$.

interactions is needed to unify the four fundamental forces. This fixes an upper bound with respect to the validity of the SM at the Planck scale $M_{Pl} = 1.2209 \times 10^{19}\ GeV$, where quantum gravity effects become important [3]. However, nothing forbids that the SM fails before this energy scale, for instance, for the appearance of new degrees of freedom, which at the energy of present colliders cannot go on shell. In addition to the absence of gravity in the SM, it is also unable to explain several phenomena from a cosmological standpoint. Here are a few examples:

- **Dark matter evidence** [4]: Galaxies in our universe are rotating with such speed that the gravity generated by their observable matter could not possibly hold them together; they should have torn themselves apart long ago. The same is true for galaxies in clusters; therefore, there is something we cannot see at work. Extra gravity needed to hold galaxies together is called "dark matter ", since it is not visible. A well-established measurement of Dark Matter abundance states that it constitutes around 26% of the energy budget of the universe. However, the only particle in the SM that can act as DM is the neutrino, but due to its small mass, it can only constitute hot dark matter and can account for a small amount of the entire energy density of DM. Therefore, an extension of the SM is needed to take this matter into account. These new particles must be stable, very weakly interacting, and non-relativistic. Several candidates have been proposed, such as the axion [5], which, through the misalignment mechanism, can provide the observed amount of cold DM. Other candidates are present in supersymmetric extensions of the SM, such as gravitinos and neutralinos.

- **Baryon asymmetry**: In our universe, the number of baryons is much larger than the number of antibaryons. It can be shown that to have such a big difference, a dynamical mechanism called baryogenesis is necessary. But in order to have baryogenesis, three conditions must be satisfied, called the Sakharov conditions. Sakharov conditions require baryon number violating interactions; however, in the SM, due to an accidental symmetry, B violation is absent[2]. In addition, CP violating interactions are also necessary, and they are present in the SM, at least in the quark sector, but in such a small amount that it is not enough to explain the asymmetry [6]. Finally, the third condition is for the interactions to happen out of thermal equilibrium.

- **Inflation**: It is a dynamical process which is supposed to happen right after the Big Bang and that can solve some early universe problems, such as the flatness problem or the horizon problem [7]. However, there is no SM field that can be identified with the inflaton field, the particle that drives the inflation mechanism.

There are also other experimental evidence that suggests the existence of new physics particles. Some of them are:

- **Neutrino oscillations** [8]: In the last decades, several experiments have shown that solar and atmospheric neutrinos change their flavor along the path between their production and their detection points. In the SM, these transitions are not allowed as neutrinos are massless, therefore, the SM must be extended to include neutrino masses. Current investigations aim at establishing the nature of neutrinos (Dirac or Majorana), their mass hierarchy and the amount of CP violation in the neutrino sector.

- **Lepton flavor universality violation** [9]: The SM predicts the electroweak interactions to have the same strength for all lepton generations. This property is called lepton flavor universality (LFU) and has been experimentally verified in meson decays, τ decays, and Z boson decays. However, in the last years, some hints of LFU violation in neutral-current as well as charged-current semi-leptonic decays have emerged. Although the current situation is not clear yet, there is an ongoing experimental and theoretical effort to shed light on this important subject.

- **The magnetic moment of the muon** [10]: For an elementary particle with spin $\vec{S}$, mass m and charge q, its magnetic moment $\vec{\mu}$ is given (in natural units) by

[2]It turns out that through non-perturbative mechanisms, the Baryon symmetry is violated. This, along with the CP violating interactions, makes sure that the SM satisfies the first two Sakharov condition

$$\vec{\mu} = g\frac{q}{2m}\vec{S} \tag{1.12}$$

where g is the gyromagnetic factor. From his original formulation of relativistic quantum mechanics in 1928, Dirac predicted $g = 2$ for any spin-$\frac{1}{2}$ elementary particle. However, this quantity receives contributions from radiative corrections. In particular, at one-loop accuracy, they amount to:

$$a_\ell = \frac{g_\ell - 2}{2} = \frac{\alpha_{\rm em}}{2\pi}\,, \qquad\qquad \ell = e, \mu, \tau\,. \tag{1.13}$$

Such deviation from the tree-level prediction $g = 2$ was fully confirmed experimentally and it represented the first great triumph of the Quantum Electro-Dynamics (QED). However, the current situation has changed: the astonishingly accurate SM prediction [11] of a_μ seems to deviate by more than 5σ from the experimental world average [12].

Besides the experimental problems of the SM listed above, there are also other theoretical problems which require to be understood, as for instance the so-called naturalness problem. To better understand this point, let us start with a classical example: the physical mass of the electron in classical field theory. Electron mass, according to electromagnetism, can be written as the sum of the bare mass and the total energy stored in the Electromagnetic field

$$m_e c^2 = m_{e,b}c^2 + \frac{e^2}{4\pi\epsilon_0 a} \tag{1.14}$$

with $a \approx 10^{-17}\ cm$ the classical radius of the electron and ϵ_0 the vacuum dielectric constant. Substituting the numbers, one finds that the Coulomb energy is about 10 GeV and therefore, to obtain the electron mass, the bare mass must be set to a very peculiar value $m_{e,b} = -9.9995\ GeV$. A so strong fine-tuning may signal physics beyond the classical field theory of electromagnetism. Indeed, at scale length of the classical electron radius, quantum effects are important and must be systematically included by means of the QED.

The most prominent examples of naturalness problems within the SM are [13]:

- **The Higgs hierarchy problem**: It consists of the huge hierarchy between the Planck mass $M_{Pl} \sim 10^{18}\ GeV$ and the Higgs mass parameter $|m_h| \sim 100\ GeV$. This problem becomes manifest in the one-loop correction to the dimension-2 Higgs mass parameter due to the top loops, as follows,

$$\Delta m_h^2 = -\frac{N_c y_t^2}{8\pi^2}\Lambda^2 + \dots \tag{1.15}$$

with Λ being the UV cut-off for the loop momentum and is typically of order M_{Pl}. Simple solutions to the hierarchy problem include, for instance, low-energy supersymmetry and composite Higgs models which predict the existence of new particles not too far from the electroweak scale.

- **The strong CP problem**[14]: The QCD Lagrangian has an additional gauge-invariant term, the so-called θ term:

$$\mathcal{L}_\theta = \frac{g_s^2}{32\pi^2}\theta G^{\mu\nu,a}\tilde{G}^a_{\mu\nu} \tag{1.16}$$

with $\tilde{G}^a_{\mu\nu} = \frac{1}{2}\epsilon_{\mu\nu\rho\sigma}G^{\rho\sigma,a}$. It turns out that the θ-term is a total derivative,

$$\frac{g_s^2}{32\pi^2}G^{\mu\nu,a}\tilde{G}^a_{\mu\nu} = \partial_\mu K^\mu \tag{1.17}$$

with

$$k^\mu = \frac{g_s^2}{32\pi^2}\epsilon^{\mu\nu\rho\sigma}G^a_\nu[G^a_{\rho\sigma} - \frac{g}{3}f^{abc}G^b_\rho G^c_\sigma]. \tag{1.18}$$

Therefore, the θ-term does not affect local QFT properties, but there is a vacuum gauge configuration with a non-trivial topological (winding) number, $n \neq 0$, due to

$$\frac{g_s^2}{32\pi^2}\int d^4x G^{\mu\nu,a}\tilde{G}^a_{\mu\nu} = \int dS^\mu K_\mu = n \tag{1.19}$$

with n being integer. The non-perturbative effects are proportional to e^{-c/g_s^2} so only the QCD θ-term is important. In fact, the QCD θ-term contributes to the neutron electric dipole moment (EDM) as

$$d_n = \frac{e}{\Lambda^2_{QCD}}\frac{m_u m_d}{m_u + m_d}\theta < 3.0 \times 10^{-26}\ ecm \tag{1.20}$$

which sets the limit to $|\theta| < 10^{-10}$. This is the strong CP problem. Nothing forbids such a small value, but it is more natural to explain it through a symmetry argument like in the Peccei-Quinn solution, where a new $U(1)_{PQ}$ symmetry is added and the parameter θ is dynamically driven to zero.

- **The Standard Model flavor puzzle** [15, 16]: It is about the hierarchical patterns of fermion masses and the mixing patterns of quarks and leptons. In particular, neutrino masses are much lighter than any of the quarks and leptons: $m_{\nu j}/m_{l,q} \lesssim 10^{-10}$. But also in the original formulation of the SM, we find that the mass spectrum ranges from around 0.5 MeV for the electron to 170 GeV for the top quark, and again this huge difference between the masses of different fermions is not natural. The flavor problem originates from the dimension-4 Yukawa couplings for quarks and leptons and partly from the dimension-5 operators for neutrino masses.

Therefore, even if the predictions of the SM in the last decades are astonishingly precise, the theory clearly needs some ultraviolet completion that is able to explain the mentioned observations and the internal consistency problems.

Chapter 2

The muon g-2

The magnetic dipole moment is a classical property of physical system. In quantum mechanics the concept of an intrinsic angular momentum, the spin $\vec{S}$, emerges. Then, for a particle with charge q and mass m, the magnetic dipole moment can be defined as

$$\vec{\mu} \equiv g\,\mu_B\,\frac{q}{2m}\,\vec{S} \tag{2.1}$$

where μ_B is the Bohr magneton and g the giroscopic ratio, also referred to as g-factor.

2.1 Standard Model prediction

The first theoretical prediction for the g-factor of point-like charged particles traces back to 1928, when the relativistic formulation of quantum mechanics obtained by Dirac provided the $g = 2$. However, this approach does not take into account radiative corrections, which modify the interaction between the lepton and the photon, through exchange of virtual particles. The theoretical estimate for the g-factor can be obtained at any order of perturbation theory exploiting corrections coming from the entirety of the Standard Model. The deviation from the quantum mechanical prediction is defined as anomalous magnetic moment as

$$a_\mu \equiv \frac{g_\mu - 2}{2} \tag{2.2}$$

This can be divided into the three different contribution that are deeply studied in the so called White Paper [11]: electromagnetic, electroweak and hadronic

$$a_\mu = a_\mu^{QED} + a_\mu^{EW} + a_\mu^{had} \tag{2.3}$$

The first correction comes from QED and was firstly computed in 1948 by Schwinger with the result of

$$a_\mu = \frac{\alpha}{2\pi}. \tag{2.4}$$

In the following we will present a brief discussion about the other contribution arising from the Standard Model.

2.1.1 Electromagnetic and weak contributions

The QED contribution arise from diagrams involving the three charged leptons ($e,\ \mu\ \tau$) interacting with the photon. It is the dominant contribution, accounting for more than 99.99 % of the value of the entire prediction. It has been computed in the framework of perturbation theory up to $\mathcal{O}(\alpha^5)$ with more then ten thousand different Feynman diagrams generating both mass dependent and independent contributions. The most recent prediction for a_μ^{QED} is [17]:

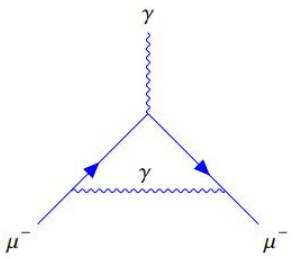

Figure 2.1: The only one loop contribution to the anomalous magnetic moment arising at one loop level

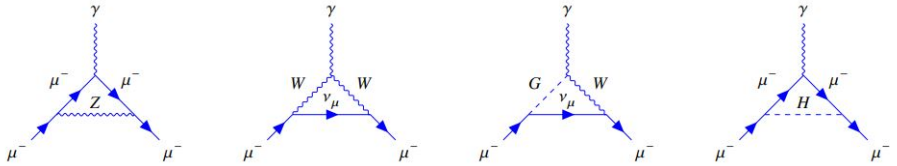

Figure 2.2: An example of some one loop diagrams in the weak sector

$$a_\mu^{QED} = 116584718.931(104) \times 10^{-11}, \tag{2.5}$$

where the uncertainty is due to the highest order contribution, the τ-lepton mass, the estimate of the $\mathcal{O}(\alpha^6)$ contribution and the measure of the fine-structure constant α.

The Electroweak term, instead, embrace all the Standard Model contributions that are not contained in the pure QED and hadronic one. The overall computation is much more complicated due to the variety of virtual particles that can appear in the loop diagrams. Differences from the QED case arise already at 1-loop, such as the presence of Goldstone boson particles like in 2.2. Overall, since the gauge bosons and the higgs masses are much heavier that the muon, these contributions are strongly suppressed. This is true in particular for those diagrams where the higgs couples to the muon, indeed these are not only suppressed by the higgs boson propagator, there is also a reduction arising by the presence of the muon-HIggs Yukawa coupling, and, for this reason, are usually neglected. The 1-loop Electroweak contribution are expressed as:

$$a_\mu^{EW} = \frac{G_F}{\sqrt{2}} \frac{m_\mu^2}{8\pi^2} \left(\frac{5}{3} + \frac{1}{3}(1 - 4s_w^2)^2 \right) \tag{2.6}$$

where G_F is the Fermi constant and the s_w is the sine of the Weinberg angle. The mass suppression can be seen in the factor $G_F m_\mu^2 \sim m_\mu^2 / M_W^2$. Among the higher order contributions an important role is played by the two-loop ones which arise from QED corrections or fermionic loop insertions in the one-loop diagrams. Surprisingly, they are the same order of magnitude of the one-loop result: this is due to the presence of $log(m_{Z,W}/m_f)$ terms associated to fermion triangular-loops, where m_f is the mass scale of the fermion in the loop, very small compared to the mass of the guage bosons. As a result, the one-loop contribution is sensibly diminished by the two-loop term.

The most recent estimate for the weak contribution is [18, 19]:

$$a_\mu^{EW} = 153.6(1.0) \times 10^{-11}. \tag{2.7}$$

2.1.2 Hadronic contribution

The hadronic contribution is given by pure QED diagrams with quarks running in the loops. The main difficulties that is encountered with this kind of terms arise from the non-perturbative behavior of QCD at low energies. The leading order contribution shows at order $\mathcal{O}(\alpha^2)$ and comes from diagrams showing an hadronic vacuum polarization insertion in the virtual photon in the loop 2.3. This contribution can be obtained exploiting the dispersion relation alongside the optical theorem combined with data

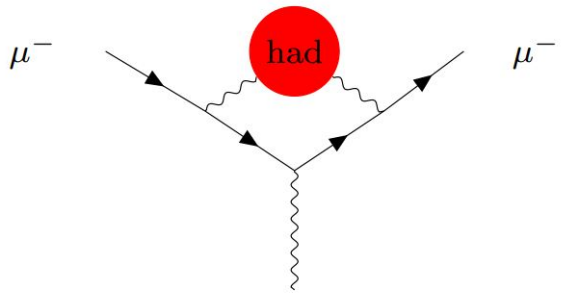

Figure 2.3: The hadronic leading order contribution to the anomalous magnetic moment

coming from the hadronic annihilation process $e^+ + e^- \longrightarrow hadrons$. The dispersive relation obtained is:

$$a_\mu^{had} = \frac{\alpha}{3\pi} \int_{m_\pi^2}^{\infty} \frac{ds}{s} K_\mu^{(2)}(s) R_{had}(s). \tag{2.8}$$

with $K_\mu^{(2)}(s)$ is a kernel function, m_π the mass of the pion and $R_{had}(s)$ is the ratio of the inclusive cross section for e^+e^- annihilation into hadrons, with electromagnetic radiative corrections subtracted off, and the cross section for muon-pair production in the high energy limit:

$$R_{had}(s) = \frac{\sigma^{(0)}(e^+ + e^- \longrightarrow \gamma^* + hadrons)}{\sigma^{(0)}(e^+ + e^- \longrightarrow \mu^+ + \mu^-)}. \tag{2.9}$$

The most recent value for the hadronic contribution is [11], where the experimental data are taken from [20, 21, 22]:

$$a_\mu^{had} = 6931(40) \times 10^{-11}. \tag{2.10}$$

The error on the measured value is mainly due to the experimental uncertainty on the hadronic cross section. As a consequence the error on the a_μ^{had} term dominates the total uncertainty on the anomalous magnetic moment, an improvement in its measurement is necessary to correctly interpret the experimental results. The hadronic higher order contribution are usually split in two terms: the first one includes QED corrections to the hadronic vacuum polarization and can be computed through the dispersive relation, the second one arise from hadronic light-by-light diagrams and cannot be extracted from experimental data, but specific models must be exploited.

The value for the vacuum polarization term is [23]:

$$a_\mu^{HHO}(vp) = -8.70(0.06) \times 10^{-10} \tag{2.11}$$

while for the light-by-light term is [24]:

$$a_\mu^{HHO}(lbl) = 10.34(2.88) \times 10^{-10} \tag{2.12}$$

Summing up the three contribution the final theoretical value for the anomalous magnetic moment of the muon can be obtained, giving the value:

$$a_\mu^{SM} = 116591810(43) \times 10^{-11} \tag{2.13}$$

2.2 Experimental status

The first measurement of the anomalous magnetic moment of the muon was performed at Columbia University in 1960. The result $a_\mu = 0.00122(8)$ at a precision of about 7% showed no difference with the electron. Shortly after, in 1961, the first precision determination was possible at the CERN

cyclotron (1958-1962). Surprisingly, nothing special was observed within the 0.4% level of accuracy of the experiment, that gave the result $a_\mu^{\text{CERN},I} = 1162(5) \times 10^{-6}$[25]. This provided the first real evidence that the muon was just a heavy electron.

Later on the idea of a muon storage ring was considered. A first one was successfully realised at CERN (1962-1968) and allowed to measure a_μ for both muons and anti-muons, giving the result $a_\mu^{\text{CERN},II}$[26], which is in excellent agreement with the QED theoretical prediction[1].

Between 1969 and 1976 another experiment (with a second muon storage ring) was realised at CERN which allowed to confirm the QED prediction with an increased accuracy, with the result $a_\mu^{\text{CERN},III} = 1165924(8.5)\times 10^{-9}$[27]. Only 20 years later, a muon storage ring experiment at Brookeven National Laboratory (BNL) was able to set new precision standards, allowing the experiment to be sensitive to the weak SM contributions and leading to the discovery of a (3.7sigma) deviation from the theoretical prediction. The collaboration yielded the following experimental value[28]:

$$a_\mu^{BNL} = 11659208.0(6.3) \times 10^{-10}. \tag{2.14}$$

A recent development in the measurement of the anomalous magnetic moment of the muon was achieved at Fermilab with the experiment Muon g-2. The first data taking started in 2018 and the result of the first run was released in 2021 [29]. Other runs have been collected in the following years and the most recent results were published in August 2023 [12].

The principle of the experiment is to measure the anomalous precession frequency of the muon in a magnetic field. This frequency is the difference between the spin precession and the cyclotron frequencies, and it's proportional to the magnetic field magnitude through a constant that contains the muon anomaly $\frac{g-2}{2}$. In particular, if the gyromagnetic factor is 2, the anomalous precession frequency should be zero.

The aim of the experiment is to measure how fast the muon spins around the momentum direction. To do this, the parity violating μ^+ decay is exploited: the high-energy positrons are emitted preferentially in the muon's spin direction, and a detector along a fixed direction will count the number of positrons modulated by the spin precession frequency. As a result, the experimental measure just requires counting the number of high-energy positrons.

The first result of the Muon g-2 collaboration came in 2021, finding an agreement with the BNL result [29]

$$a_\mu^{\text{FNAL},2021} = 116592040(54) \times 10^{-11}. \tag{2.15}$$

More recently, the same collaboration presented the results from the second and third runs of the experiment, increasing the overall precision of the measurement [12]:

$$a_\mu^{\text{FNAL},2023} = 116592059(22) \times 10^{-11}. \tag{2.16}$$

Combining the SM value in 2.13 with the experimental world average, it is found that

$$\Delta a_\mu^{2023} = 24.9(4.8) \times 10^{-10}. \tag{2.17}$$

where the uncertainties are combined in quadrature. Interestingly, 2.17 shows a 5.0σ discrepancy which could be a hint of new physics effects[12].

2.3 New physics contributions

New interactions emerging at a scale Λ larger than the electroweak scale can be described at energies $E \ll \Lambda$ by an effective Lagrangian containing non-renormalizable $SU(3)_c \otimes SU(2)_L \otimes U(1)_Y$ invariant operators. Focusing on the leptonic g-2, the relevant effective Lagrangian contributing to them, up to one-loop order.

[1]Actually, this experiment found a 1.7σ deviation from the QED theoretical prediction, which was subsequently explained by including the so far missing 3-loop QED contribution.

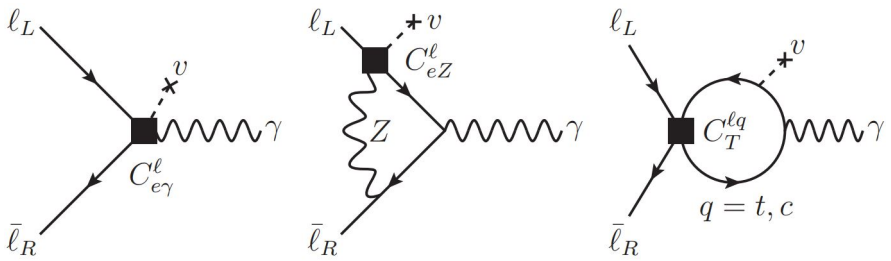

Figure 2.4: Feynman diagrams contributing to the leptonic g-2 up to one-loop order in the Standard Model EFT.

$$\begin{aligned}\mathcal{L} = &\frac{C^\ell_{eB}}{\Lambda^2}\left(\bar{\ell}_L\sigma^{\mu\nu}e_R\right)HB_{\mu\nu} + \frac{C^\ell_{eW}}{\Lambda^2}\left(\bar{\ell}_L\sigma^{\mu\nu}e_R\right)\tau^I HW^I_{\mu\nu} \\ &+ \frac{C^\ell_T}{\Lambda^2}(\bar{\ell}^a_L\sigma_{\mu\nu}e_R)\varepsilon_{ab}(\overline{Q}^b_L\sigma^{\mu\nu}u_R) + h.c. \end{aligned} \tag{2.18}$$

where it is assumed that the NP scale $\Lambda \gtrsim 1$ TeV. The Feynman diagrams relevant for the leptonic g-2 are displayed in figure 2.4. They lead to the following result

$$\begin{aligned}\Delta a_\ell \simeq &\frac{4m_\ell v}{e\Lambda^2}\left(C^\ell_{e\gamma} - \frac{3\alpha}{2\pi}\frac{c^2_W - s^2_W}{s_W c_W}C^\ell_{eZ}\log\frac{\Lambda}{m_Z}\right) \\ &- \sum_{q=c,t}\frac{4m_\ell m_q}{\pi^2}\frac{C^{\ell q}_T}{\Lambda^2}\log\frac{\Lambda}{m_q},\end{aligned} \tag{2.19}$$

where s_W, c_W are the sine and cosine of the weak mixing angle, $C_{e\gamma} = c_W C_{eB} - s_W C_{eW}$ and $C_{eZ} = -s_W C_{eB} - c_W C_{eW}$. Additional loop contributions from the operators $H^\dagger HW^I_{\mu\nu}W^{I\mu\nu}$, $H^\dagger HB_{\mu\nu}B^{\mu\nu}$, and $H^\dagger\tau^I HW^I_{\mu\nu}B^{\mu\nu}$ are suppressed by the lepton Yukawa couplings and can be neglected. Moreover, in equation 2.19, we assumed for simplicity that C_{eB}, C_{eW} and C_T are real. Since only the first two operators of equation 2.18 generate electromagnetic dipoles at tree-level, we include their one-loop renormalization effects to $C^\ell_{e\gamma}$

$$C^\ell_{e\gamma}(m_\ell) \simeq C^\ell_{e\gamma}(\Lambda)\left(1 - \frac{3y^2_t}{16\pi^2}\log\frac{\Lambda}{m_t} - \frac{4\alpha}{\pi}\log\frac{m_t}{m_\ell}\right). \tag{2.20}$$

In order to see where we stand, let us determine the NP scale probed by Δa_ℓ. From equation 2.19 we find that

$$\frac{\Delta a_\mu}{3\times10^{-9}} \approx \left(\frac{250\,TeV}{\Lambda}\right)^2\left(C^\mu_{e\gamma} - 0.2C^{\mu t}_T - 0.001C^{\mu c}_T - 0.05C^\mu_{eZ}\right).$$

A few comments are in order:

- The Δa_μ discrepancy can be solved for a NP scale up to $\Lambda \approx 250$ TeV. This requires a strongly coupled NP sector where $C^\mu_{e\gamma}$ and/or $C^{\mu t}_T \sim g^2_{NP}/16\pi^2 \sim 1$ and a chiral enhancement v/m_μ compared with the weak SM contribution.
- If the underlying NP sector is weakly coupled, $g_{NP} \lesssim 1$, then $C^\mu_{e\gamma}$ and $C^{\mu t}_T \lesssim 1/16\pi^2$, implying $\Lambda \lesssim 20\,TeV$ to solve the Δa_μ anomaly.
- If the NP sector is weakly coupled, and further Δa_μ scales with lepton masses as the SM weak contribution, then $\Delta a_\mu \sim m^2_\mu/16\pi^2\Lambda^2$. Here, the experimental value of Δa_μ can be accommodated only provided that $\Lambda \lesssim 1\,TeV$.

Chapter 3

The Dark Matter problem

Increasing curiosity in the study of our cosmos has driven astronomers to research the sky with a variety of experiments during the last century [30, 31, 32]. Galaxies and clusters of galaxies were of great interest and were investigated by exploiting gravitational interactions and electromagnetic signals. Performing these kinds of studies, astronomers began to realize that there is a large discrepancy between the amount of mass deduced by the analysis of gravitational interactions and the mass that interacts with us through electromagnetic fields. The name "dark matter"was introduced to denote the hypothesis that this discrepancy is due to a component of matter subject to the gravitational interaction but not to the electromagnetic one, resulting in an opaque component of the mass budget inside the structures of the universe. Decades of subsequent astronomical observations, and the recent striking developments in observational cosmology, have nearly ruled out alternative proposals to explain this discrepancy. This explains why the idea that dark matter is made of a new type of particle, subject to yet unknown interactions with ordinary matter, is widely shared today in the scientific community.

3.1 Evidence for Dark Matter

Oort made the first observations of non-luminous matter in 1932. His measurements of the brightest stars in the Milky Way suggested that part of the galaxy's gravitational mass was missing if only those stars were considered, leading him to claim that the disk of the galaxy was made up of two-thirds "dark matter", which included stars less luminous than the Sun and gas and dust in the interstellar medium. Many years later, in 1959, Kinman detected some deviations in the velocities of the Milky Way's globular clusters from what was expected from a pure disk mass model and proposed a linearly growing mass distribution beyond the disk. Also, the observations of the spiral galaxy nearest to us, M31 (Andromeda), done by Babcock in 1939, suggested that the ratio between gravitational and luminous mass was increasing in the outer regions of the galaxy. The studies were deepened in the following years, in particular by Vera Rubin, who showed that, for a large sample of spiral galaxies, the rotation curve of stars inside the galaxy did not fall off as predicted by Keplerian gravity, but kept a flat profile for a large distance outside the main disk. Since the radial velocity, in the approximation of a circular motion and spherical symmetry, is given by $v = \sqrt{GM(r)/r}$ (where $G = 6.67 \times 10^{-11}\ Nm^2kg^{-2}$ is the gravitational constant and $M(r)$ is the gravitational mass contained inside a sphere of radius r centered in the barycenter of the galaxy) according to Newtonian gravity, these results imply a dark matter mass density proportional to r^{-2} within a large region outside the main disk of the galaxy. The large set of observations gathered from the early '30s to the end of the '80s provided plenty of evidence that, in the framework of general relativity, a large part of the mass inside and surrounding galaxies is not interacting through electromagnetic or nuclear interactions.

The Cosmic Microwave Background (CMB) searches (Maxima, Boomerang in 2000 and WMAP in 2003) provided another crucial hint for the existence of dark matter. A comprehensive observation of the CMB on a small angular scale enabled the measurement of the spectrum of anisotropies in the CMB's temperature, which constrains numerous cosmological parameters, including the ratio between the total matter's energy density (given by the sum of dark and standard matter energy density) and

the critical density, denoted by Ω_m. Ω_m affects the shape of the spectrum through many mechanisms, but mainly influences the heights of the first peaks. Already the first measurements of Maxima and Boomerang pointed to a value of Ω_m around 30%, and the current best measurement of the CMB, obtained by the Planck satellite, gives $\Omega_m = 31.6\%$ [33], and an energy density of dark matter equal to 26.7% of the total one. Another important probe for the distribution of dark matter is the observation of strong gravitational lensing, i.e., the study of images of faraway galaxies bent or replicated because of the passage of light near a very massive galaxy cluster. This kind of observations showed that the most massive clusters are largely dominated by dark matter, with ratios of gravitational to luminous matter of the order of some hundreds.

3.2 Dark Matter production

Once the existence of Dark Matter is assumed in order to explain the cosmological observations, it is necessary to specify the mechanism through which these particles are produced and their consequent abundance in the universe. There are two alternative mechanisms, named "freeze out"and "freeze in", which we shall explain briefly in the following.

Freeze out is the simplest mechanism that fixes the abundance of a species in an expanding Universe [32]. If two particles, say A and X, can interact with each other through the reaction $AA \rightleftarrows XX$, then, when initially the Universe is very hot (at energies much greater than the masses of the two particles), the two species annihilate into each other maintaining the chemical equilibrium. When the temperature T of the Universe drops below the higher of the two masses, say m_X, then the number density n_X of X, in the hypothesis that X remains in thermal equilibrium, must follow the non-relativistic Boltzmann distribution, which includes a suppression factor $e^{-m_X/kT}$. Hence, the particles X will annihilate into particles A so as to follow the Boltzmann distribution. As a result, n_X should drop to zero as the universe cools down, unless the reaction $XX \to AA$ becomes inefficient at a certain point. Indeed, this will happen because of the expansion of the Universe, which dilutes the concentration of non-relativistic particles proportionally to a^{-3}, where a is the scale factor appearing in the Friedman-Roberson-Walker metric. Then, when the annihilation rate $n_X\langle\sigma v\rangle$ (where $\langle\sigma v\rangle$ is the thermally averaged cross section for the reaction $XX \to AA$) will decrease below the Hubble rate of expansion $H \equiv \dot{a}/a$, the annihilation of the X particles will substantially cease. The consequence is that n_X keeps the same value it had at the moment of the freeze out, when $n_X\langle\sigma v\rangle \approx H$.

This mechanism can be specialized to the case of Dark Matter, denoting by X the corresponding Dark Matter candidate, we can assume that it can interact with another species, like SM particles, through some yet unknown interaction (or possibly only through gravitational ones), and that it is in thermal equilibrium in the early Universe.

This discussion can be made quantitative through the numerical solution of the Boltzmann equations, a set of differential equations that describe the evolution of the number densities of interacting species in an expanding universe. In the case we are discussing, the equation for n_X reads

$$\frac{dn_X}{dt} = -3Hn_X - \langle\sigma v\rangle(n_X^2 - n_{X,eq}^2) \tag{3.1}$$

where $n_{X,eq}$ is the equilibrium number density of X. The first term on the right-hand side of equation 3.1 accounts for the dilution due to the expansion, the second term comes from the $XX \to AA$ process, while the third one comes from the opposite reaction $AA \to XX$. This equation can be solved numerically.

Let us focus on the freeze-out moment (denoted with a subscript f): the condition $\langle\sigma v\rangle = H$, together with the Friedmann equation for a radiation-dominated Universe, $H^2 \sim T_f^4/M_{Pl}^2$, brings to

$$n_{X,f} \sim \frac{T_f^2}{M_{Pl}\langle\sigma v\rangle}. \tag{3.2}$$

It is customary to define $x \equiv m/T$, and the yield $Y_X \equiv n_X/s$, where s is the entropy density of the Universe. The thermal relic density of X is then (the subscript 0 denotes present-day quantities)

$$\Omega_X = \frac{m_X n_{X,0}}{\rho_c} = \frac{m_X T_0^3}{\rho_c}\frac{n_{X,0}}{T_0^3} \sim \frac{m_X T_0^3}{\rho_c}\frac{n_{X,f}}{T_f^3} \approx \frac{x_f T_0^3}{\rho_c M_{Pl}}\frac{1}{\langle\sigma v\rangle}, \tag{3.3}$$

where the first approximation follows from $Y_{X,f} = Y_{X,0}$ and $s_f = s_0$ (isoentropic expansion of the universe) with the approximation $g_{*,f} \approx g_{*,0}$, and in the last step we used equation 3.2.

If we impose $\Omega_X \sim 0.3$ in equation 3.3, assuming that X is weakly interacting with A and therefore we can write, on dimensional grounds, $\langle\sigma v\rangle \sim g_{weak}^4/(16\pi^2 m_X^4)$, then m_X turns out to be in the range $100\ GeV - 1\ TeV$. Then, a weakly interacting particle with a weak scale mass naturally leads to the correct relic abundance. This exciting coincidence was called the "WIMP miracle", where WIMP stands for Weakly Interacting Massive Particle, and motivated in the last decades a wide belief that the most likely particle candidate for dark matter is a WIMP. An important point in this result is that the thermal relic density is mainly dependent on the cross section σ, rather than on the mass m_X. Indeed, the Dark Matter mass appears in equation 3.3 only through x_f, which is typically of the order of 20 for a WIMP candidate and does not vary much for different choices of m_X. Moreover, this mechanism is independent of the early thermal history of the Universe and of the interactions at high energy scales.

We conclude this discussion about the freeze-out mechanism by recalling the corresponding requirements for dark matter: the DM particle X should be stable on cosmological scales and in thermal equilibrium in the early Universe (moreover, its mass should be lower than the reheating temperature), it should annihilate to other particles, and the corresponding cross section must satisfy a lower bound, so that X is not over-abundant. A peculiarity of the freeze-out mechanism is that a weakly interacting particle X with a mass of the order of the weak scale implies the correct total relic abundance of dark matter.

On the other hand, the production mechanism called freeze-in can be seen for various reasons as the "opposite" with respect to the freeze-out mechanism, in particular for its constraints on the properties of the dark matter candidate. We will sketch here only its basic features.

The following is the basic framework of this production method. The assumptions about the initial conditions of the dark matter candidate X are that, unlike for freeze-out, the species X is weakly interacting with the particle not in thermal equilibrium. Another assumption is that the initial number density of X is negligible; a possible explanation for this is that the reactions that produce X are inefficient after the reheating era. Although the interactions with the thermal bath are feeble, X is still produced, with a yield that turns out to be inversely proportional to the temperature T, and therefore increasing in time. Then the number density of X keeps growing until the temperature drops below m_X, and the reactions that produce X become kinematically disfavoured. From that moment on, the number density of X will substantially remain frozen because the interaction rate will be lower than the Hubble rate.

The most relevant feature of this mechanism is that the number density of X is greater for higher couplings of X to the thermal bath, contrary to the freeze-out case.

We will now estimate the yields expected for two possible renormalisable interaction terms to show that they turn out to be decreasing with temperature (and hence increasing with time). The yield, being an adimensional quantity (once we set $k = 1$), must be the ratio of the two dimensionful quantities that are involved: the decay rate Γ (for a three field interaction, or $n\langle\sigma v\rangle$ for a two-to-two particles scattering) and the Hubble rate $H \sim T^2/M_{Pl}$.

For a Yukawa interaction $\mathcal{L}_{int} = \lambda\psi_1\psi_2 X$ among three fields with masses $m_1 > m_2, m_X$, the decay rate in the rest frame of ψ_1 must be $\Gamma^{RF} \sim \lambda^2 m_1$. The corresponding rate in the comoving frame can be obtained by dividing for the boost factor T/m_1; then $Y_X \sim \Gamma/H \sim \lambda^2 m_1^2 M_{Pl}/T^3$. By evaluating the yield for the temperature $T \approx m_1$ at which the production is dominant (with respect to later times when $T < m$) we get

$$Y_X \sim \lambda\frac{M_{Pl}}{m_1}$$

.

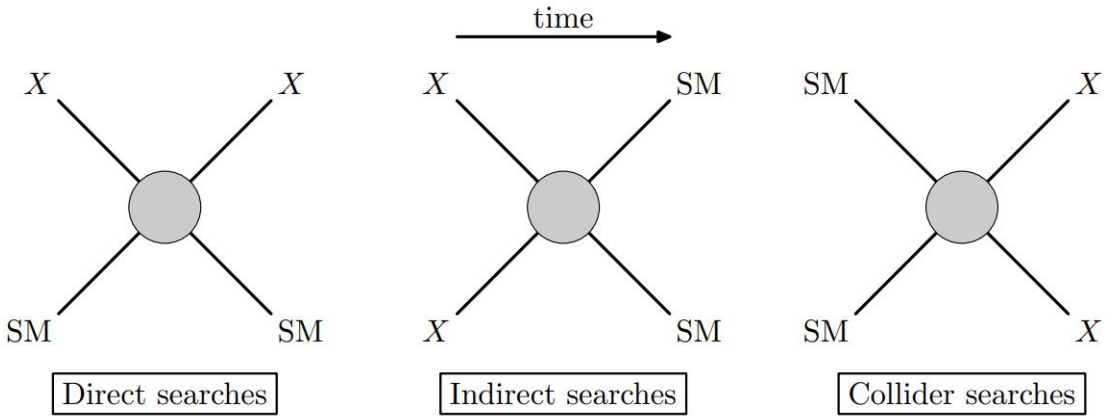

Figure 3.1: Schematic Feynman diagrams involved in the three possible searches for dark matter.

In the case of the quadrilinear interaction $\mathcal{L}_{int} = \lambda X^2 \psi_1^2$, the corresponding cross section will be proportional to λ^2/T^2 for dimensional reasons (for early times, the two species are relativistic, $T \gtrsim m_1,\, m_X$), $n \sim T^3$ and $Y_X \sim n\langle\sigma v\rangle H^{-1} \sim \lambda^2 M_{Pl}/T$ which gives a final yield (for $T \approx m_1$) of the same order as before, $Y_X \sim \lambda^2 M_{Pl}/m_1$.

Even if the details of the freeze-in mechanism and the calculation of the relic density change from case to case, the relevant point that emerges from these estimates is that the yield predicted by this mechanism has opposite features with respect to the one predicted by freeze-out. We can estimate the latter from equation 3.2 by inserting $\langle\sigma v\rangle \sim \lambda^2/M_X^2$ and $T \sim M_X$:

$$Y_{FO} \sim \frac{1}{\alpha^2}\frac{m_X}{M_{Pl}} \tag{3.4}$$

.

We can see that the two mechanisms generally yield the correct relic abundance of dark matter for different regimes of mass scales and interaction couplings.

3.3 Dark Matter Searches

Keeping in mind the previous discussion about the possible scenarios for dark matter production in the early Universe, we can argue that, in addition to the gravitational interaction to which all particles in Nature are subject (according to General Relativity), dark matter must couple to some of the other components of the Universe via some kind of weak interaction. Furthermore, each of the mechanisms outlined in the preceding section requires an interaction that, while possibly weak, must have been efficient at some point in the Universe's history. In particular, the freeze-out mechanism produces consistent relic densities in the hypothesis of an interaction with the SM with a strength comparable to the one of the SM $SU(2)_L$ interaction: this possibility leaves room for detection in the near future with some of the methods described below.

Because of these reasons, it is reasonable to assume that there is a non-gravitational interaction between the DM and the SM. The generic Feynman diagram involving two DM particles (that we will denote by X) and two SM particles on the external lines implies three possible search channels.

From this image, it is clear that a positive result from any of these searches could be probed by the other ones, depending on the regions of higher sensitivity specific to each experiment. Therefore, it is likely that the best constraints we can get about any DM candidate will come from an interplay of all three research channels.

3.3.1 Direct Searches

Direct searches try to detect the motion of Earth through the dark matter distribution of our galaxy [34]. Indeed, the relative motions of the Earth with respect to the Sun (at a speed of 30 km/s) and of the Sun with respect to the galaxy and therefore with respect to the dark matter distribution (at

a speed of around 220 km/s) imply a relatively large flux of dark matter particles through the Earth. This flux, also called "dark matter wind", can be quantified as $\Phi_{DM} \sim 10^{11}\ m^{-2}s^{-1}/(m_X/GeV)$.

A possible experimental search consist in monitoring a large detector looking for energy signals that stem from nuclei recoiling from a dark matter interaction. Since dark matter-nucleus interactions are very unlikely, this kind of experiments must use high-density materials in order to maximize the cross section and must be built underground so that the background of cosmic rays and other sources is minimized. For this reason they are typically held in old mines or inside mountains. Eventually, an important point that can allow us to distinguish the expected signal from the background is the periodicity: indeed, the flux of DM through the Earth should show an annual modulation, as we will discuss below.

In order to quantify the expected number of events, many inputs from different research fields must be specified:

- **Astrophysical input**: we should have a precise estimate of the flux of DM particles, which depends both on the local density distribution and on the velocity distribution of dark matter. The only way to get a detailed prediction is to compare some ansatz for these functions, which depend on some unspecified parameters, with the result of numerical simulations and with phenomenological inputs from astrophysics and cosmology. For example, all the density profiles for dark matter that have been proposed display the common behavior $\rho \propto r^{-2}$, i.e., a density proportional to the inverse of the square of the radial distance from the center of the galaxy for r of the order of the galactic visible disk dimension.

- **Experimental and Particle Physics input**: a careful choice of material for the detector must be done. Indeed, depending on the nuclear mass and spin of the nucleus, the event rate is different if the dark matter interacts or not with the nucleus spin; we will talk of spin-dependent and spin-independent cross section respectively. Furthermore, in order to maximize the cross section of the interaction, it is better to choose a material with a high density. Finally, the cost of the experiment must also be taken into account. Just to mention some relevant examples for the spin-independent searches, the chosen material in some current experiments are xenon (e.g., XENON100, LUX, ZEPLIN), germanium (CDMS, EDELWEISS, CoGeNT), calcium tungstate (CRESST), and sodium iodide (DAMA).

We will now discuss shortly how these inputs enter in the definition of the differential scattering rate for a target nuclei recoiling with energy E_R[1].

Let us first observe that the scattering of dark matter with electrons can be safely neglected. Indeed, the dark matter particle moves at non-relativistic speed, and when it interacts with the nucleus, it does not have enough energy to resolve its constituent. For this reason, the nucleus can be seen as a bound state, and its cross section is by far larger than the one with an electron.

The rate R of nuclear recoils due to dark matter scatterings (event rate) is usually calculated as a differential rate with respect to the recoil energy $E_R \equiv q^2/(2m_T)$, where m_X is the dark matter mass, m_T the target nuclei mass, and q is the momentum transferred in the scattering. E_R is the amount of kinetic energy left by the incoming dark matter particle in the detector after the interaction. Since Dark Matter has a non-relativistic speed of order $\sim 10^{-3}$, and the typical mass of a nucleus is $m_T \sim 100\ GeV$, the maximum momentum transfers is $q \lesssim 200\ MeV$ and the scattering is elastic.

The scattering rate per unit of time and volume, for a dark matter particle travelling through the detector with velocity $\vec{v}$ is given by:

$$R = \frac{dN_T}{dtdV} \equiv n_T n_X v \sigma_{XN}(v) \tag{3.5}$$

where n_T and n_X are the number density of target nuclei and dark matter, respectively. σ_{XN} is the cross section of the interaction and can be obtained from a particle physics model that describes the interactions between dark matter and nucleons[2]. Since the dark matter particles are not

[1] We assume that the detector does not contain impurities and is composed of nuclei of the same species and isotope

[2] In general, the cross section can depend on the full velocity vector $\vec{v}$, but if the dark matter flux and the nuclei in the detector are both unpolarized, as we assume, it will depend only on the dark matter speed.

monochromatic in velocity, the density in equation 3.5 must be replaced by its differential

$$dn = \frac{\rho_X}{m_X} f_E(\vec{v}, t) d^3v \tag{3.6}$$

where ρ_X is the local dark matter density and $f_E(\vec{v}, t)$ is the velocity distribution at Earth's location, normalized to one. The density ρ_X can be determined from the study of the vertical kinematics of stars near the Sun. The value $\rho_X = 0.3\ GeV/cm^3$ is the historical reference used in direct detection literature. The velocity distribution is deduced from the comparison of observations and numerical simulations. The usual ansatz for the velocity distribution is the Maxwell distribution with two modifications. First, we must consider that an upper limit for v is given by the so-called escape velocity v_{esc}, above which a dark matter particle is not gravitationally bound to the Milky Way. A standard value is $v_{esc} \approx 650\ km/s$. Secondly, the WIMP speed distribution in the detector frame is obtained through a time-dependent Galilean transformation $\vec{v} \to \vec{v} + \vec{v}_E(t)$, where $\vec{v}_E(t)$ is the velocity of the Earth in the galaxy rest frame, equal to the sum of the Sun's peculiar motion $\vec{v}_\odot$, with $|\vec{v}_\odot| \approx 220\ km/s$, and the revolution velocity $\vec{v}_E^{orb}$ of the Earth around the Sun. This vectorial sum can be approximated to $|\vec{v}_E t| = |\vec{v}_\odot| + V_\oplus cos(2\pi t)$, where t is measured in years (starting from the 1st June), and $V_\oplus \approx 30\ km/s$. From the time dependence of the velocity distribution arises the modulation of the expected signals.

Taking this into consideration and dividing by the mass density of the detector (ρ_{det})), we get for the differential scattering rate:

$$\frac{dR}{dE_R}(E_R, t) = \frac{\rho_X}{m_X} \frac{n_{det}}{\rho_{det}} \int_{v_{min}}^{v_{max}} f_E(\vec{v}, t) v \frac{d\sigma_{XN}}{dE_R}(E_R, v) \tag{3.7}$$

where v_{max} is determined by v_{esc} and $\vec{v}_E(t)$, and v_{min} is the minimum dark matter speed which can cause a recoil of energy E_R, which turns out to be $v_{min} = \sqrt{(m_N E_R)/2\mu_N^2}$, with $\mu_N = m_X m_N/(m_X + m_N)$ the reduced mass of X and the nucleus. This formula follows from this alternative expression for ER, which can be derived from kinematical considerations:

$$E_R = \left(\frac{1}{2} m_X v_{in}^2\right) \frac{4\mu_N}{m_X + m_N} \left(\frac{1 - cos\theta*}{2}\right) \tag{3.8}$$

,

where θ^* is the recoil angle in the center-of-mass frame. We notice that E_R is maximum for a value of m_X equal to m_N: if we recall that the detector is sensitive to the recoil energy E_R, we can understand why the limits on the cross sections coming from direct detection experiments are stronger in the range $m_X \approx 10 - 100\ GeV$, near to the mass of the nuclei of the target material of the experiment. Moreover, from equation 3.7, we can understand the qualitative behavior of the sensitivity of direct detection for high values of m_X: the cross section in a first approximation will be proportional to a parameter with mass dimension (the cut-off scale Λ, that will be introduced in equation 3.9) raised to the power (-4), thus for dimensional reasons it will also be proportional to the reduced mass μ_N, that for m_X much greater than m_N tends to the smaller of the two, i.e. m_N. Thus the cross section tends to a constant for $m_X > m_N$, but the number density of dark matter, which is the first multiplicative factor in equation 3.7, can be written as ρ_X/m_X, where ρ_X is basically fixed by the observed energy density of dark matter. Therefore, this factor $1/m_X$ mildly reduces the sensitivity of direct detection for masses $m_X > m_N$.

At this point, in equation 3.7, the only quantity to be discussed is the cross section σ_{XN} for the elastic scattering between X and the nucleus. This cross section can be derived from the microscopic theory through three steps.

The first step requires to define a theory that describes the interactions between the dark matter field and partons (either a quark or a gluon). This can be done in a specific model by using a complete theory (also called ultraviolet or UV theory) or by using an effective field theory (EFT) approach. In an effective Lagrangian, one considers all the possible effective non-renormalisable operators $\mathcal{O}_i^{(d)}$ of mass dimension d between two quarks (or gluons) and two X fields, each of them with an unknown coefficient $c_i^{(d)}$ called Wilson coefficient,

$$\mathcal{L}_{EFT} = \sum_{d\geq 5} \sum_{i} \frac{c_i^{(d)}}{\Lambda^{d-4}} \mathcal{O}_i^{(d)} \tag{3.9}$$

where Λ is the cutoff scale, which allows to quantify the goodness of the truncation up to a certain dimension d. Indeed, depending on the energy scale E of the interaction and the value of Λ, one can approximate equation 3.9 by truncating the first sum up to a dimension d such that $(E/\Lambda)^d \ll 1$. One thinks about the Lagrangian 3.9 from the Wilsonian point of view, in which all the degrees of freedom of a renormalisable UV theory, with energy higher than Λ, have been integrated out; therefore, in the resulting Lagrangian, the operators of dimension $d \geq 5$ listed in equation 3.9 appear. From this perspective, we can be more precise about the condition $(E/\Lambda)^d \ll 1$: in fact, we can relate the cut-off scale Λ to the masses and the couplings of heavy fields which have been integrated out in the Wilsonian Lagrangian. A more detailed discussion of the EFTs describing the interactions between Dark Matter and SM particles will be given at the beginning of the next chapter.

Once the dark matter-partons interactions are specified, we need to derive the interaction of the dark matter particles with the nuclei. This can be achieved using the hadronic matrix elements, i.e., the matrix elements for the operators containing quark or gluon fields, which introduce the form factors. These are functions depending on the momentum exchanged in the interaction; they must be determined experimentally and represent the greatest source of error in the total scattering rate. It is then possible to match the relativistic operators onto a set of non-relativistic operators that describe the interaction of dark matter with a single nucleon, obtaining the effective Lagrangian:

$$\mathcal{L}_{eff} = \sum_{i,N} c_i^N(q^2) \mathcal{O}_i^N \tag{3.10}$$

where $N = p, n$ refers to proton and neutron respectively and i runs over the 14 non-relativistic operators $\mathcal{O}_i^N$.

Finally, to get the scattering rate $d\sigma_{XN}/dE_R$ with the whole nucleus, a multipole expansion is performed, and the nuclear response functions are defined. These and other nuclear parameters are experimentally measured by nuclear physicists.

To conclude, we note that the $\mathcal{O}_i^N$ operators can be divided into two categories: those that do not depend on the nucleon spin and those that do. This distinction is important since operators depending on the nucleon spin (for example, $\mathcal{O}_4^N = \vec{S}_X \cdot \vec{S}_N$) will produce a so-called spin-dependent cross section that is suppressed due to interference between the nucleon's spins. On the other hand, operators that do not depend on the nucleon spin (like $\mathcal{O}_1^N = \mathbb{I}_X \mathbb{I}_N$) generate a spin-independent cross section that is coherently enhanced and hence proportional to A^2 (A being the mass number of the nucleus). This point is very important from the experimental point of view because, in order to probe spin-dependent interactions, it is necessary to use a target with nuclei with a non-vanishing total spin. As a result, only some studies are sufficiently sensitive to spin-dependent interactions, and the exclusion limits are weaker in that case.

3.3.2 Indirect Searches

Indirect techniques are based on the search for radiation produced in dark matter annihilations. Indeed, the reactions that produced dark matter in the early Universe are now inefficient, and their impact on the dark matter relic density is negligible, but dark matter annihilation continues and may be observable. The flux of the radiation produced by these annihilations is proportional to the annihilation rate Γ_{ann}, which in turn depends on the square of the dark matter density, $\Gamma_{ann} \propto \rho_X^2$. As a result, the places where dark matter accumulates, also known as amplifiers, are the most attractive directions to investigate in order to maximize the probability of finding the products of these interactions. Dense regions of the galactic halo, as the galactic center, are therefore the target of many astrophysical searches, but also the Sun or the Earth could act as amplifiers for dark matter annihilations since dark matter could lose energy through the scattering with nucleons inside these objects. Astronomers then aim to detect the possible products of these annihilations; these can be photons (both X-rays and Gamma rays), neutrinos, electrons and positrons, or protons and antiprotons. The latters being

charged can be deviated by electromagnetic fields encountered along the line of sight, meaning that their spatial distribution is random and the source cannot be tracked down. As said before, dark matter can accumulate towards the Earth's or Sun's center because of their gravitational field and the loss of energy due to interaction with nuclei. The only products of annihilations happening in this context that can be detected are high-energy neutrinos, which are more likely to leave a track in a Cherenkov detector.

3.3.3 Collider Searches

If dark matter interacts weakly with standard model particles, there is the possibility for it to be produced in collider experiments.

Because of this extremely weak interaction with matter, dark matter is not expected to leave track inside the detector, and the experimental signature is characterized by a large amount of missing transversal energy [35, 36]. Typically, the analysis for dark matter searches focuses on single jet (from quark or gluon initial state radiation) plus missing transversal energy or a single photon (from electromagnetic initial state radiation) plus missing transversal energy. The background for these kinds of events stems from Z boson production and decays into two neutrinos with initial state radiation (either a jet or a photon). This kind of background can be reduced in a e^+e^- collider, where the total energy of the collision can be tuned far away from the Z resonance. The same tuning cannot be done in a hadron collider like LHC since it is not possible to control the parton's energy. We must make an additional remark about this type of search. The observation of missing particles at colliders simply reveals that some particles weakly interacting with the SM were produced, but it is far from a compelling evidence that this can be the DM candidate. In the case of a positive detection by the experimental collaborations, further studies (or even further collider experiments) are needed to understand the mass and lifetime of that particle, and possibly the branching ratios for its decays. Then, on the basis of these data, one should compute the thermal relic density and check that the result is consistent with cosmological observations.

Chapter 4

New Physics Models for the Dark Matter and the muon g-2 anomaly

4.1 New Physics models Lagrangians

As already anticipated in the previous chapter, a possible explanation of the a_μ anomaly can be achieved by extending the Standard Model through the introduction of new fields coupling to muons. The aim of this section is to build and classify a set of simplified models following the lines of [37]. Since the currently observed a_μ anomaly is of the same size as the SM weak contribution, one would be naturally tempted to invoke weakly coupled particles emerging at the electro-weak scale. Remarkably, this possibility could be connected with the solution of the hierarchy problem and could provide, at the same time, a WIMP dark matter candidate. Unfortunately, the lack for new particles at LEP and LHC strongly disfavours this interpretation. As a result, two possibilities seem to emerge: either NP is very light and feebly coupled to SM particles, or NP is very heavy and strongly coupled.

Here, we take the second direction. Heavy NP contributions to the muon g-2 arise from the dimension-6 dipole operator $\mu_L \sigma_{\mu\nu} \mu_R H F^{\mu\nu}$ where $H = (v+h)/\sqrt{2}$ contains both the Higgs boson field h and its vacuum expectation value $v = 246$ GeV. After electroweak symmetry breaking, one obtains the prediction $\Delta a_\mu \sim (g_{\rm NP}^2/16\pi^2) \times (m_\mu v\, y_{\rm NP}/\Lambda^2)$, where $g_{\rm NP}$ is the typical coupling of the NP sector to SM particles while $y_{\rm NP}$ represents the NP Yukawa coupling of the new states to the Higgs boson. Therefore, the NP chiral enhancement $v/m_\mu \sim 10^3$ with respect to the SM weak contribution, together with the assumption of a new strong dynamics with $g_{\rm NP}, y_{\rm NP} \gtrsim 1$, enable us to bring the sensitivity of the muon g-2 to NP scales well above the TeV scale, in agreement with the LHC bounds. Since such a required chiral enhancement implies NP couplings with both left-handed and right-handed fermions, it is clear that the minimal particle content of a simplified NP model addressing the muon g-2 anomaly has to entail at least two states (either boson or fermion states).

Moreover, the requirement of having a good dark matter candidate poses further restrictions. In particular, a good DM candidate must be an electromagnetically neutral color singlet state and must be stable on cosmological time scales. While the first requirement will affect the transformation properties of the fields under the electroweak gauge group $G_{weak} = SU(2)_L \times U(1)_Y$, the second one can be realized by imposing a Z_2 symmetry under which the new fields are odd while the Standard Model fields are even. Therefore, to ensure the Z_2 symmetry, the new sector must contain at least one fermion and one scalar. As a result, a successful explanation of both the muon g-2 anomaly (through a chiral enhancement) and the observed DM relic abundance selects models with at least three fields, either two fermions and one scalar or viceversa.

We are now ready to present the two possible scenarios:

- **FH Models:** the Higgs couples to new fermions through the following Lagrangian

$$\mathcal{L}^{NP}_{int,FH} = y_F H F_L F_R + \lambda_L L_L^2 F_R S_R + \lambda_R \mu_R F_L S_R^* + h.c.\ . \tag{4.1}$$

  Introducing the two fields $\bar{F}_R$ and $\bar{F}_L$, that transform under the conjugate representation of the electroweak gauge gruop, the mass term for these fields can be written as

$$-\mathcal{L}_{mass} = (M_{F_L} F_L \bar{F}_L + M_{F_R} F_R \bar{F}_R + h.c.) + M^2_{S_R} S^*_R S_R \ . \tag{4.2}$$

- **SH Models:** the Higgs couples to new scalars through the following Lagrangian

$$\mathcal{L}^{NP}_{int,SH} = aH S_L S_R + \lambda_L L^2_L F_R S_L + \lambda_R \mu_R \bar{F}_R S_L + h.c. \tag{4.3}$$

  where the field $\bar{F}_R$ transform under the conjugate representation of the electroweak gauge group. Then, the mass term for these fields can be written as

$$-\mathcal{L}_{mass} = (M_{F_R} F_R \bar{F}_R + h.c.) + M^2_{S_R} S^*_R S_R + M^2_{S_L} S^*_L S_L \ . \tag{4.4}$$

The possible transformation properties of the fields introduced in equations 4.1 and 4.3 can be obtained by requiring the operator in those Lagrangians to be gauge invariant and then selecting all the possible combinations that allow a dark matter candidate, hence an electromagnetically neutral state[1]. We have to note that the dark matter candidate can still interact under weak neutral interaction if the hypercharge $Y_{F,S}$ is not null, but these possibilities are strongly constrained by the experimental bounds on dark matter direct detection. We will find all possible models containing fields transforming up to a $SU(2)_L$ triplets and collect them in 4.1 and 4.2.

We will sketch the general procedure to get the possible field representation for the FH model; the procedure for the SH case is completely analogous. Let's first define the notation we will use:

$$F_R \sim (n_{F_R})_{Y_{F_R}} \ , \qquad F_L \sim (n_{F_L})_{Y_{F_L}} \ , \qquad S_R \sim (n_{S_R})_{Y_{S_R}} \ . \tag{4.5}$$

From the interaction term with the right-handed muon, it is straightforward to see that the product $F_L S^*_R$ must transform as a singlet, and, using the summation rule for angular momentum from quantum mechanics, we have that F_L and S_R must transform in the same representation, i.e. $n_{F_L} = n_{S_R}$. From the interaction term with the left-handed muon, we deduce that the product $F_R S_R$ must transform as a doublet. Using this, we can show that n_{F_R} must satisfy the following constraint $|n_{F_R} - n_{S_R}| \leq 1$. Since n_{F_R} and n_{S_R} are positive integers, we have:

$$n_{F_R} = n_{S_R} \pm 1 \tag{4.6}$$

.

Once the transformation properties under $SU(2)_L$ of the scalar S_R are specified, $n_{F_{R,L}}$ are fixed. Each of the interaction terms in the Lagrangian shown above must be a singlet under the $U(1)_Y$ group; this provides us with a set of three equations for the hyercharges of the new fields:

$$\frac{1}{2} + Y_{F_R} + Y_{F_L} = 0 \, , \tag{4.7}$$

$$\frac{1}{2} - Y_{F_R} - Y_{S_R} = 0 \, , \tag{4.8}$$

$$1 + Y_{F_L} - Y_{S_L} = 0 \, . \tag{4.9}$$

The three equations are not independent from each other; indeed, the third one can be obtained by subtracting the second equation from the first one. This implies that we can express the hypercharges of the fermion fields in terms of Y_{S_R}:

$$Y_{F_R} = \frac{1}{2} - Y_{S_R} \, , \tag{4.10}$$

$$Y_{F_L} = Y_{S_R} - 1 \, . \tag{4.11}$$

[1]The condition for the new particle to be color singlet was implicitly assumed.

For the SH models, analogous arguments apply. We can then express the transformation properties of $S_{R,L}$ as a function of those pertaining to F_R as:

$$n_{S_R} = n_{F_R} \pm 1\,, \tag{4.12}$$

$$Y_{S_R} = \frac{1}{2} - Y_{F_R}\,, \tag{4.13}$$

$$Y_{S_L} = Y_{F_R} - 1\,. \tag{4.14}$$

Finally, in all these possible FH and SH models, we need to focus on those that admit a dark matter candidate. To find them, it is sufficient to require that at least one of the multiplets admits a neutral component, imposing the condition $Q_i = T^3_{L,i} + Y_i = 0$ (with $i = F_R, F_L, S_R, S_L$) to be valid for some value of the third component of the weak isospin T^3_L, where $-\frac{n_i-1}{2} \leq T^3_L \leq \frac{n_i-1}{2}$.

FH										
S_R	$2^*_{\frac{1}{2}}$	$2^*_{-\frac{1}{2}}$	1_1	3^*_1	1^*_0	3^*_0	3^*_{-1}	$2_{\frac{3}{2}}$	$2^*_{\frac{1}{2}}$	$2^*_{-\frac{1}{2}}$
F_R	1^*_0	1_1	$2^*_{-\frac{1}{2}}$	$2^*_{-\frac{1}{2}}$	$2^*_{\frac{1}{2}}$	$2^*_{\frac{1}{2}}$	$2_{\frac{3}{2}}$	3^*_{-1}	3^*_0	3^*_1
F_L	$2^*_{-\frac{1}{2}}$	$2_{\frac{3}{2}}$	1^*_0	3^*_0	1_{-1}	3^*_{-1}	3_{-2}	$2^*_{\frac{1}{2}}$	$2^*_{-\frac{1}{2}}$	$2_{-\frac{3}{2}}$

Table 4.1: FH models up to $SU(2)_L$ triplets. Fields with a $\star$ contain a dark matter candidate.

SH										
F_R	1_1	1^*_0	$2^*_{\frac{1}{2}}$	$2^*_{\frac{1}{2}}$	$2_{\frac{3}{2}}$	$2^*_{-\frac{1}{2}}$	$2^*_{-\frac{1}{2}}$	3^*_1	3^*_0	3_{-1}
S_L	1^*_0	1_{-1}	$2^*_{-\frac{1}{2}}$	$2^*_{-\frac{1}{2}}$	$2^*_{\frac{1}{2}}$	$2_{-\frac{3}{2}}$	$2_{-\frac{3}{2}}$	3^*_0	3^*_{-1}	3_{-2}
S_R	$2^*_{-\frac{1}{2}}$	$2^*_{\frac{1}{2}}$	1^*_0	3^*_0	3^*_{-1}	1_1	3^*_1	$2^*_{-\frac{1}{2}}$	$2^*_{\frac{1}{2}}$	$2_{\frac{3}{2}}$

Table 4.2: SH models up to $SU(2)_L$ triplets. Fields with a $\star$ contain a dark matter candidate.

4.1.1 Benchmark models

Direct detection tests place strong constraints on the parameter space of dark matter models. The most critical restrictions in our framework arise from gauge interactions. It is well known that bounds on dark matter-nucleus scattering due to the tree-level Z boson exchange exclude models with non-zero hypercharged weak-scale Dirac fermions or scalar dark matter multiplets. In the light of the above considerations, hereafter, we will focus on two simple models containing dark matter candidates with $Y = 0$ and arising in the smallest representations of the electroweak gauge group.

$FH1$ model

The $FH1$ model is the simplest model where new physics couples to the Higgs and has a viable dark matter candidate. The quantum numbers for the new sector content can be read from the first column of table 4.1, $F_R \sim 1_0$ is a heavy Majorana fermion, $F_L \sim 2_{-\frac{1}{2}}$ is a vector-like fermion doublet (we also need $\bar{F}_L$ transforming in the conjugate representation of the gauge gruop), and finally $S_R \sim 2_{\frac{1}{2}}$ is a vector-like scalar doublet. We will change the notation to a more suggestive one

$$F_S \equiv F_R \;\; F_D \equiv F_L \;\; \bar{F}_D \equiv \bar{F}_L \;\; S \equiv S_R \tag{4.15}$$

given these field content the new physics sector Lagrangian is,

$$\mathcal{L}_{FH1} = \frac{1}{2}\left(F_S^\dagger i\bar{\sigma}^\mu \partial_\mu F_S - F_S F_S + h.c.\right) \tag{4.16}$$

$$+ F_D^\dagger i\bar{\sigma}^\mu D_\mu F_D + \bar{F}_D^\dagger i\bar{\sigma}^\mu D_\mu^* \bar{F}_D - M_{F_D} F_D \bar{F}_D \tag{4.17}$$

$$+ (D_\mu S)^*(D^\mu S) - M_S^2 S^* S \tag{4.18}$$

$$+ (\lambda_{1H} H F_D F_S + \lambda_{2H} \tilde{H} \bar{F}_D F_S + \lambda_1 \mu F_S S + \lambda_2 \bar{\mu} F_D S^* + h.c.) \tag{4.19}$$

Where the covariant derivative is given by $D_\mu = \partial_\mu - i\frac{g_2}{2}\tau^i W_\mu^i - i g_Y Y_{NP} B_\mu$ and D_μ^* is the one for fields transforming in the conjugate representation, $\bar{\sigma}^\mu = (\mathbb{I}, -\tau^i)$ are two-by-two matrices and Y_{NP} is the hypergarge of the new field. We have introduced four complex dimensionless couplings $\lambda_{1,2}$ and $\lambda_{1H,2H}$ that can be taken to be of $\mathcal{O}(\infty)$.

This model has the following matter content:

- A charge complex scalar S_+ and a neutral complex scalar S_0 from the scalar doublet S;
- A Dirac fermion $F_- = \begin{pmatrix} F_{D-} \\ \bar{F}_{D+}^\dagger \end{pmatrix}$ obtained combining the charged components of F_D and $\bar{F}_D$;
- Three Majorana fermions, $F_S = \begin{pmatrix} F_S \\ F_S^\dagger \end{pmatrix}$, $F_{D0} = \begin{pmatrix} F_{D0} \\ F_{D0}^\dagger \end{pmatrix}$ and $\bar{F}_{D0} = \begin{pmatrix} \bar{F}_{D0} \\ \bar{F}_{D0}^\dagger \end{pmatrix}$, the last two being the neutral components of F_D and $\bar{F}_D$ respectively

We can thus rewrite the Lagrangian in terms of Dirac and Majorana fields. The Higgs-fermions interactions will induce a mixing between the three Majorana fields after Electroweak Symmetry Breaking. We can define the mixing matrix V that diagonalizes the Majorana mass matrix:

$$V^T \begin{pmatrix} M_{F_S} & \frac{\lambda_{1H} v}{\sqrt{2}} & \frac{\lambda_{2H} v}{\sqrt{2}} \\ \frac{\lambda_{1H} v}{\sqrt{2}} & 0 & M_{F_D} \\ \frac{\lambda_{2H} v}{\sqrt{2}} & M_{F_D} & 0 \end{pmatrix} V = \begin{pmatrix} M_1 & 0 & 0 \\ 0 & M_2 & 0 \\ 0 & 0 & M_3 \end{pmatrix} \tag{4.20}$$

where the mass eigenvalue satisfy $M_1 \leq M_2 \leq M_3$ and are related to mass eigenstate as:

$$F_{0i} = \begin{pmatrix} F_i \\ F_i^\dagger \end{pmatrix}, \quad i = 1, 2, 3 \tag{4.21}$$

In terms of these eigenstate, the Lagrangian is given by

$$\mathcal{L}_{FH} = \mathcal{L}_{kin} + \mathcal{L}_{NP} + \mathcal{L}_h + \mathcal{L}_{gauge} + \mathcal{L}_{scalar} \tag{4.22}$$

with

$$\mathcal{L}_{kin} = \bar{F}_-(i\partial\!\!\!/ - M_{F_D})F_- + \frac{1}{2}\left(\bar{F}_{0i}(i\partial\!\!\!/ - M_i)F_{0i}\right) \tag{4.23}$$

$$\mathcal{L}_{NP} = \lambda_1 V_{1j}(S_0 \bar{F}_{0j}\nu_{\mu L} - S_+ \bar{F}_{0j}\mu_L) + \lambda_2 S_0^*(\bar{\mu} P_L F_-) + \lambda_2 V_{2j} S_+^*(\bar{\mu} P_L F_{0j}) + h.c. \tag{4.24}$$

$$\mathcal{L}_h = -\frac{h}{\sqrt{2}}(\lambda_{1H} V_{2i} V_{1j} + \lambda_{2H} V_{3i} V_{1j})\bar{F}_{0i} P_L F_{0j} + h.c. \tag{4.25}$$

$$\mathcal{L}_{gauge} = \frac{g_2}{c_W} Z_\mu \left[\frac{1}{4}(V_{2i}^* V_{2j} - V_{3i}^* V_{3j})\bar{F}_{0i}\gamma^\mu P_L F_{0j} - \frac{1}{4}(V_{2i} V_{2j}^* - V_{3i} V_{3j}^*)\bar{F}_{0i}\gamma^\mu P_R F_{0j}\right] \tag{4.26}$$

$$- \left(\frac{1}{2} - s_W^2\right)\bar{F}_-\gamma^\mu F_- + e A_\mu \bar{F}_-\gamma^\mu F_- \tag{4.27}$$

$$+ \frac{g_2}{\sqrt{2}}\left[W_\mu^+(V_{2i}^* \bar{F}_{0i}\gamma^\mu P_L F_- + V_{3i}\bar{F}_{0i}\gamma^\mu P_R F_-) + h.c.\right] \tag{4.28}$$

We do not give the expression for $\mathcal{L}_{scalar}$ since it is not relevant for the following discussion. This model presents different neutral particles, but only two are viable dark matter candidates: S_0 and F_{01}. Since we require the dark matter to have $Y_{DM} = 0$, only F_{01} remains as a possible candidate.

$SH1$ model

The $SH1$ model is the simplest model that introduces two new scalars, interacting with the Higgs, and one fermion. The quantum numbers for the new particles can be read from the first column of table 4.2. The two scalars are a real singlet $S_L \sim 1_0$ and a complex scalar doublet $S_R \sim 2_{-\frac{1}{2}}$, and finally a pair of vector-like Weyl fermions $F_R \sim 1_1$ and $\bar{F}_R \sim 1_{-1}$. As before, we changed the notation to a more suggestive one,

$$F \equiv F_R, \quad \bar{F} \equiv \bar{F}_R, \quad S \equiv S_L, \quad D \equiv S_R \tag{4.29}$$

From this field content we can build the following Lagrangian:

$$\begin{aligned}
\mathcal{L}_{SH} =& \frac{1}{2}\left(\partial_\mu S \partial^\mu S - M_s^2 S^2\right) && (4.30)\\
&+ (D^\mu D)^* D_\mu D - M_D^2 D^* D && (4.31)\\
&+ F^\dagger i\bar{\sigma}^\mu D_\mu F + \bar{F}^\dagger i\bar{\sigma}^\mu D_\mu^* \bar{F} - M_f F\bar{F} + h.c. && (4.32)\\
&+ a_H HSD + \lambda_1 D\mu F + \lambda_2 S\bar{\mu}\bar{F} + h.c. && (4.33)
\end{aligned}$$

Where the covariant derivative is given by $D_\mu = \partial_\mu - i\frac{g_2}{2}\tau^i W_\mu^i - ig_Y Y_{NP} B_\mu$ and D_μ^* is the one for fields transforming in the conjugate representation, $\bar{\sigma}^\mu = (\mathbb{I}, -\tau^i)$ are two-by-two matrices and Y_{NP} is the hypergarge of the new field. In this model, we have introduced two dimensionless complex couplings, $\lambda_{1,2}$ of $\mathcal{O}(1)$ and a dimensionfull coupling a_H that can be taken to be of $\mathcal{O}(v)$.

From this Lagrangian we can deduce the following matter content:

- Two CP-even neutral scalar S and D_0 from the singlet and one of the neutral component of the complex scalar D respectively;
- A CP-odd neutral scalar A_0 from the doublet D;
- A complex scalar S_- again from th complex scalar D;
- A charged Dirac fermion $F_- = \begin{pmatrix} \bar{F} \\ F^\dagger \end{pmatrix}$ obtained combining the two Weyl fermions.

The Higgs-scalar interactions will induce a mixing between the two CP-even neutral scalar fields after Electro-Weak Symmetry Breaking. We can define the mixing matrix U that diagonalizes the scalar mass matrix:

$$U^T \begin{pmatrix} M_S^2 & va_H \\ va_H & M_D^2 \end{pmatrix} U = \begin{pmatrix} M_1^2 & 0 \\ 0 & M_2^2 \end{pmatrix} \tag{4.34}$$

.

where the mass eigenvalues satisfy $M_1^2 \leq M_2^2$ and are associated to the neutral scalars $S_\alpha, \quad \alpha = 1, 2$.

Then the Lagrangian can be rewritten in terms of the mass eigenstate:

$$\mathcal{L}_{SH1} = \mathcal{L}_{kin} + \mathcal{L}_{NP} + \mathcal{L}_h + \mathcal{L}_{gauge} + \mathcal{L}_{fermion} \tag{4.35}$$

with

$$\mathcal{L}_{kin} = \bar{F}_-(i\partial\!\!\!/ - M_f)F_- + \frac{1}{2}(\partial^\mu S_\alpha \partial_\mu S_\alpha - M_\alpha^2 S_\alpha^2) + \frac{1}{2}(\partial^\mu A_0 \partial_\mu A_0 - M_D^2 A_0^2) + \partial^\mu S_-^* \partial_\mu S_- - M_D^2 S_-^* S_- \tag{4.36}$$

$$\mathcal{L}_{NP} = \frac{\lambda_1}{\sqrt{2}}(U_{2\alpha}S_\alpha + iA_0)(\bar{F}_- P_L \mu) - \lambda_1 S_-(\bar{F}_- P_L \nu) + \lambda_2 U_{1\alpha} S_\alpha(\bar{\mu} P_L F_-) + h.c. \tag{4.37}$$

$$\mathcal{L}_h = -\frac{a_H}{2} h U_{1\alpha} U_{2\beta} S_\alpha S_\beta \tag{4.38}$$

$$\mathcal{L}_{gauge} = \frac{g_2}{c_W} Z_\mu \left[(-\frac{1}{2} + s_W^2)(S_-^* i \overleftrightarrow{\partial}^\mu S_-) + \frac{1}{2} U_{2\alpha}(A_0 \overleftrightarrow{\partial}^\mu S_\alpha) \right] + ieA_\mu (S_-^* \overleftrightarrow{\partial}^\mu S_-) \tag{4.39}$$

$$+ \frac{g_2^2}{8c_W^2}(iA_0 + U_{2\alpha}S_\alpha)(-iA_0 + U_{2\beta}S_\beta)(2c_W^2 W_\mu^+ W_-^\mu + Z_\mu Z^\mu) \tag{4.40}$$

$$+ S_-^* S_- \left[\frac{1}{2} g_2^2 W_\mu^+ W_-^\mu + \left(eA_\mu + \frac{g_2}{C_W}\left(-\frac{1}{2} + s_W^2 \right) \right)^2 \right] \tag{4.41}$$

$$+ \frac{g_2}{2} W_\mu^+ \left[U_{2\alpha}(S_\alpha \overleftrightarrow{\partial}^\mu S_-) + A_0 \overleftrightarrow{\partial}^\mu S_- + S_-(U_{2\alpha}S_\alpha - iA_0)\left(eA^\mu + \frac{g-2}{c_W} s_W^2 Z^\mu \right) \right] + h.c. \tag{4.42}$$

We do not give the explicit expression for $\mathcal{L}_{fermion}$ since it will not be of interest for this model discussion.

The dark matter candidate in this model is represented by the lightest scalar S_1.

4.2 The muon g-2

In order to compute the Δa_μ^{NP} we use an $SU(3)_c \times U(1)_{em}$ Lagrangian that captures the general structure of the new physics-muon interactions,

$$\mathcal{L}_{kin} = (D_\mu s)^* D^\mu s - M_s s^* s + \bar{f}\left(i\partial\!\!\!/ - M_f \right) f + \bar{\mu}\left(i\partial\!\!\!/ - m_\mu \right)\mu \tag{4.43}$$

$$\mathcal{L}_{int} = s^* \bar{\mu}\left(\lambda_2^R P_L + \lambda_2^R P_R \right) f + h.c \tag{4.44}$$

where s and f are a scalar and a vector-like fermion representative of the new physics fields, with electric charge Q_s and Q_f. Applying charge conservation to the interaction term in the Lagrangian 4.44, the relation between $Q_f = Q_s - 1$ is found. The covariant derivative is $D_\mu = \partial_\mu - ieQ_{s,f}$. While the couplings $\lambda_2^{L,R}$ are functions of the coupling constants and mixing angles of the specific model $FH1$ or $SH1$.

The Feynman rules for the two Lagrangians 4.43 and 4.44 are drawn in A.11 and A.10 respectively.

The anomalous magnetic moment of the muon, a_μ, is one of the most important tests of the Standard Model and provides a powerful probe of new physics. The discrepancy first discovered at the BNL laboratory has triggered many speculations about new physics scenarios that give additional contributions to a_μ.

The most general of those can be described by the effective Lagrangian

$$\mathcal{L} = \frac{em_l}{8\pi^2} C_{ll'}(\vec{l}_R \sigma_{\mu\nu} l_L) + h.c.), \quad l, l' = e, \mu, \tau \tag{4.45}$$

where $C_{ll'}$ is a Wilson coefficient with mass dimension $(GeV)^{-2}$. This leads to the general expression for the new physics contribution to the anomalous magnetic moment, Δa_l,

$$\Delta a_l = \frac{1}{2\pi^2} m_l^2 \Re(C_{ll'}) \tag{4.46}$$

and to a flavor violating transitions, with branching ratios that are in the $m_l \gg m_{l'}$ limit given by

$$\frac{BR(l \to l'\gamma)}{BR(l \to l'\nu\nu')} = \frac{3\alpha}{\pi G_F^2}(|C_{ll'}|^2 + |C_{l'l}|^2) \tag{4.47}$$

.

We will deal in particular with Δ_μ and the branching ratios for the two decays $\tau \to \mu\gamma$ and $\mu \to e\gamma$ in the remaining of this section.

The contributions to the anomalous magnetic moment from the two models shown in the previous section arise from the one-loop level $\mu\mu\gamma$ vertex function and are described by the Feynman diagrams in Figure 4.1. The general expression for the vertex can is written in terms of two forms factor F_1^μ and F_M^μ as:

$$V^\mu = \bar{u}(p')[F_1^\mu(q^2)\gamma^\mu - i\frac{1}{2m_\mu}F_2^\mu(q^2)\sigma^{\mu\nu}q_\nu]u(p) \tag{4.48}$$

From 4.48 the expression for a_μ is obtained:

$$g = 2 + 2F_2^\mu \tag{4.49}$$

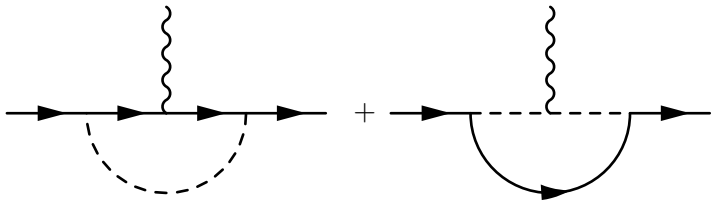

Figure 4.1: The two 1-loop Feynman diagrams contributing to the $(g-2)_\mu$ induced by the new physics described in the simplified Lagrangians in 4.43 and 4.43.

In the following, we will show the computation for the amplitudes related to the Feynman diagrams above.

As can be seen from a naive dimensional analysis, the two diagrams are UV divergent; for this reason, dimensional regularization will be used. We need to note that, since the models we have built are renormalizable, any divergence appearing in the one-loop computations can either be absorbed by counterterms or cancelled. An example of this is explicitly shown in the following section.

For the leftmost diagram in Figure 4.1, we can write the amplitude:

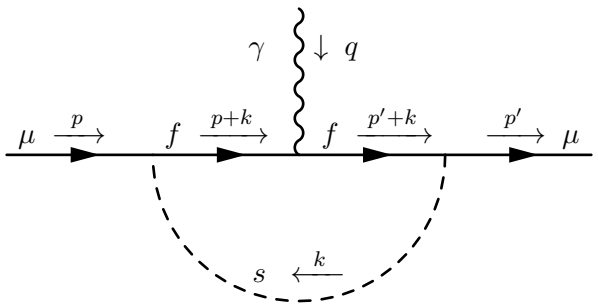

Figure 4.2: Momentum convention for the leftmost diagram in FIgure 4.1

$$\mathcal{M}_1 = -i^6 Q_f e \mu^{3\epsilon/2} \int \frac{d^d k}{(2\pi)^d} \frac{\bar{u}(p')C_2^{RL}(\not{p}' + \not{k} + M_f)\gamma^\mu(\not{p} + \not{k} + M_f)(C_2^{RL})^* u(p)}{\left((p'+k)^2 - M_f^2\right)\left((p+k)^2 - M_f^2\right)(k^2 - M_s^2)} \tag{4.50}$$

Introducing the Feynman parameter, it can be rewritten as:

$$\mathcal{M}^\mu = Q_f e \mu^{3\epsilon/2} \int dx_1 dx_2 dx_3 2\delta(x_1 + x_2 + x_3 - 1) \int \frac{d^d k}{(2\pi)^d} \frac{\bar{u}(p')\mathcal{N}^\mu u(p)}{\mathcal{D}} \tag{4.51}$$

Where, after the momentum shift $k \to k - x_1 p' - x_2 p$ is performed, the denominator can be written as in the last step of 4.52.

$$\begin{aligned}\mathcal{D}^\mu &= \left(x_1\left((p'+k)^2 - M_f^2\right) + x_2\left((p+k)^2 - M_f^2\right) + x_3(k^2 - M_s^2)\right)^3 \\ &= (k^2 - D)^3\end{aligned} \tag{4.52}$$

with

$$D = (1-x_3)M_f^2 + x_3 M_s^2 - x_1 x_3 p'^2 - x_2 x_3 p^2 - x_1 x_2 q^2 \tag{4.53}$$

As regard the numerator, after the momentum shift and neglecting linear terms in the loop momentum k, we have:

$$\begin{aligned}\mathcal{N}^\mu &= C_2^{RL}(\not{k} + (1-x_1)\not{p}' - x_2\not{p})\gamma^\mu(\not{k} - x_1\not{p}' + (1-x_2)\not{p})C_2^{RL*} \\ &= C_2^{RL}[\not{k}\gamma^\mu\not{k} + ((1-x_1)\not{p}' - x_2\not{p} + M_f)\gamma^\mu(-x_1\not{p}' + (1-x_2)\not{p} + M_f)]\end{aligned} \tag{4.54}$$

From this using the relations $\gamma^\mu\gamma^\nu\gamma_\mu = -(d-2)\gamma^\nu$ and $k^\mu k^\nu \to \frac{1}{d}k^2 g^{\mu\nu}$ (valid only inside the d-dimensional momentum integral) combined with the equation of motion for the spinor, the numerator becomes

$$\begin{aligned}\bar{u}(p')\mathcal{N}^\mu u(p) = &-\frac{d-2}{2}k^2\bar{u}(p')\gamma^\mu(|\lambda_2^R|^2 P_R + |\lambda_2^L|^2 P_L)u(p) \\ &+ m_\mu^2\bar{u}(p')[(1-x_1)(1-x_2) - x_1x_2]\gamma^\mu(|\lambda_2^R|^2 P_L + |\lambda_2^L|^2 P_R)u(p) \\ &+ \bar{u}(p')[x_1(1-x_1)p'^2 + x_2(1-x_2)p^2 - 2x_1x_2 p\dot{p}' + M_f^2]\gamma^\mu(|\lambda_2^R|^2 P_R + |\lambda_2^L|^2 P_L)u(p) \\ &+ m_\mu\bar{u}(p')[-x_1(x_2+1-x_1)q^\mu - x_1x_3(p+p')^\mu](|\lambda_2^R|^2 P_R + |\lambda_2^L|^2 P_L)u(p) \\ &+ m_\mu\bar{u}(p')[x_2(x_1+1-x_2)q^\mu - x_2x_3(p+p')^\mu](|\lambda_2^R|^2 P_L + |\lambda_2^R|^2 P_R)u(p) \\ &+ 2m_\mu M_f \Re\lambda_2^R\lambda_2^{L*}\bar{u}(p')\gamma^\mu u(p) \\ &+ M_f\bar{u}(p')[(x_2-x_1)q^\mu + (x_3-1)(p+p')^\mu](\lambda_2^R\lambda_2^{L*}P_L + \lambda_2^L\lambda_2^{R*}P_R)u(p)\end{aligned} \tag{4.55}$$

The terms contributing to the F_M^μ can be obtained applying the Gordon Identities (equation A.9) and are summarized in 4.56.

$$\begin{aligned}\bar{u}(p')\tilde{N}^\mu u(p) = &-\{|\lambda_2^R|^2 m_\mu x_1 x_3\bar{u}(p')i\sigma^{\mu\nu}q_\nu P_R u(p) + |\lambda_2^R|^2 m_\mu x_2 x_3\bar{u}(p')i\sigma^{\mu\nu}q_\nu P_L u(p) \\ &+ |\lambda_2^L|^2 m_\mu x_1 x_3\bar{u}(p')i\sigma^{\mu\nu}q_\nu P_L u(p) + |\lambda_2^L|^2 m_\mu x_2 x_3\bar{u}(p')i\sigma^{\mu\nu}q_\nu P_R u(p) \\ &+ \lambda_2^R\lambda_2^{L*}M_f(1-x_3)\bar{u}(p')i\sigma^{\mu\nu}q_\nu P_L u(p) + \lambda_2^R\lambda_2^{L*}M_f(1-x_3)\bar{u}(p')i\sigma^{\mu\nu}q_\nu P_R u(p)\}\end{aligned} \tag{4.56}$$

Since the momentum integral is finite, it can be performed using A.7 with $d = 4$ and $n = 3$. Then, evaluating 4.53 at $q^2 = 0$ and exploiting the fact that $M_s >> m_\mu$, the two loop functions I_{LL}^f and I_{LR}^f, respectively in A.11 and A.12, can be defined through the integral over the Feynman parameters. These two functions depend on the ratio $r = M_f^2/M_s^2$.

So the terms contributing to the $F_M^\mu(0)$ form factor are given by:

$$\begin{aligned}&eQ_f\int dx_1dx_2dx_3 2\delta(x_1+x_2+x_3-1)\int\frac{d^4k}{(2\pi)^4}\frac{\bar{u}(p')\tilde{N}^\mu u(p)}{\mathcal{D}} \\ &= -i\frac{e}{2m_\mu}\left[-\frac{Q_f(|\lambda_2^R|^2+|\lambda_2^L|^2)m_\mu^2}{8\pi^2M_s^2}I_{LL}^f(r) - \frac{Q_f\lambda_2^L\lambda_2^{R*}m_\mu M_f}{8\pi^2M_s^2}I_{LR}^f(r)\right]\bar{u}(p')i\sigma^{\mu\nu}q_\nu P_R u(p) \\ &\quad\left[-\frac{Q_f(|\lambda_2^R|^2+|\lambda_2^L|^2)m_\mu^2}{8\pi^2M_s^2}I_{LL}^f(r) - \frac{Q_f\lambda_2^R\lambda_2^{L*}m_\mu M_f}{8\pi^2M_s^2}I_{LR}^f(r)\right]\bar{u}(p')i\sigma^{\mu\nu}q_\nu P_L u(p)\end{aligned} \tag{4.57}$$

And finally the contribution to the Δa_μ coming from this first diagram can be written as:

$$\Delta a_\mu = -\frac{|\lambda_2^R|^2 + |\lambda_2^L|^2}{8\pi^2}\frac{m_\mu^2}{M_s^2}Q_f I_{LL}^f(r) - \frac{Re(\lambda_2^L \lambda_2^{R*})}{8\pi^2}\frac{m_\mu M_f}{M_s^2}Q_f I_{LR}^f(r) \tag{4.58}$$

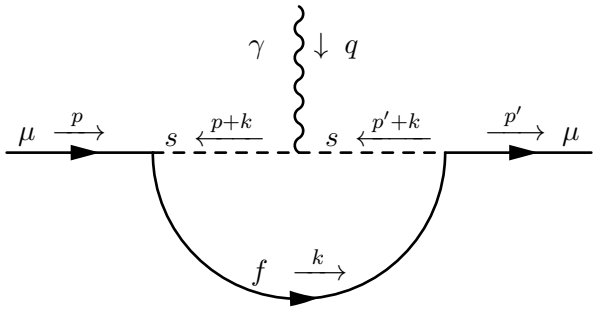

Figure 4.3: Momentum convention for the rightmost diagram in FIgure 4.1

Instead, for the rightmost diagram of 4.1 the amplitude is:

$$\mathcal{M}^\mu = -i^6 Q_s e \mu^{3\epsilon/2}\int \frac{d^dk}{(2\pi)^d}\frac{\bar{u}(p')C_2^{RL}(\not{k}+M_f)C_2^{RL*}u(p)(2k-p'-p)^\mu}{(k^2-M_f^2)\left((k-p)^2-M_s^2\right)\left((k-p')^2-M_s^2\right)} \tag{4.59}$$

Also in this case the Feynman parameter are introduced so that the denominator can be recast as in the last step of 4.61, performing the momentum shift $k \to k + x_2 p + x_3 p'$.

$$\mathcal{M}^\mu = eQ_s\mu^{3\epsilon/2}\int dx_1 dx_2 dx_3 2\delta(x_1+x_2+x_3-1)\int \frac{\bar{u}(p')\mathcal{N}^\mu u(p)}{\mathcal{D}} \tag{4.60}$$

$$\begin{aligned}\mathcal{D} &= \left(x_1(k^2-M_f) + x_2\left((k-p)^2-M_s^2\right) + x_3\left((k-p')^2-M_f\right)\right)^3 \\ &= (k^2-D)^3\end{aligned} \tag{4.61}$$

with

$$D = x_1 M_f^2 + (1-x_1)M_s^2 + x_2 x_1 p^2 + x_3 x_1 p'^2 - x_2 x_3 q^2 \tag{4.62}$$

The numerator, after the momentum shift and neglecting the linear term in the loop momentum k, looks like:

$$\begin{aligned}\mathcal{N}^\mu &= C_2^{RL}(\not{k}+M_f)C_2^{RL*}(2k-p'-p)^\mu \\ &= C_2^{RL}[\not{k}k^\mu + (x_2\not{p}+x_3\not{p}')((2x_2-1)p+(2x_3-1)p')^\mu]C_2^{RL*}\end{aligned} \tag{4.63}$$

This can be rewritten using the equation of motion for the spinor and the relation $k^\mu k\nu = \frac{1}{d}k^2 g^{\mu\nu}$ as:

$$\begin{aligned}\bar{u}(p')\mathcal{N}^\mu u(p) = &\frac{2}{d}k^2\bar{u}(p')\gamma^\mu(|\lambda_2^R|^2P_R + |\lambda_2^L|^2P_L)u(p) \\ &+ m_\mu\bar{u}(p')[x_3(x_3-x_2)q^\mu - x_1x_3(p'+p)^\mu](|\lambda_2^R|^2P_R + |\lambda_2^L|^2P_L)u(p) \\ &++ m_\mu\bar{u}(p')[x_2(x_3-x_2)q^\mu - x_1x_2(p'+p)^\mu](|\lambda_2^R|^2P_L + |\lambda_2^L|^2P_R)u(p) \\ &+ \lambda_2^R\lambda_2^{L*}M_f\bar{u}(p')[(x_3-x_2)q^\mu - x_3(p'+p)^\mu]P_L u(p) \\ &+ \lambda_2^L\lambda_2^{R*}M_f\bar{u}(p')[(x_3-x_2)q^\mu - x_3(p'+p)^\mu]P_R u(p)\end{aligned} \tag{4.64}$$

As for the previous diagram the relevant terms to compute the contribution to the muon's anomalous magnetic moment are obtained exploiting the Gordon identities A.9, the result is presented in 4.65.

$$\begin{aligned}\bar{u}(p')\tilde{N}^{\mu}u(p) = &-\{|\lambda_2^R|^2 m_\mu x_1 x_3 \bar{u}(p') i\sigma^{\mu\nu} q_\nu P_R u(p) + |\lambda_2^R|^2 m_\mu x_1 x_2 \bar{u}(p') i\sigma^{\mu\nu} q_\nu P_L u(p) \\ &+ |\lambda_2^L|^2 m_\mu x_1 x_3 \bar{u}(p') i\sigma^{\mu\nu} q_\nu P_L u(p) + |\lambda_2^L|^2 m_\mu x_1 x_2 \bar{u}(p') i\sigma^{\mu\nu} q_\nu P_R u(p) \\ &+ \lambda_2^R \lambda_2^{L*} x_3 \bar{u}(p') i\sigma^{\mu\nu} q_\nu P_L u(p) + \lambda_2^L \lambda_2^{R*} x_3 \bar{u}(p') i\sigma^{\mu\nu} q_\nu P_R u(p)\}\end{aligned} \tag{4.65}$$

The momentum integral can now be performed using A.7 with $d = 4$ and $n = 3$; then, evaluating 4.62 at $q^2 = 0$ in the limit in which $M_s >> m_\mu$, the two loop function I^s_{LL} and I^s_{RL} can be defined as in A.13 and A.14, depending on the ratio $r = M_f^2/M_s^2$. e

$$\begin{aligned}&eQ_s \int dx_1 dx_2 dx_3 2\delta(x_1 + x_2 + x_3 - 1) \int \frac{d^4}{(2\pi)^4} \frac{\bar{u}(p')\tilde{N}u(p)}{\mathcal{D}} \\ &= -i\frac{e}{2m_\mu}\left[-\frac{Q_s(|\lambda_2^R|^2 + |\lambda_2^L|^2)m_\mu^2}{8\pi^2 M_s^2} I^s_{LL}(r) - \frac{Q_s \lambda_2^L \lambda_2^{R*} m_\mu M_f}{8\pi^2 M_s^2} I^s_{LR}(r)\right] \bar{u}(p') i\sigma^{\mu\nu} q_\nu P_R u(p) \\ &\quad \left[-\frac{Q_s(|\lambda_2^R|^2 + |\lambda_2^L|^2)m_\mu^2}{8\pi^2 M_s^2} I^s_{LL}(r) - \frac{Q_s \lambda_2^R \lambda_2^{L*} m_\mu M_f}{8\pi^2 M_s^2} I^s_{LR}(r)\right] \bar{u}(p') i\sigma^{\mu\nu} q_\nu P_L u(p)\end{aligned} \tag{4.66}$$

The contribution of this second diagram to the anomalous magnetic moment is then:

$$\Delta a_{mu} = -\frac{|\lambda_2^R|^2 + |\lambda_2^L|^2}{8\pi^2}\frac{m_\mu^2}{M_s^2} Q_s I^s_{LL}(r) - \frac{Re(\lambda_2^L \lambda_2^{R*})}{8\pi^2}\frac{m_\mu M_f}{M_s^2} Q_s I^s_{LR}(r) \tag{4.67}$$

Finally the total contribution to Δa_μ^{NP} is given adding the expression in 4.58 and 4.67.

$$\begin{aligned}\Delta a_\mu^{tot} = &\frac{m_\mu^2}{8\pi^2 M_s^2}(|\lambda_2^R|^2 + |\lambda_2^L|^2)[Q_f I^f_{LL} + Q_s I^s_{LL}] \\ &+ \frac{m_\mu M_f}{8\pi^2 M_s^2} Re(\lambda_2^L \lambda_2^{R*})[Q_f I^f_{LR} + Q_s I^s_{LR}]\end{aligned} \tag{4.68}$$

We will now apply the above results to the $FH1$ and $SH1$ models, assuming real coupling constants.

For the $FH1$ model, the one-loop contribution to the Δa_μ comes from two different sets of diagrams. The first one comes from the interaction term $\lambda_2[S_0^*(\bar{\mu}P_L F_-) + h.c.]$, and the particles running in the loops are a neutral complex scalar and a charged Dirac fermion; only the latter one can couple to the photon. Since in this interaction new physics couples just to the left-handed muon, we will not have the chirality flip term in 4.68. Then, for the effective coupling and the particle's charges, we have

$$Q_f = Q_{F_-} = -1 \tag{4.69}$$
$$Q_s = Q_{S_0} = 0 \tag{4.70}$$
$$\lambda_2^R = \lambda_2 \tag{4.71}$$
$$\lambda_2^L = 0 \tag{4.72}$$

The ratio appearing in the loop function is $r = M^2_{F_D}/M_s^2$. Given these, the contribution to the anomalous magnetic moment can be written as:

$$\Delta a_\mu^{FH1,1} = \frac{m_\mu^2}{8\pi^2 M_s^2}\lambda_2^2 I^f_{LL}\left(\frac{M^2_{F_D}}{M_s^2}\right) \tag{4.73}$$

Instead, the second contribution comes from the interaction term $-\lambda_1 V_{1j}(S_+ \bar{F}_{0j}\mu_L) + \lambda_2 V_{2j} S_+^*(\bar{\mu}P_L F_{0j}) + h.c.$. In this case, the particles running in the loop are a charged complex scalar and one of the three

Mayorana fermions. In this case, we have couplings to both the left- and right-handed muon components. In this case, the effective coupling and the particle's charges are

$$Q_f = Q_{F_{0i}} 0\,, \tag{4.74}$$
$$Q_s = Q_{S_+} = +1\,, \tag{4.75}$$
$$\lambda_2^R = \lambda_2 V_{2i}\,, \tag{4.76}$$
$$\lambda_2^L = -\lambda_1 V_{1i}\,. \tag{4.77}$$

Then Δa_μ is obtained by summing over the three Mayorana fermions running in the loop:

$$\begin{aligned}\Delta a_\mu^{FH1,2} =& -\frac{m_\mu^2}{8\pi^2 M_s^2}\sum_{i=1,2,3}(\lambda_2^2|V_{2i}|^2+\lambda_1^2|V_{1i}|^2) I_{LL}^s\left(\frac{M_i^2}{M_s^2}\right)\\ &+\frac{m_\mu}{8\pi^2 M_s^2}\sum_{i=1,2,3} M_i \Re\left[\lambda_1\lambda_2 V_{1i}V_{2i}\right] I_{LR}^s\left(\frac{M_i^2}{M_s^2}\right)\end{aligned} \tag{4.78}$$

The total contribution is given by the sum of $\Delta a_\mu^{FH1,1}$ and $\Delta a_\mu^{FH1,2}$.

Also in the $SH1$ model, two different sets of Feynamn diagrams contribute to Δa_μ. The first one arises from the interaction term $\frac{\lambda_1}{\sqrt{2}} i A_0(\bar{F}_- P_L \mu) + h.c.$ The running particles in the loop are a neutral CP-odd scalar and a charged Dirac fermion. For this interaction, the effective coupling constant along with the particle charges are

$$Q_f = Q_{A_0} = 0\,, \tag{4.79}$$
$$Q_s = Q_{F_-} = -1\,, \tag{4.80}$$
$$\lambda_2^R = 0\,, \tag{4.81}$$
$$\lambda_2^L = \frac{\lambda_1}{\sqrt{2}}\,. \tag{4.82}$$

Then the anomalous magnetic moment can be expressed as

$$\Delta a_\mu^{SH1,1} = \frac{\lambda_1^2 m_\mu^2}{16\pi^2 M_D^2} I_{LL}^f\left(\frac{M_f^2}{M_D^2}\right) \tag{4.83}$$

The second contribution comes from the interaction term $\frac{\lambda_1}{\sqrt{2}} U_{2\alpha} S_\alpha(\bar{F}_- P_L \mu) + \lambda_2 U_{1\alpha} S_\alpha(\bar{\mu} P_L F_-) + h.c.$ The particles running in the loop are a complex Dirac fermion and one of the two neutral scalars. We can write the effective couplings and the charges as

$$Q_f = Q_{F_-} = -1 \tag{4.84}$$
$$Q_s = Q_{S_\alpha} = 0 \tag{4.85}$$
$$\lambda_2^R = \frac{\lambda_1}{\sqrt{2}} U_{2\alpha} \tag{4.86}$$
$$\lambda_2^L = \lambda_2 U_{1\alpha} \tag{4.87}$$

In this case, the mass ratio for the loop function is $r = M_f^2/M_{S_\alpha}^2$. Then the Δa_μ can be written as

$$\begin{aligned}\Delta a_\mu^{SH1,2} =& \frac{m_\mu^2}{16\pi^2}\sum_{\alpha=1,2}\frac{\lambda_1^2|U_{2\alpha}|^2+2\lambda_2^2|U_{1\alpha}|^2}{M_{S_\alpha}} I_{LL}^f\left(\frac{M_f^2}{M_{S_\alpha}^2}\right)\\ &+\frac{m_\mu M_f}{8\sqrt{2}\pi^2}\sum_{\alpha=1,2}\frac{\lambda_1\lambda_2 U_{2\alpha}U_{1\alpha}}{M_{S_\alpha}} I_{LR}^f\left(\frac{M_f^2}{M_{S_\alpha}^2}\right)\end{aligned} \tag{4.88}$$

The total contribution is obtained summing $\Delta a_\mu^{SH1,1}$ and $\Delta a_\mu^{SH1,2}$.

4.3 Flavour violating processes

The models analyzed in the previous section can be extended to the whole standard model's lepton sector; this can be achieved by substituting the Weyl muon fields μ and $\bar{\mu}$ in equations 4.1 and 4.3 with the generic Weyl lepton fermions l^i and $\bar{l^i}$. They are related to the Dirac field as for the muon case,

$$L_L^i = \begin{pmatrix} l^i \\ 0 \end{pmatrix}, \quad e_R^i = \begin{pmatrix} 0 \\ \bar{l^i} \end{pmatrix} \tag{4.89}$$

The coupling constants for the new physics-lepton interactions can be expressed as λ^i where the index refers to the three lepton flavors. The same argument can be applied for the simplified model of 4.43, and the couplings can be written as $\lambda_i^{R,L}$. In this scenario, Lepton Flavour Violating decays are possible at loop level. These processes are described by the Feynman diagrams in the upper row of 4.4, while the two diagrams in the bottom row are needed in order for the full amplitude to be convergent.

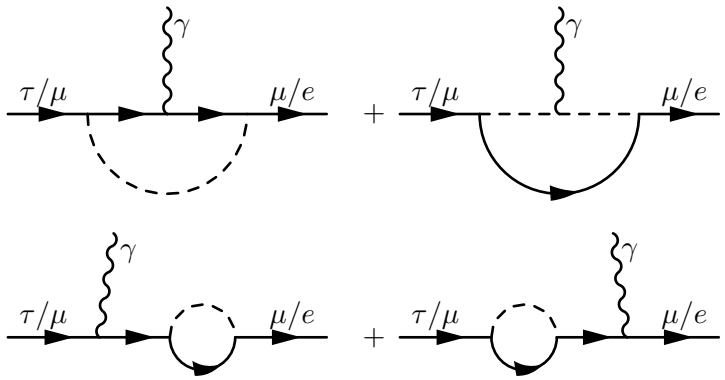

Figure 4.4: Diagrams contributing to the lepton flavour violation decays. The two diagram in the bottom row are needed in order for the full amplitude to be convergent.

For the sake of simplicity, we will perform the computation for the branching ratio for the decay $\mu \to e\gamma$ in the assumption that the coupling constants are real and $\lambda_i^R = 0$.

First of all we specify the cinematic of the decay. In the center of mass reference frame we have:

$$p^\mu = (m_\mu, 0, 0, 0) \tag{4.90}$$
$$p'^\mu = (E_e, 0, 0, p) \tag{4.91}$$
$$q^\mu = (E_\gamma, 0, 0, p) \tag{4.92}$$

Where the three 4-momentum are respectively of them muon, the elecrton and the photon; they satisfy the momentum conservation $p^\mu = p'^\mu + q^\mu$ relation. Finally to compute the width of the process the equation 4.93 is exploited.

$$\Gamma = \int \frac{d\Omega_{cm}}{4\pi} \frac{1}{8\pi} \frac{2p}{E_{cm}} \tag{4.93}$$

The first two diagrams in 4.4 are similar to the one computed in the previous section, with the only difference being that now λ_2^R is absent, the incoming and outgoing particles are a muon and an electron, and the photon elicity vector must be included. Keeping this in mind, the amplitude for the first diagram can be derived from 4.2, giving the result in 4.94. To deal with the divergences of the amplitude, Dimensional Regularization was exploited with $\epsilon = d - 4$.

$$\mathcal{M}_1 = eQ_s\lambda_1^L\lambda_2^L\mu^{3\epsilon/2}\int\frac{d^dk}{(2\pi)^d}\frac{\bar{u}_e(p')\mathcal{N}_1^\mu u_\mu(p)}{\mathcal{D}_1}\epsilon_\mu^\lambda(q) \tag{4.94}$$

The numerator and denominator in 4.94 are given respectively in 4.95 and 4.96.

$$\mathcal{D}_1 = \left((k+p')^2 - M_f^2\right)\left((k+p)^2 - M_f^2\right)\left(k^2 - M_s^2\right) \tag{4.95}$$

$$\mathcal{N}_1^\mu = P_R(\not{k} + \not{p}' + M_f)\gamma^\mu(\not{k} + \not{p} + M_f)P_L \tag{4.96}$$

To proceed in the computation the numerator and denominator are rewritten after the Feynman parameters are introduced. Moreover the numerator is divided in two components, N_{1D}^μ represents the divergent part of the amplitude while N_{1C}^μ the finite one.

$$\begin{aligned}\mathcal{N}_1^\mu &= P_R[\not{k}\gamma\not{k}]P_L + P_R((1-x_3)\not{p}' - x_2\not{p} + M_f)\gamma^\mu(-x_3\not{p}' + (1-x_2)\not{p} + M_f)P_L \\ &= N_{1D}^\mu + N_{1C}^\mu\end{aligned} \tag{4.97}$$

$$\begin{aligned}\mathcal{D}_1 &= \left[x_1\left(k^2 - M_s^2\right) + x_2\left((k+p)^2 - M_f^2\right) + x_3\left((k+p')^2 - M_f^2\right)\right]^3 \\ &= \left[k^2 - \left(x_1M_s^2 + (1-x_1)M_s^2 - x_2x_1p^2 - x_3x_1p'^2 - x_2x_3q^2\right)\right]^3 \\ &= [k^2 + D]^3\end{aligned} \tag{4.98}$$

The computations for the two components of the amplitude are shown below. As in the previous section, D_1 can be simplified under the hypothesis that the new physics particles are much heavier than the standard model lepton and evaluating it at low energies, $q^2 = 0$. Using the properties of the gamma matrices and the relations $\gamma^\nu\gamma^\mu\gamma_\nu = -(d-2)\gamma^\mu$, $k^\mu k^\nu = \frac{1}{d}k^2g^{\mu\nu}$, the numerator of the divergent integral can be simplified. Then the momentum integral can be performed using equation A.8 with $n = 3$. The result is expressed in 4.100 as a Laurent series in ϵ up to terms of order $\mathcal{O}(\epsilon)$.

$$N_{1D}^\mu = \not{k}\gamma^\mu\not{k}P_L = \frac{2-d}{d}k^2\gamma^\mu P_L \tag{4.99}$$

$$\mathcal{M}_{1D} = \frac{ieQ_f\lambda_1^L\lambda_2^L}{32\pi^2}\left[-\frac{2}{\epsilon} + 1 + \gamma - \int_0^1 dx_1 2(1-x_1)log\left(\frac{4\pi\mu^2}{D_1}\right)\right]\bar{u}_e(p')\gamma^\mu P_L u_\mu(p)\epsilon_\mu^\lambda(q) \tag{4.100}$$

To deal with the convergent part, similar steps can be done using the equation of motion for the two spinors. The momentum integral is computed using A.7 with $n = 3$. The result is shown in 4.101, where $I_{LL}^F(r)$, $K_{LL}^f(r)$ and $H_{LL}(r)$ are loop functions defined in A.11, A.16 and A.17, respectively. Note that also terms proportional to $q\cdot\epsilon$ are considered even if they are null due to the properties of the photon polarization.

$$\begin{aligned}\mathcal{M}_{1C} = -\frac{ieQ_f\lambda_1^L\lambda_2^L}{32\pi^2}\epsilon_\mu^\lambda(q)\Bigg[&\frac{m_em_\mu}{M_s^2}K_{LL}^f(r)\bar{u}_e(p')\gamma^\mu P_R u_\mu(p) \\ &+ \frac{m_e^2+m_\mu^2}{M_s^2}I_{LL}^f(r)\bar{u}_e(p')\gamma^\mu P_L u_\mu(p) \\ &+ \frac{m_e}{M_s^2}\left(H_{LL}^f(r)q^\mu - I_{LL}^f(r)(p+p')^\mu\right)\bar{u}_e(p')P_L u_\mu(p) \\ &+ \frac{m_\mu}{M_s^2}\left(-H_{LL}^f(r)q^\mu - I_{LL}^f(r)(p+p')^\mu\right)\bar{u}_e(p')P_R u_\mu(p)\Bigg]\end{aligned} \tag{4.101}$$

The computation for the second diagram proceeds as for the previous one. The amplitude 4.102 can be evaluated from 4.3; the numerator and denominator are in 4.103 and 4.104, respectively.

$$\mathcal{M}_2 = eQ_s\mu^{3\epsilon/2}\lambda_1^L\lambda_2^L\int\frac{d^dk}{(2\pi)^d}\frac{\bar{u}_e(p')\mathcal{N}_2^\mu u_\mu(p)}{\mathcal{D}_2}\epsilon_\mu^\lambda \tag{4.102}$$

$$\mathcal{N}_2^\mu = P_R(\not{k}+M_f)P_L(2k-p'-p)^\mu \tag{4.103}$$
$$\mathcal{D}_2 = \left(k^2-M_f^2\right)\left((k-p)^2-M_s^2\right)\left((k-p')^2-M_s^2\right) \tag{4.104}$$

The calculation follows the same steps as for 4.94, treating separately the diverging part, given by N_{2D}^μ, from the converging one, arising from N_{2C}^μ. Also in this case, the masses of the standard model particles are neglected in D_2, setting also $q^2=0$.

$$\begin{aligned}\mathcal{N}_2^\mu &= P_R 2k^\mu \not{k} P_L + P_R(x_2\not{p}+x_3\not{p}'+M_f)\left((2x_2-1)p+(2x_3-1)p'\right)^\mu P_L \\ &= N_{2D}^\mu + N_{2C}^\mu\end{aligned} \tag{4.105}$$

$$\begin{aligned}\mathcal{D}_2 &= \left[x_1\left(k^2-M_f^2\right)+x_2\left((k-p)^2-M_s^2\right)+x_3\left((k-p')^2-M_f^2\right)\right]^3 \\ &= \left[k^2-\left(x_1M_f^2+(1-x_1)M_s^2-x_1x_2p^2-x_1x_3p'^2-x_2x_3q^2\right)\right]^3 \\ &= \left[k^2-D_2\right]^3\end{aligned} \tag{4.106}$$

For the divergent component of the amplitude, the calculation leads to 4.107.

$$\mathcal{M}_{2D} = \frac{ieQ_s\lambda_1^L\lambda_2^L}{32\pi^2}\left[\frac{2}{\epsilon}-\gamma+\int_0^1 dx_1 2(1-x_1)log\left(\frac{4\pi\mu^2}{D_2}\right)\right]\bar{u}_e(p')\gamma^\mu P_L u_\mu(p)\epsilon_\mu^\lambda(q) \tag{4.107}$$

As for the convergent component the result in 4.108 is obtained, where the loop functions H_{LL}^s and I_{LL}^s are defined in A.15 and A.13 respectively.

$$\begin{aligned}\mathcal{M}_{2C} = \frac{-ieQ_s\lambda_1^L\lambda_2^L}{32\pi^2}\epsilon_\mu^\lambda(q)\Bigg[&\frac{m_e}{M_s^2}\left(H_{LL}^s(r)q^\mu+I_{LL}^s(r)(p+p')^\mu\right)\bar{u}_e(p')P_L u_\mu(p') \\ &+\frac{m_\mu}{M_s^2}\left(-H_{LL}^s(r)q^\mu+I_{LL}^s(r)(p+p')^\mu\right)\bar{u}_e(p')P_R u_\mu(p)\Bigg]\end{aligned} \tag{4.108}$$

The total amplitude is written as $\mathcal{M}_{tot}=\mathcal{M}_{1C}+\mathcal{M}_{2C}$ and its modulus squared is given by 4.109, where it is expressed in terms of the anomalous magnetic moment and in the limit in which $m_\mu >> m_e$.

$$|\mathcal{M}_{tot}|^2 = \pi^2\alpha^2\left(\frac{\lambda_1^L}{\lambda_2^L}\right)^2\left(\Delta a_{tot}^\mu\right)^2 m_\mu \tag{4.109}$$

Now the width for $\Gamma(\mu\to e\gamma)$ can be computed using the formula in 4.93.

$$\Gamma(\mu\to e\gamma) = \frac{\pi}{8}\alpha^2\left(\frac{\lambda_1^L}{\lambda_2^L}\right)^2\left(\Delta a_{tot}^\mu\right)^2 m_\mu \tag{4.110}$$

To evaluate the decay width for $\tau\to\mu\gamma$ the same calculation can be done leading to the same result as in 4.110 with m_μ replaced by m_τ These results can be generalized to the scenario in which the new physics particles couple both to the left- and right-handed leptons by the substitution $\left(\frac{\lambda_1^L}{\lambda_2^L}\right)^2 \to \left(\frac{\lambda_1^L}{\lambda_2^L}\right)^2+\left(\frac{\lambda_1^R}{\lambda_2^R}\right)^2$.

The two divergent amplitudes 4.100 and 4.107 are canceled by the divergent diagrams in 4.5, where Λ is given in 4.6 and the corresponding amplitude is given by

$$\mathcal{M}_3 = \bar{u}_e(p')\left\{\Lambda(p')\frac{i}{\not{p}'-m_\mu}(-ie\mu^{\epsilon/2})+(-ie\mu^{\epsilon/2})\frac{i}{\not{p}-m_e}\Lambda(p)\right\}u_\mu(p)\epsilon_\mu^\lambda(q) \tag{4.111}$$

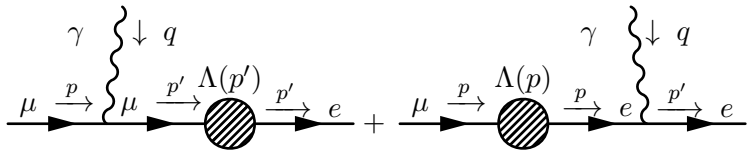

Figure 4.5: Momentum convention for the two diagrams in the bottom row of 4.4. Here Λ represent the vacuum polarization due to the new physics field.

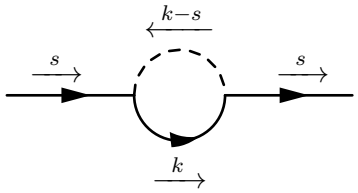

Figure 4.6: Definition of the vacuum polarization defined in 4.5 as Λ.

$$\Lambda(s) = \int \frac{d^d k}{(2\pi)^d} \frac{(i\lambda_1^L \mu^{\epsilon/2} P_R)(\not{k} + M_f)(i\lambda_2^L \mu^{\epsilon/2} P_L)}{(k^2 - M_f^2)\left((k-s)^2 - M_s^2\right)} \tag{4.112}$$

The loop integral in $\Lambda(s)$ is computed in 4.113, where the Feynman parameters are introduced, then, in the second step, the momentum shift $k \to k + (1-x_1)p'$ is performed and linear terms in momentum are neglected.

$$\begin{aligned} &\int dx_1 dx_2 \delta(x_1 + x_2 - 1) \int \frac{d^d k}{(2\pi)^d} \frac{-\lambda_1^L \lambda_2^L P_R \mu^\epsilon (\not{k} + M_f) P_L}{\mathcal{D}_3} \\ &= -\lambda_1^L \lambda_2^L \mu^\epsilon \int_0^1 dx_1 \int \frac{d^d k}{(2\pi)^d} \frac{P_R \left((1-x1)\not{s} + M_f\right) P_L}{\mathcal{D}_3} \end{aligned} \tag{4.113}$$

$$\begin{aligned} \mathcal{D}_3 &= \left[x_1(k^2 - M_f^2) + (1-x_1)\left((k-s)^2 - M_s^2\right)\right]^2 \\ &= \left[k^2 - \left(x_1 M_f^2 + (1-x_1)M_s^2 - x_1(1-x_1)p'^2\right)\right]^2 \\ &= \left[k^2 - D_3\right]^2 \end{aligned} \tag{4.114}$$

The momentum integral can be calculated exploiting the Master Integral A.8 with $n = 2$ and the result is then expanded as a Laurent series of ϵ up to $\mathcal{O}(\epsilon)$.

$$\Lambda(s) = -\frac{i\lambda_1^L \lambda_2^L \mu^\epsilon}{16\pi^2} \int_0^1 dx_1 (1-x_1) \left(\frac{2}{\epsilon} - \gamma + log\left(\frac{4\pi\mu^2}{D_3}\right)\right) \not{s} P_L \tag{4.115}$$

The expression 4.115 obtained for $\Lambda(s)$ is substituted back into 4.111 and can be simplified into 4.116 using the anticommutation properties of the γ matrices, the equation of motion for the two spinors, and the on-shell condition for the momenta.

Adding up the three divergent amplitudes in 4.100, 4.107, and 4.116 and recalling the relation existing between the New Physics particle charges, it is clear that the total amplitude is finite. Note that using the dimensional regularization to treat the divergences introduces a scale dependence in the amplitude; this is cancelled by the implicit scale dependence of the coupling constants e and $\lambda_2^{L/R}$.

$$\mathcal{M}_3 = -\frac{ie\lambda_1^L\lambda_2^L\mu^{\epsilon/2}}{32\pi^2}\left[\frac{2}{\epsilon} - \gamma + 2\int_0^1 dx_1(1-x_1)log\left(\frac{4\pi\mu^2}{D_3}\right)\right]\bar{u}_e(p')\gamma^\mu P_L u_\mu(p)\epsilon_\mu^\lambda(q) \tag{4.116}$$

Exploiting the experimental value for the Δa_μ and the most recent constrain for $BR(\mu \to e\gamma)$ and $BR(\tau \to \mu\gamma)$, a bound on the ratios $\lambda_{1,3}^{L,R}/\lambda_2^{L,R}$ is found [38, 39].

$$\frac{\lambda_1^{L,R}}{\lambda_2^{L,R}} \leq 1.7 \times 10^{-5}, \quad \frac{\lambda_3^{L,R}}{\lambda_2^{L,R}} \leq 1.3 \times 10^{-2} \tag{4.117}$$

The new physics states thus need to couple muons much more strongly than electrons and taus. Although not common, such muon-philic structures are possible. In the remainder of this work, we will assume this bound to be fulfilled, and we will not investigate possible mechanisms that can explain this kind of characteristic.

4.4 Dark Matter relic density

The final objective of this work is to find new physics models able to explain both the moun's $g-2$ anomaly and the Dark Matter paradigm at the same time. Based on this assumption, the models in 4.1.1 were built so that they contain a possible Dark Matter candidate. In this Chapter, we will focus on the properties of the Dark Matter particles, and in particular, we will compute the relic abundance.

The two models $FH1$ and $SH1$ predict two very different Dark Matter particles; indeed, in the first model, the candidate is a Mayorana fermion, while in the second one, a neutral scalar. Although, in both cases, we will assume that the Dark Matter particles are in thermal equilibrium with the primordial bath and that they decouple from it after they become non-relativistic. The decoupling process takes place through the freeze-out mechanism, as was said in Section 3.2 and will be treated more carefully in the following discussion[40]. The abundance of Dark Matter in the universe nowadays is quantified by the parameter:

$$\Omega_{DM}h^2 = \frac{\rho_{X,0}}{\rho_c} \tag{4.118}$$

where $\rho_{X,0}$ represents the Dark Matter density, which for a non-relativistic particle can be expressed in terms of the number density as $\rho_{X,0} = m_X n_{X,0}$. The experimental value for this parameter can be inferred from the CMB, which represents the most powerful cosmological data source, assuming a flat Universe. The matter density can be measured from the CMB spectra, exploiting the scale-dependence of the amplitude. The result obtained by the Planck experiment for Dark Matter is [33]:

$$\Omega_{DM}h^2 = 0.1200 \pm 0.0012 \tag{4.119}$$

at 68% confidence level, where $h = 0.674 \pm 0.005$ is the Hubble parameter.

The relic desity can be written with good approximation as

$$\Omega_{DM}h^2 \approx 9 \times 10^{-11}\frac{x_f}{\sqrt{g_*(T_f)}}\frac{GeV^{-2}}{\langle\sigma v\rangle} \tag{4.120}$$

Where $g_*(T_f$ is the effective number of relativistic degrees of freedom evaluated at the freeze-out temperature T_f. The ratio $x_f = m_X/T_f$ is determined solving the transcendental equation

$$x_f = log\left[3.8 \times 10^9 \frac{g_X\sqrt{x_f}}{\sqrt{g_*(T_f)}\frac{m_X}{1GeV}\frac{\langle\sigma v\rangle}{1pb}}\right] \tag{4.121}$$

valid for a Dark Matter particle with g_X degrees of freedom

In order to compute the relic density, we need to evaluate the thermal average of the cross section times the relative velocity σv. In particular, we will need the annihilation cross section of the Dark Matter particles into SM fields. The most relevant annihilations are those into gauge bosons and

muons. In general, σv is expanded in terms of v^2, for our purposes, the dominant contribution stems from the zero-order term of the expansion (that will be referred to as "s-wave"), which can be computed simply by performing the substitution $s \to 4m_X^2$.

The annihilation cross section for a Dark Matter $SU(2)_L$ n-dimensional multiplet with hypercharge Y_X can be easily computed in the $SU(2)_L \times U(1)_Y$ symmetric limit, assuming that $m_X \gg m_W$. Moreover, if the mass splitting of the components of the multiplet is small, also coannihilation must be considered; thus, an effective annihilation cross section is obtained $(\sigma v)_{eff} = \frac{1}{n^2}\sum_{mn}\sigma_{mn}v$, where the indices m, n run over the different components of the multiplet. Since only the amplitude squared depends on these indices, the sum over the multiplet component can be performed when computing the unpolarized amplitude. The computation is done for two general scenarios in which the Dark Matter candidate is a Dirac fermion or a complex scalar; these results can then be translated trivially to the case of a Mayorana fermion

4.4.1 Scalar Dark Matter

As a first scenario, let's consider the decay of complex scalar Dark Matter s into gauge bosons. The Lagrangian for a generic complex scalar multiplet transforming under $SU(2)_L \times U(1)_Y$ in the n-dimensional representation with hypergarge Y_s is

$$\mathcal{L}_S = (D_\mu s)^\dagger D^\mu s - M_s^2 s^\dagger s \tag{4.122}$$

Where $D_\mu = -ig_2 T^i W_\mu^i - ig_{Y_s} B_\mu$ is the usual covariant derivative. From this Lagrangian, we can infer three different annihilation channels: one given by the processes $s_m s_n \to W^i W^j$, another one is instead given by $s_m s_m \to BB$, and finally the last one is $s_m s_n \to W^i B$.

All the relevant Feynman rules are given explicitly in Appendix A.

The computation will be done in the center of the mass reference frame, where we will denote with $p_{1/2}^\mu$ the momentum of the incoming scalar particles and with $k_{1,2}^\mu$ the ones for the boson. The 4-momentum will satisfy the relation

$$p_{1/2}^2 = M_s^2, \quad k_{1/2}^2 = 0 \tag{4.123}$$

This same notation is used for the computations of each diagram in this section.

Moreover, the explicit computation for the amplitude square and then for the s-wave cross section is done exploiting the Mathematica package Feyncalc [41, 42, 43].

The four different Feynman diagrams contributing to the first channel are given in Figure 4.7: the first two of them are t-channel interactions, then there is a s-channel interaction involving the three-linear gauge boson vertex, and finally a last term coming from the $ssWW$ interaction term.

The corresponding amplitude is

$$\begin{aligned}\mathcal{M}_{WW} = g_2^2 \Bigg[-i \Bigg(& \frac{(p_1 - k_1 - p_2)^\nu (2p_1 - k_1)^\mu}{(p_1 - k_1)^2 - m_s^2} \sum_k T_{nk}^i T_{km}^j + \frac{(p_1 - k_2 - p_2)^\nu (2p_1 - k_2)^\mu}{(p_1 - k_2)^2 - m_s^2} \sum_k T_{nk}^j T_{km}^i \Bigg) \\ & + \Bigg(\frac{(p_1 - p_2)_\rho}{(p_1 + p_2)^2} V^{\mu\nu\rho}(-k_1, -k_2, p_1 + p_2) T_{nm}^c f^{abc} + ig^{\mu\nu}(2T^i T^j - if^{ijk}T^k)_{nm} \Bigg) \Bigg] \epsilon_\mu^*(k_1)\epsilon_\nu^*(k_2) \\ = & \left[-ig_2^2 \mathcal{M}_{WW,1}^{\mu\nu}(T^i T^j)_{nm} + g_2^2 \mathcal{M}_{WW,2}^{\mu\nu} f^{ijk} T_{nm}^k \right] \epsilon_\mu^*(k_1)\epsilon_\nu^*(k_2)\end{aligned} \tag{4.124}$$

Where $V^{\mu\nu\rho}(q1, q2, q3) = g^{\mu\nu}(q_1 - q_2)^\rho + g^{\nu\rho}(q_2 - q_3)^\mu + g^{\rho\mu}(q_3 - q_1)^\nu$ is the tensor related to the three-linear gauge boson interaction, and we have used the anticommutation relation for the generators of the $su(2)$ algebra $\left[T^i, T^j\right] = i\sum_k f^{ijk}T^k$.

The modulus squared of the amplitude can be obtained as

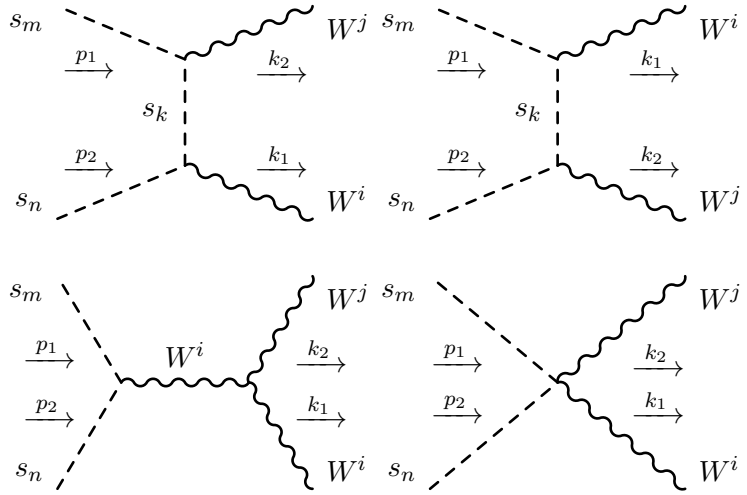

Figure 4.7: Feynman diagrams contributing to the annihilation cross section of the Dark Matter into W^i.

$$
\begin{aligned}
|\bar{\mathcal{M}}_{WW}|^2 =& \frac{g_2^2}{n^2}\sum_{mn}\sum_{ij}\Bigg[\mathcal{M}^2_{WW,1}(T^iT^j)_{nm}(T^iT^j)_{mn} + \mathcal{M}^2_{WW,2}\sum_{kl} f^{ijk}f^{ijl}(T^k_{nm}T^l_{mn}) \\
&+\mathcal{M}_{WW,1}\mathcal{M}_{WW,2}i\sum_k f^{ijk}\left[(T^jT^i)_{nm}T^k_{mn} - (T^iT^j)_{mn}T^k_{nm}\right]\Bigg]
\end{aligned}
\tag{4.125}
$$

Where we have taken the sum over the physical polarization of the gauge boson

$$\mathcal{M}^2_{WW,1} = \sum_{p.p.}\mathcal{M}^{\mu\nu}_{WW,1}\mathcal{M}^{\rho\sigma}_{WW,1}\epsilon^*_\mu(k_1)\epsilon^*_\nu(k_2)\epsilon_\rho(k_1)\epsilon_\sigma(k_2) \tag{4.126}$$

$$\mathcal{M}^2_{WW,2} = \sum_{p.p.}\mathcal{M}^{\mu\nu}_{WW,2}\mathcal{M}^{\rho\sigma}_{WW,2}\epsilon^*_\mu(k_1)\epsilon^*_\nu(k_2)\epsilon_\rho(k_1)\epsilon_\sigma(k_2) \tag{4.127}$$

$$\mathcal{M}_{WW,1}\mathcal{M}_{WW,2} = \sum_{p.p.}\mathcal{M}^{\mu\nu}_{WW,1}\mathcal{M}^{\rho\sigma}_{WW,2}\epsilon^*_\mu(k_1)\epsilon^*_\nu(k_2)\epsilon_\rho(k_1)\epsilon_\sigma(k_2) \tag{4.128}$$

Evaluating the sum over the gauge indices the amplitude squared is obtained

$$|\bar{\mathcal{M}}_{WW}|^2 = g_2^2(\mathcal{M}^2_{WW,1}\frac{dim(R)C_2(R)^2}{n^2} + (\mathcal{M}^2_{WW,1} + \mathcal{M}_{WW,1}\mathcal{M}_{WW,2})\frac{2dim(R)C_2(R)}{n^2}) \tag{4.129}$$

where $dim(R)$ and $C_2(R)$ are the dimension and Casimir for the representation in which the scalar transforms. The s-wave cross section can be derived as was specified at the beginning of this section:

$$\sigma v(s^\dagger s \to WW) = \frac{g_2^4}{16\pi M_s^2 n^2}C_2(R)(2C_2(R)-1)dim(R) \tag{4.130}$$

As for the second channel, there are three Feynman diagram, see FIgure 4.8: two are t-channel processes and one comes from the $ssBB$ interaction term in the Lagrangian:

The corresponding amplitude is:

$$
\begin{aligned}
\mathcal{M} &= -i(g_Y Y_s)^2\left[\frac{(2p_1-k_1)^\mu(p_1-k_1-p_2)^\nu}{(p_1-k_1)^2-M_s^2} + \frac{(2p_1-k_2)^\nu(p_1-k_2-p_2)^\mu}{(p_1-k_2)^2-M_s^2} - 2g^{\mu\nu}\right]\epsilon^*_\mu(k_1)\epsilon^*_\nu(k_2) \\
&= -i(g_Y Y_s)^2\mathcal{M}^{\mu\nu}_{ZZ}\delta_{nm}\epsilon^*_\mu(k_1)\epsilon^*_\nu(k_2)
\end{aligned}
\tag{4.131}
$$

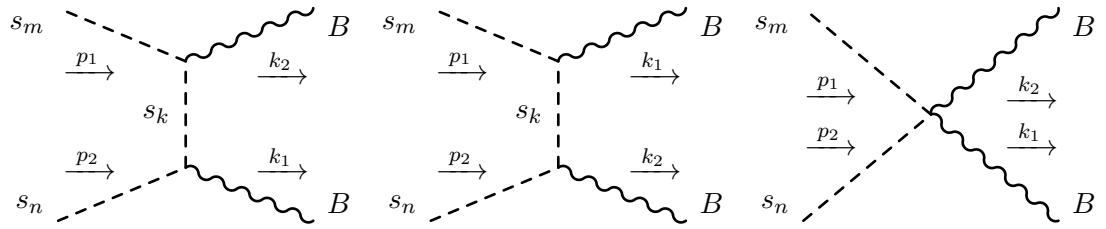

Figure 4.8: Feynman diagrams contributing to the annihilation cross section of the Dark Matter into B.

Its modulus squared can be computed as before leading to

$$|\bar{\mathcal{M}}_{BB}|^2 = (g_Y Y_s)^4 \mathcal{M}_{BB}^2 \frac{1}{n^2} \sum_{nm} \delta_{nm}\delta_{nm} \tag{4.132}$$

where

$$\mathcal{M}_{BB}^2 = \sum_{p.p.} \mathcal{M}_{BB}^{\mu\nu} \mathcal{M}_{BB}^{\rho\sigma} \epsilon_\mu^*(k_1)\epsilon_\nu^*(k_2)\epsilon_\rho(k_1)\epsilon_\sigma(k_2) \tag{4.133}$$

and, performing the sum over the multiplet indices, we would get for the s-wave cross section:

$$\sigma v(s^\dagger s \to BB) = \frac{(g_Y Y_s)^4}{8\pi M_s^2 n} \tag{4.134}$$

Finally we can find three diagrams that contribute to the third channel: two of them are again t-channel processes and one arise from the $ssBW$ interaction term. They are represented in FIgure 4.9

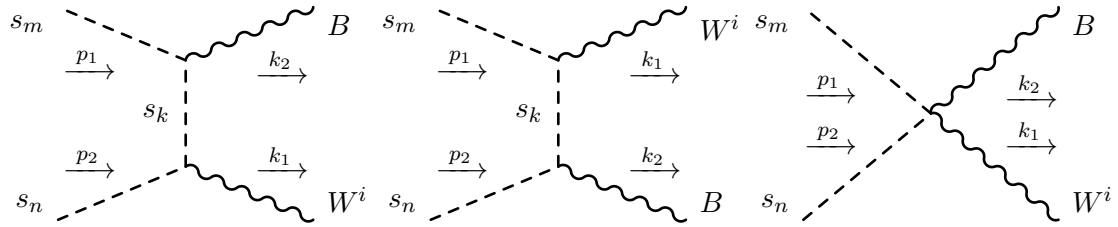

Figure 4.9: Feynman diagrams contributing to the annihilation cross section of the Dark Matter into W^i and B.

The amplitude is given by

$$\begin{aligned}\mathcal{M} &= -ig_2 g_Y Y_s \left[\frac{(p_1 - k_1 - p_2)^\nu (2p_1 - k_1)^\mu}{(p_1 - k_1)^2 - M_s^2} + \frac{(p_1 - k_2 - p_2)^\nu (2p_1 - k_2)^\mu}{(p_1 - k_1)^2 - M_s^2} - 2g^{\mu\nu}\right] T_{mn}^i \epsilon_\mu^*(k_1)\epsilon_\nu^*(k_2) \\ &= -ig_2 g_Y Y_s \mathcal{M}_{WB}^{\mu\nu} T_{mn}^i \epsilon_\mu^*(k_1)\epsilon_\nu^*(k_2)\end{aligned} \tag{4.135}$$

We can then write the unpolarized amplitude, taking the sum over the physical polarization of the bosons

$$|\bar{\mathcal{M}}_{WB}|^2 = (g_2 g_Y Y_s)^2 \mathcal{M}_{WB}^2 \sum_{mn} \sum_i T_{nm}^i T_{nm}^i \tag{4.136}$$

where as before

$$\mathcal{M}^2_{WB} = \sum_{p.p.} \mathcal{M}^{\mu\nu}_{WB} \mathcal{M}^{\rho\sigma}_{WB} \epsilon^*_\mu(k_1)\epsilon^*_\nu(k_2)\epsilon_\rho(k_1)\epsilon_\sigma(k_2) \tag{4.137}$$

Then evaluating the sum's over the multiplet and gauge indices, we get

$$|\bar{\mathcal{M}}_{WB}|^2 = (g_2 g_Y Y_s)^2 \mathcal{M}^2_{WB} \frac{dim(R)C_2(R)}{n^2} \tag{4.138}$$

giving for the s-wave cross section

$$\sigma v(s^\dagger s \to WB) = \frac{g_2^2 g_Y^2 Y_s^2}{4\pi M_s^2 n^2} dim(R)C_2(R) \tag{4.139}$$

Summing up the three equation 4.130, 4.134 and 4.139, and keeping in mind that the multiplet is in an n-dimensional representation so we can substitute $dim(R) = n$ and $C_2(R) = \frac{n^2-1}{4}$, we get the total annihilation cross section times velocity as:

$$(\sigma v)^{C-scalar}_{eff} = \frac{g_2^2(n^4 - 4n^2 + 3) + 16 g_Y^4 Y_s^4 + 8 g_2^2 g_Y^2 Y_s^2 (n^2-1)}{128\pi M_s^2 n} \tag{4.140}$$

The same computations can be done for the case in which s is a real scalar, the two final cross section will differ only for a factor of two

$$(\sigma v)^{R-scalar}_{eff} = \frac{g_2^2(n^4 - 4n^2 + 3) + 16 g_Y^4 Y_s^4 + 8 g_2^2 g_Y^2 Y_s^2 (n^2-1)}{64\pi M_s^2 n} \tag{4.141}$$

The other important annihilation process that we need to discuss is the one into muon's arising from the interaction terms introduced in the new physics models. We will present the computations under the assumption that the Dark Matter particle is a real scalar or a Mayorana fermion, as in the $FH1$ model and in the $SH1$ model respectively.

In order to perform the computation, we can use the simplified Lagrangian defined in 4.44. In the real scalar case, there are two different diagrams contributing to the annihilation, Figure 4.10.

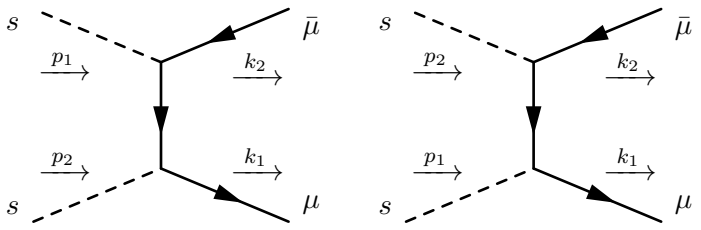

Figure 4.10: Feynman diagrams contributing to the annihilation cross section of scalar Dark Matter into muons due to the new physics couplings.

The corresponding amplitude is:

$$\mathcal{M}_{\mu\mu} = -i\bar{q_1}\left[\frac{C_{RL}(\not{q}_1 - \not{p}_1 + M_f)C_{LR}}{(q_1-p_1)^2 - M_f^2} + \frac{C_{RL}(\not{q}_1 - \not{p}_2 + M_f)C_{LR}}{(q_1-p_2)^2 - M_f^2}\right] \tag{4.142}$$

where for sake of simplicity, we denoted $C_{RL} = \lambda_2^R P_L + \lambda_2^L P_R$ and $C_{LR} = \lambda_2^R P_R + \lambda_2^L P_L$. Taking the sum over the final state spin the amplitude modulus square in the limit of $m_{NP} \gg m_\mu$

$$\begin{aligned}|\mathcal{M}_{\mu\mu}|^2 =& \frac{Tr\left[C_{RL}(\not{q}_1 - \not{p}_1 + M_f)C_{LR}\not{q}_2 C_{RL}(\not{q}_1 - \not{p}_1 + M_f)C_{LR}\not{q}_1\right]}{\left((q_1-p_1)^2 - M_f^2\right)^2} + \\ & \frac{\left[C_{RL}(\not{q}_1 - \not{p}_1 + M_f)C_{LR}\not{q}_2 C_{RL}(\not{q}_1 - \not{p}_2 + M_f)C_{LR}\not{q}_1\right]}{\left((q_1-p_1)^2 - M_f^2\right)\left((q_1-p_2)^2 - M_f^2\right)} + (p_1 \longleftrightarrow p_2)\end{aligned} \tag{4.143}$$

Then evaluating the traces the s-wave cross section can be obtained as

$$(\sigma v)_{\mu\mu}^{R-scalar} = \frac{1}{\pi M_f^2}\frac{(\lambda_2^L)^2(\lambda_2^R)^2}{(1+r_s^2)^2} \tag{4.144}$$

A scalar Dark Matter candidate appear in the $SH1$ model, then comparing the Lagrangian 4.43 with the one for the model in 4.23 we have for the effective coupling $\lambda_2^{R/L}$:

$$\lambda_2^R = \lambda_2 U_{11} \tag{4.145}$$

$$\lambda_2^L = \frac{\lambda_1}{\sqrt{2}} U_{21} \tag{4.146}$$

then the cross section can be written as

$$(\sigma v)_{\mu\mu}^{R-scalar} = \frac{1}{\pi M_f^2}\frac{(\lambda_1\lambda_2 U_{11}U_{21})^2}{2(1+r_s^2)^2} \tag{4.147}$$

where we introduce the parameter $r_s = M_s/M_f < 1$.

4.4.2 Fermionic Dark Matter

For the scenario in which the Dark Matter is a Dirac fermion transforming in the n-dimensional representation with hypergarge Y_s, the Lagrangian can be written as

$$\mathcal{L}_F = \bar{f}(i\not{D} - M_f)f \tag{4.148}$$

with D_μ the usual covariant derivative. The fermion annihilation into a gauge boson is described by the same three channels as for the scalar Dark Matter case. The main difference is that for a fermion, both Higgs and Standard Model fermion final states contribute to the s-wave cross section of annihilations plus coannihilations.

The contribution to the $\bar{f}_m f_n \to W^i W^j$ comes from three Feynman diagrams, as can be seen from Figure 4.11: two of them refer to t-channel processes, and one of them is an s-channel process involving the three-linear gauge boson vertex.

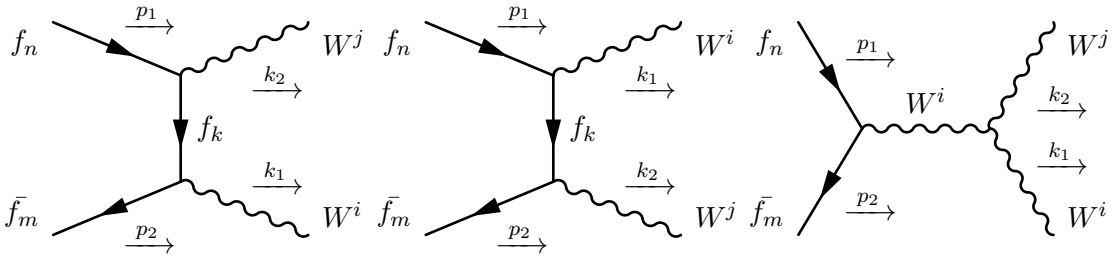

Figure 4.11: Feynman diagram contributing to the Dark Matter annihilation into W^i.

The amplitude is given by

$$\begin{aligned}\mathcal{M} = -ig_2^2\bar{v}(p_2)\Bigg[&\frac{\gamma^\mu(\not{p}_1 - \not{k}_1 + M_f)\gamma^\nu}{(p_1-k_1)^2 - M_f^2}(T^jT^i)_{nm} + \frac{\gamma^\nu(\not{p}_1 - \not{k}_2 + M_f)\gamma^\mu}{(p_1-k_2)^2 - M_f^2}(T^iT^j)_{nm} \\ &+ i\gamma_\rho V^{\mu\nu\rho}(-k_1, k_2, p_1+p_2)T^k_{nm}f^{ijk}\Bigg] u(p_1)\epsilon^*_\mu(k_1)\epsilon^*_\nu(k_2) \\ = -ig_2^2&\left[\mathcal{M}^{\mu\nu}_{WW,1}(T^iT^j)_{nm} + \mathcal{M}^{\mu\nu}_{WW,2}\sum_k f^{ijk}T^k_{nm}\right]\epsilon^*_\mu(k_1)\epsilon^*_\nu(k_2)\end{aligned} \tag{4.149}$$

To get the unpolirized modulus squared amplitude, we can procede excactly as for the scalar multiplet, the only difference being that in the fermion case, in the definition of $\mathcal{M}_{WW,i}$, $i = 1, 2, 12$,

we need also to take the average over the initial spins and evaluate the corresponding Dirac traces. Summing over the gguage group indices:

$$|\bar{\mathcal{M}}_{WW}|^2 = g_2^2 \left[\mathcal{M}^2_{WW,1} \frac{dim(R) C_2(R)}{n^2} + (\mathcal{M}^2_{WW,2} + \mathcal{M}^2_{WW,12}) \frac{2dim(R) C_2(R)}{n^2} \right] \tag{4.150}$$

Then the s-wave cross section is:

$$(\sigma v)(\bar{f} f \to WW) = \frac{g_2^4}{32\pi M_f^2 n^2} C_2(R)(2C_2(R) - 1) dim(R) \tag{4.151}$$

The Feynman diagrams contributing to the annihilation into B's are depicted in FIgure 4.12 and the corresponding amplitude is evaluated to be:

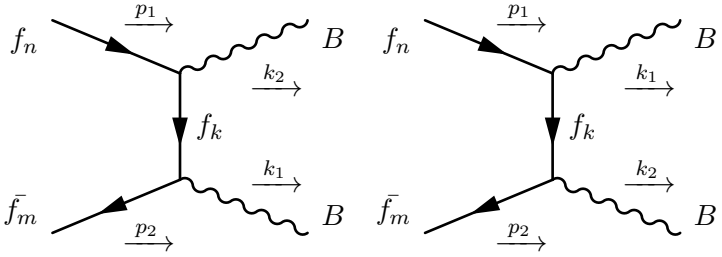

Figure 4.12: Feynman diagram contributing to the Dark Matter annihilation into B.

$$\begin{aligned} \mathcal{M}_{BB} &= -i(g_Y Y_f)^2 \left[\bar{v}(p_2) \left(\frac{\gamma^\nu (\not{p}_1 - \not{k}_1 + M_f)\gamma^\mu}{(p_1 - k_1)^2 - M_f^2} + \frac{\gamma^\mu (\not{p}_1 - \not{k}_2 + M_f)\gamma^\nu}{(p_1 - k_2)^2 - M_f^2} \right) u(p_1) \right] \delta_{nm} \epsilon^*_\mu(K_1) \epsilon^*_\nu(K_2) \\ &= -i(g_Y Y_f)^2 \mathcal{M}^{\mu\nu}_{BB} \delta_{nm} \epsilon^*_\mu(K_1) \epsilon^*_\nu(K_2) \end{aligned} \tag{4.152}$$

The unpolarized amplitude squared and the corresponding s-wave cross section are

$$|\bar{\mathcal{M}}_{BB}|^2 = (g_Y Y_f)^4 \mathcal{M}^2_{BB} \frac{1}{n} \tag{4.153}$$

$$(\sigma v)(\bar{f} f \to BB) = \frac{g_Y^4 Y_f^4}{16\pi M_f^2 n^2} dim(R) \tag{4.154}$$

The third annihilation channel gets contribution from the two Feynman diagram in 4.13.

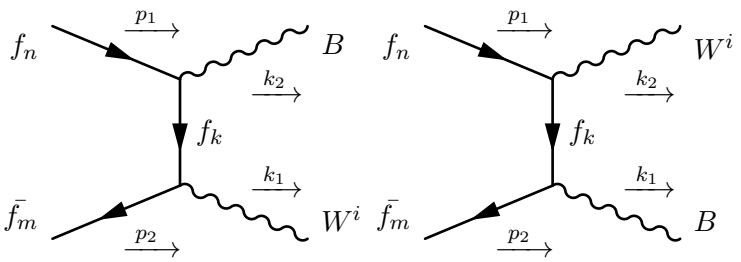

Figure 4.13: Feynman diagram contributing to the Dark Matter annihilation into W^i and B.

The amplitude is given by:

$$\mathcal{M}_{WB} = -ig_2 g_Y Y_f \left[\bar{v}(p_2) \left(\frac{\gamma^\nu (\not{p}_1 - \not{k}_1 + M_f)\gamma^\mu}{(p_1 - k_1)^2 - M_f^2} + \frac{\gamma^\mu (\not{p}_1 - \not{k}_2 + M_f)\gamma^\nu}{(p_1 - k_2)^2 - M_f^2} \right) u(p_1) \right] T^i_{nm} \epsilon^*_\mu(k_1) \epsilon^*_\nu(k_2) \tag{4.155}$$

From this expression, following the same steps as for the previous computation, we derive the unpolarized amplitude and the cross section

$$|\bar{\mathcal{M}}_{WB}|^2 = (g_2 g_Y Y_f)^2 \mathcal{M}^2_{WB} \frac{dim(R)C_2(R)}{n^2} \tag{4.156}$$

$$(\sigma v)(\bar{f}f \to WB) = \frac{g_2^2 g_Y^2 Y_f^2}{8\pi M_f^2 n^2} dim(R)C_2(R) \tag{4.157}$$

The Dark Matter annihilation into the Higgs doublets is mediated by the B or the W^i for the coannihilation, as in FIgure 4.14

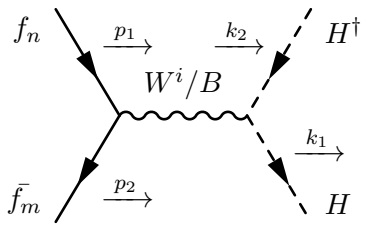

Figure 4.14: Feynman diagram contributing to the Dark Matter annihilation into Higgs doublets.

The amplitude is

$$\begin{aligned}\mathcal{M}_{HH} &= ig_2^2 \bar{v}(p_2)\frac{\gamma^\mu (k_1-k_2)_\mu}{(p_1+p_2)^2}u(p_1)\sum_i T^i_{nm}\tilde{T}^i_{\bar{n}\bar{m}} + ig_Y^2 Y_f Y_H \bar{v}(p_2)\frac{\gamma^\mu (k_1-k_2)_\mu}{(p_1+p_2)^2}u(p_1)\delta_{nm}\delta_{\bar{n}\bar{m}} \\ &= i\mathcal{M}_{HH}(g_2^2\sum_i T^i_{nm}\tilde{T}^i_{\bar{n}\bar{m}} + g_Y^2 Y_f Y_H \delta_{nm}\delta_{\bar{n}\bar{m}})\end{aligned} \tag{4.158}$$

Where $\tilde{T}^i$ are the $su(2)$ generators in the fundamental representation. Then, taking the average over the initial spins and summing over all possible final states, we can write the unnpolarized amplitude squared

$$|\bar{\mathcal{M}}_{HH}|^2 = \mathcal{M}^2_{HH}\frac{1}{n^2}\sum_{nm}\sum_{\bar{n}\bar{m}}(g_2^2\sum_i T^i_{nm}\tilde{T}^i_{\bar{n}\bar{m}} + g_Y^2 Y_f Y_H \delta_{nm}\delta_{\bar{n}\bar{m}})^2 \tag{4.159}$$

keeping in mind that the generators are traceless, we can then derive the expression for the s-wave cross section

$$(\sigma v)(\bar{f}f \to HH) = \frac{g_2^4 dim(R)C_2(R) + g_Y^4 Y_\Psi^2 Y_H^2 dim(R)}{128\pi m_\Psi^2 n^2} \tag{4.160}$$

For the annihilation into Standard Model fermion doublets we have the analogous Feynamn diagram as for the annihilation into Higgs doublet, while the annihilation into fermion singlet can only be mediated by the B boson. They are both represented in 4.15.

The amplitude is given by

$$\begin{aligned}\mathcal{M}_{\Psi\Psi} &= i[g_2^2\frac{\bar{v}(p_2)\gamma^\mu u(p_1)\bar{u}(k_1)\gamma_\mu v(p_2)}{(p_1+p_2)^2}\sum_i T^i_{nm}T^i_{\bar{n}\bar{m}} + ig_Y^2 Y_f Y_\Psi \frac{\bar{v}(p_2)\gamma^\mu u(p_1)\bar{u}(k_1)\gamma_\mu v(p_2)}{(p_1+p_2)^2}\delta_{nm}\delta_{\bar{n}\bar{m}} \\ &= i\mathcal{M}^2_{\Psi\Psi}(g_2^2\sum_i T^i_{nm}\tilde{T}^i_{\bar{n}\bar{m}} + g_Y^2 Y_f Y_\Psi \delta_{nm}\delta_{\bar{n}\bar{m}})\end{aligned} \tag{4.161}$$

we can notice that to compute the unpolarized amplitude we can follow exactly the steps for the Higgs annihilation channel, keeping in mind that we have also to take the sum over the outgoing spinors in the definition of $\mathcal{M}^2_{\Psi\Psi}$. We can then recover the amplitude squered as

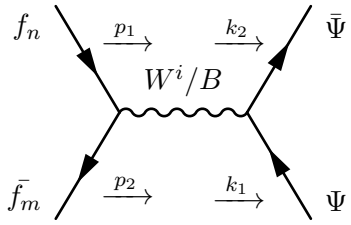

Figure 4.15: Feynman diagram contributing to the Dark Matter annihilation into Standard Model fermions.

$$|\bar{\mathcal{M}}_{\Psi\Psi}|^2 = N_c^{\Psi}\mathcal{M}_{ff}^2\frac{1}{n^2}(g_2^4 dim(R)C_2(R) + 2g_Y^4 Y_s^2 Y_f^2 dim(R)) \tag{4.162}$$

where N_c^{Ψ} is the color factor, and assume the values of 1 for leptons and 3 for quarks. From this amplitude, describing the Dark Matter annihilation into doublets, we can recover the amplitude for the annihilation into fermions by simply substituting $g_2 = 0$ and dividing by 2 the $g_Y^2 Y^2$ terms to cancel the factor of 2 coming from the sum over the fermion doublets components. We finally get the s-wave cross sections:

$$(\sigma v)^{fD}(\bar{f}f \to \Psi\Psi) = \frac{N_c^{\Psi} g_2^4 dim(R)C_2(R) + g_Y^4 Y_{\Psi}^2 Y_f^2 dim(R)}{32\pi M_f^2 n^2} \tag{4.163}$$

$$(\sigma v)^{fS}(\bar{f}f \to \Psi\Psi) = \frac{N_c^{\Psi} g_Y^4 Y_{\Psi}^2 Y_f^2}{16\pi M_f^2 n^2} dim(R) \tag{4.164}$$

Taking the sum over all the Standard Model fermions and adding the result to the other channels, we get the final expression for the annihilation of fermion Dark Matter

$$(\sigma v)_{eff}^{D-fermion} = \frac{g_2^4(2n^4 + 49n^2 - 51) + 4g_Y^4 Y_f^2(81 + 8Y_f^2) + 16g_2^2 g_Y^2 Y_f^2(n^2 - 1)}{512\pi M_f^2 n} \tag{4.165}$$

If instead of a Dirac fermion, f is a Mayorana fermion, the computation follows the same steps leading to the same result up to a factor of two

$$(\sigma v)_{eff}^{M-fermion} = \frac{g_2^4(2n^4 + 49n^2 - 51) + 4g_Y^4 Y_f^2(81 + 8Y_f^2) + 16g_2^2 g_Y^2 Y_f^2(n^2 - 1)}{256\pi M_f^2 n} \tag{4.166}$$

If the Dark Matter is a Mayorana fermion the are additional contributions to take into account which are represented by the Feynman diagrams of FIgure 4.16

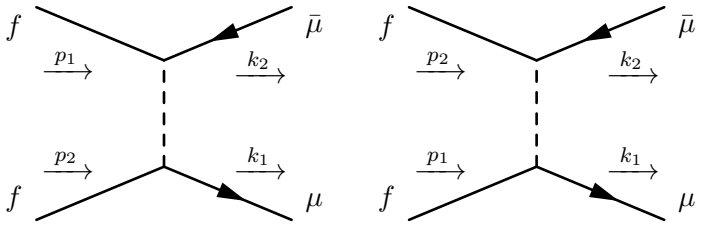

Figure 4.16: Feynman diagrams contributing to the annihilation cross section of fermionic Dark Matter into muons due to the new physics couplings.

The amplitude is

$$\mathcal{M}_{\mu\mu} = -i\left[\frac{\bar{u}(q_1)C_{RL}u(p_1)\bar{v}(p_2)C_{LR}v(q_2)}{\left((q_1-p_1)^2-M_s^2\right)^2}+\frac{\bar{u}(q_1)C_{RL}u(p_2)\bar{v}(p_1)C_{LR}v(q_2)}{\left((q_1-p_2)^2-M_s^2\right)^2}\right] \tag{4.167}$$

Taking the average over the initial spin and the sum over the final one, we get the unpolarized amplitude squared in the $m_{NP} \gg m_\mu$ limit as

$$\begin{aligned}|\mathcal{M}_{\mu\mu}|^2 =& \frac{Tr\left[C_{RL}(\not{p}_1+M_f)C_{LR}\not{q}_1\right]Tr\left[C_{LR}\not{q}_2C_{RL}(\not{p}_2-M_f)\right]}{4\left((q_1-p_1)^2-M_s^2\right)^2}+\\ &\frac{Tr\left[\not{q}_1C_{RL}(\not{p}_2+M_f)C^TC_{RL}^T\not{q}_2^TC_{LR}^TC^{-1}(\not{p}_2-M_f)C_{LR}\right]}{4\left((q_1-p_1)^2-M_s^2\right)\left((q_1-p_2)^2-M_s^2\right)}+(p_1\longleftrightarrow p_2)\end{aligned} \tag{4.168}$$

Where C is the charge conjugation operator, using its anticommutation properties with the chiral projectors the second trace can be computed and then the s-wave cross section is derived

$$(\sigma v)_{\mu\mu}^{M-fermion} = \frac{1}{8\pi M_s^2}\frac{r_f^2\lambda_L^2\lambda_R^2}{(1+r_f^2)^2} \tag{4.169}$$

where we introduce the parameter $r_f = M_f/M_s < 1$.

A fermion Dark Matter candidate appears in the $FH1$ model, then we can compare the couplings in 4.44 with the one in 4.36 we get:

$$\lambda_2^R = \lambda_2 V_{21} \tag{4.170}$$

$$\lambda_2^L = -\lambda_1 V_{11} \tag{4.171}$$

then the cross section can be rewritten as:

$$(\sigma v)_{\mu\mu}^{M-fermion} = \frac{1}{8\pi M_s^2}\frac{r_f^2(\lambda_1\lambda_2 V_{11}V_{21})^2}{(1+r_f^2)^2}\,. \tag{4.172}$$

4.5 Dark Matter direct detection

The problem of Dark Matter direct detection can be approached through an effective field theory approach [34, 44, 45]. The first ingredient needed in order to compute the Dark Matter-nucleus interaction amplitude is a parton model that describes the Dark Matter interaction with quarks. Thus, we start with an effective Lagrangian describing the Dark Matter interactions with SM particles through a sum of higher dimension operators,

$$\mathcal{L}_{UV} = \sum_{a,d}\hat{C}_a^{(d)}\mathcal{Q}_a^{(d)} \tag{4.173}$$

with $\hat{C}_a^{(d)}$ are dimensionfull Wilson coefficient and can be written in terms of their corresponding dimensionless coefficient as $\hat{C}_a^{(d)} = \frac{C_a^{(d)}}{\Lambda^{d-4}}$, where Λ is the energy cut off at which the effective theory fails and can be identified with the mass of the mediator between Dark Matter and the Standard Model for couplings of order unity. The sum in the effective Lagrangian runs over the operator dimension $d = 5, 6, 7$ and over the index a which denotes the operator number and, if it contains Standard Model fermion bilinear, a flavor index[2].

The kinds of operators appearing in the Lagrangian vary depending on the Dark Matter nature. The full set of operators will be given in the following for each of the two cases.

[2]Among the dimension seven operator we will exclude those which are additionally suppressed by derivatives.

Since the Dark Matter nucleus scattering pertaining to the direct detection experiments happens at low energy, we take the non-relativistic limit of 4.173. This is achieved by computing the hadronization of the operators, exploiting the definition of the form factors, and taking the non-relativistic expansion of the Dark Matter currents. It is then possible to define a Lagrangian describing the interaction between the Dark Matter and non-relativistic nucleons.

$$\mathcal{L}_{eff}^{N} = \sum_{l} c_l^N \mathcal{O}_l \tag{4.174}$$

The index l runs over the 14 different non relativistic operators

$$\mathcal{O}_1^N = \mathbb{I}_X \mathbb{I}_N \tag{4.175}$$
$$\mathcal{O}_2^N = v_\perp^2 \mathbb{I}_X \mathbb{I}_N \tag{4.176}$$
$$\mathcal{O}_3^N = \mathbb{I}_X \vec{s}_N \cdot \left(\vec{v}_\perp \times \frac{i\vec{q}}{m_N} \right) \tag{4.177}$$
$$\mathcal{O}_4^N = \vec{s}_X \cdot \vec{s}_N \tag{4.178}$$
$$\mathcal{O}_5^N = \vec{s}_X \cdot \left(\vec{v}_\perp \times \frac{i\vec{q}}{m_N} \right) \mathbb{I}_N \tag{4.179}$$
$$\mathcal{O}_6^N = \left(\vec{s}_X \cdot \frac{\vec{q}}{m_N} \right) \left(\vec{s}_N \cdot \frac{\vec{q}}{m_N} \right) \tag{4.180}$$
$$\mathcal{O}_7^N = \mathbb{I}_X \vec{s}_X \cdot \vec{v}_\perp \tag{4.181}$$
$$\mathcal{O}_8^N = (\vec{s}_X \cdot \vec{v}_\perp) \mathbb{I}_N \tag{4.182}$$
$$\mathcal{O}_9^N = \vec{s}_X \left(\frac{i\vec{q}}{m_N} \times \vec{s}_N \right) \tag{4.183}$$
$$\mathcal{O}_{10}^N = -\mathbb{I}_X \left(\vec{s}_N \cdot \frac{i\vec{q}}{m_N} \right) \tag{4.184}$$
$$\mathcal{O}_{11}^N = -\left(\vec{s}_X \cdot \frac{i\vec{q}}{m_N} \right) \mathbb{I}_N \tag{4.185}$$
$$\mathcal{O}_{12}^N = \vec{s}_X \cdot (\vec{s}_N \times \vec{v}_\perp) \tag{4.186}$$
$$\mathcal{O}_{13}^N = -(\vec{s}_X \cdot \vec{v}_\perp) \left(\vec{s}_N \cdot \frac{i\vec{q}}{m_N} \right) \tag{4.187}$$
$$\mathcal{O}_{14}^N = -\left(\vec{s}_X \cdot \frac{i\vec{q}}{m_N} \right) (\vec{s}_N \cdot \vec{v}_\perp) \tag{4.188}$$

where $\vec{s}_X$ and $\vec{s}_N$ are the Dark Matter and nucleon spins, respectively, while $\vec{v}_\perp$ is the Dark Matter transversal velocity and $\vec{q}$ is the momentum transferred during the reaction. Of these 14 operators, those depending on the nucleon spin will produce the so-called spin-dependent cross section, while the others are responsible for the spin-independent one. As can be seen, most of these operators depend on the Dark Matter velocity; hence, they produce a velocity-suppressed contribution to the amplitude squared. Since the Dark Matter velocity can be estimated to be approximately $v \approx 10^{-3}$, we will neglect such operators. There are only two operators that are not velocity suppressed and thus responsible for the dominant contribution to the scattering cross section, the $\mathcal{O}_1^N$ and the $\mathcal{O}_4^N$, responsible respectively for the spin-independent and the spin-dependent interactions.

The Dark Matter nucleus differential cross section can be written as

$$\frac{d\sigma_T}{dE_R} = \frac{1}{32\pi} \frac{1}{m_X^2 m_T} \frac{1}{v^2} |\bar{\mathcal{M}}|^2 \tag{4.189}$$

It is important to note that we have implicitly assumed that both the Dark Matter and the target nucleus are unpolarized; this implies that the scattering cross section can only depend on the modulus square of the Dark Matter velocity, v^2.

In order to compare the theoretical prediction to the experimental result of the XENON1T experiment, we need to compute the differential scattering rate for a target nuclei recoiling with an energy E_R. This is achieved by performing the integral of the scattering cross section weighted by the Dark Matter velocity distribution over the velocity, leading to the expression:

$$\frac{dR_T}{dE_R}(E_R,t) = \frac{\rho_X}{m_X}\frac{1}{m_T}\int_{v\geq v_{min}(E_R)} d^3v f_E(v,t) v \frac{d\sigma_T}{dE_R}(E_R,v) \tag{4.190}$$

The lower bound of the integral is given by the minimum velocity a Dark Matter particle must have in order to produce a nucleus recoiling with energy E_R.

In the following discussion, we will neglect any non-relativistic operator that gives rise to a velocity suppressed amplitude. This means that the velocity integral appearing in 4.190 does not depend on the particular interaction and will be parameterized by the function $\eta_0(v_{min},t)$

$$\eta_0(v_{min},t) = \int_{v\geq v_{min}} d^3v \frac{f_E(v,t)}{v} \tag{4.191}$$

The time dependence in the velocity integral comes from the velocity distribution $f_E(v,t)$ and is due to the Earth motion. Indeed, the Dark Matter can be considered at rest in the galactic reference frame; thus, the Earth's motion around the Sun will produce a periodic variation of the Dark Matter flux at Earth, which will then produce an annual modulation of the signal in the experimental setup. This modulation effect will not be considered in our discussion; the main interest will be in the annual average interaction rate.

Finally, the number of events can be evaluated by performing the integral over the recoil energy E_R or equivalently, over v_{min}; XENON1T results are compatible with the hypothesis that no dark matter events were observed[46, 47].

4.5.1 $FH1$ model and Mayorana Dark Matter

For a Dark Matter Mayorana fermion, we define in the following the base of the relativistic operators appearing in the Lagrangian 4.173. The relevant operators start at dimension-six

$$\mathcal{Q}^{(6)}_{2,q} = (\bar{f}\gamma_\mu\gamma_5 f)(\bar{q}\gamma^\mu q), \quad \mathcal{Q}^{(6)}_{4,q} = (\bar{f}\gamma_\mu\gamma_5 f)(\bar{q}\gamma^\mu\gamma_5 q) \tag{4.192}$$

while for dimension-seven we will consider a subset of operators, namely

$$\mathcal{Q}^{(7)}_1 = \frac{\alpha_s}{12\pi}(\bar{f}f)G^{a,\mu\nu}G^a_{\mu\nu}, \quad \mathcal{Q}^{(7)}_2 = \frac{\alpha_s}{12\pi}(\bar{f}i\gamma_5 f)G^{a,\mu\nu}G^a_{\mu\nu}, \tag{4.193}$$

$$\mathcal{Q}^{(7)}_3 = \frac{\alpha_s}{8\pi}G^{a,\mu\nu}\tilde{G}^a_{\mu\nu}, \quad \mathcal{Q}^{(7)}_4 = \frac{\alpha_s}{8\pi} - (\bar{f}i\gamma_5 f)G^{a,\mu\nu}\tilde{G}^a_{\mu\nu}, \tag{4.194}$$

$$\mathcal{Q}^{(7)}_{5,q} = m_q(\bar{f}f)(\bar{q}q), \quad \mathcal{Q}^{(7)}_{6,q} = m_q(\bar{f}i\gamma_5 f)(\bar{q}q), \tag{4.195}$$

$$\mathcal{Q}^{(7)}_{7,q} = m_q(\bar{f}f)(\bar{q}i\gamma_5 q), \quad \mathcal{Q}^{(7)}_{8,q} = m_q(\bar{f}i\gamma_5 f)(\bar{q}i\gamma_5 q) \tag{4.196}$$

Where $q = u,d,s$ are the light quarks fields. Of all these operators, we are interested in those that, once hadronized, produce the non-relativistic operators $\mathcal{O}^N_1$ and $\mathcal{O}^N_4$. The $\mathcal{O}^N_1$ arise from the hadronization of $\mathcal{Q}^{(6)}_{1,q}$, $\mathcal{Q}^{(7)}_1$ and $\mathcal{Q}^{(7)}_{5,q}$. The operator $\mathcal{Q}^{(6)}_{4,q}$ in the non relativistic limit produces both $\mathcal{O}^N_4$ and $\mathcal{O}^N_6$ that interfere between themselves, but since the latter one is q^2/m^2_N suppressed and we are interested in the leading order contribution to the scattering rate, we will neglect its contribution to the amplitude.

To get the explicit expression of the non-relativistic coefficients c^N_1 and c^N_4 we need to match the $FH1$ model Lagrangian onto the relativistic Lagrangian 4.173. For our porpous, it will be sufficient to perform tree-level matching with just one exception regarding the $\mathcal{Q}^{(7)}_1$ operator. At tree level, the interaction between Dark Matter and quarks can be mediated either by the Z boson or by the Higgs field. Below the Electroweak scale, these interactions can be described with an Effective Field Theory approach integrating out the heavy mediators from the model Lagrangian 4.23. This is achieved by exploiting the equation of motion technique applied to the Lagrangian relevant to our case.

$$\begin{aligned}\mathcal{L} =& -\lambda_H h\bar{F}_{01}F_{01} - \frac{g_2}{c_W}Z_\mu g_A^F \bar{F}_{01}\gamma^\mu\gamma_5 F_{01}) \\ &- \frac{g_2}{c_W}\sum_{q=u,d,s} Z_\mu \bar{q}\gamma^\mu(g_V^q + g_A^q\gamma_5)q - \sum_{q=u,d,s}\frac{m_q}{v}h\bar{q}q \\ &- \frac{1}{4}Z^{\mu\nu}Z_{\mu\nu} - \frac{1}{2}M_Z^2 Z^\mu Z_\mu + \frac{1}{2}\left(\partial^\mu h\partial_\mu h - M_h^2 h^2\right)\end{aligned} \tag{4.197}$$

for simplicity, we have introduced the couplings$\lambda_H = \frac{\lambda_{1H}V_{21}V_{11}+\lambda_{2H}V_{31}V_{11}}{\sqrt{2}}$, $g_A^F = \frac{1}{4}(V_{21}V_{21} - V_{31}V_{31})$, while g_V^q and g_A^q are the coupling of standard model quark currents to the Z boson. By writing the equation of motion for Z and h neglecting the kinetics terms, and substituting the results back into the Lagrangian, we get the effective operators:

$$\mathcal{L} = 4\sqrt{2}G_F g_A^f \bar{f}\gamma^\mu\gamma_5 f\sum_{q=u,d,s}\bar{q}\gamma_\mu(g_V^q + g_A^q\gamma_5)q + \sum_{q=u,d,s}\frac{\lambda_H m_q}{vM_h^2}\bar{f}f\bar{q}q \tag{4.198}$$

which corresponds to the operators $\mathcal{Q}_{2,q}^{(6)}$, $\mathcal{Q}_{4,q}^{(6)}$ and $\mathcal{Q}_{5,q}^{(7)}$ respectively.

Another important contribution comes from the dimension-seven operator $\mathcal{Q}_1^{(7)}$ that arise at one-loop level from the diagrams in Figure 4.17.

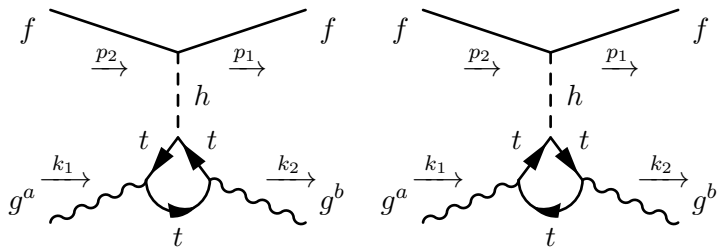

Figure 4.17: The two Feynman diagram responsible for the $\mathcal{Q}_1^{(7)}$ operator.

The one-loop computation is a standard result in the Standard Model theory, using this result we can derive the operator

$$\mathcal{L} = -\frac{1}{2\pi}\frac{\lambda_J y_t}{vM_h^2}\frac{\alpha_s}{12\pi}(\bar{f}f)G^{\mu\nu,a}G^a_{\mu\nu} \tag{4.199}$$

where we have exploited the fact that for the transferred momentum inside the h boson propagator we have the relation $q^2 \ll M_h^2$.

From what we have found up to now and considering the definition of the hadronic form factors, we can derive the expression for the Wilson coefficient of the non-relativistic theory

$$c_1^N = 4m_X m_N\left[\sum_{q=u,d,s} m_N f_{Tq}^{(N)} 2\hat{C}_{5,q}^{(7)} - \frac{2}{27}m_N f_{TG}^{(N)} 2\hat{C}_1^{(7)}\right] = 4m_X m_N \tilde{c}_1^N \tag{4.200}$$

$$c_4^N = 4m_X m_N\left[-4\sum_{q=u,d,s}\Delta_q^N 2\hat{C}_{4,q}^{(6)}\right] = 4m_X m_N \tilde{c}_4^N \tag{4.201}$$

We added a factor of two for each Wilson coefficient that arise from the non relativistic limit of the operators.

To get a rough estimate of the interaction cross section we will exploit the point like nucleus hypothesis. In this hypothesis we can neglect nuclear response during the process, the amplitude can then be written as

$$\mathcal{M}_{PLN} = \sum_{N=p,n} \sum_i (c_1^N \delta_{ss'} \delta_{MM'} + c_4^N \vec{s}_f \cdot \langle J, M | \vec{s}_N | J, M' \rangle) \tag{4.202}$$

We can then compute the amplitude modulus square remembering that, for unpolarized Dark Matter the $\mathcal{O}_1^N - \mathcal{O}_4^N$ interference term is null. The amplitude we get is

$$|\mathcal{M}_{PLN}|^2 = 16 m_X^2 m_N^2 (Z c_1^p + (A - Z) c_1^n)^2 + \frac{J+1}{4J} (\mathcal{S}_p c_4^p + \mathcal{S}_n c_4^n)^2 \tag{4.203}$$

Substituting this result into 4.189 we obtain the cross section

$$\frac{d\sigma_T}{dE_R} = \frac{m_T}{2\pi} \frac{1}{v^2} \left[A^2 \left(\frac{Z}{A} \tilde{c}_1^p + \frac{(A-Z)}{A} \tilde{c}_1^n \right)^2 + \frac{J+1}{4J} (\mathcal{S}_p \tilde{c}_4^p + \mathcal{S}_n \tilde{c}_4^n)^2 \right] \tag{4.204}$$

As can be seen, the cross section is obtained as the sum of a spin-indipendent and a spin-dependent term. The first of these terms arises from the operator $\mathcal{O}_1^N$ and is coherently enhanced by a factor of $A^2 \sim 10^4$ and thus can be dominant with respect to the spin-dependent term. But in our particular case, the situation is not so clear; indeed, the $\mathcal{O}_4^N$ operator arises from dimension-six relativistic operators that are suppressed by a factor of M_W^{-2} while the operators inducing $\mathcal{O}_1^N$ are all of dimension seven and are suppressed by a factor of $1/(v M_h^2)$. As a consequence, the two cross sections are of comparable size. Indeed, if we evaluate the two contributions for the case of the tungsten 183, we get for the two contributions the values of $\sim 10^{-13} Mev^{-2}$ and $\sim 10^{-12} Mev^{-2}$ respectively for the spin independent and the spin dependent terms.

4.5.2 $SH1$ model and real scalar Dark Matter

For a real scalar Dark Matter the set of relativistic operator is quite smaller, in particular also in this case there are not dimension-five operators moreover neither dimension seven operators are relevant. We will then consider the following set of dimension-six operators:

$$\mathcal{Q}_{3,q}^{(6)} = m_q(s^2)(\bar{q}q) \quad \mathcal{Q}_{4,q}^{(6)} = m_q(s^2)(\bar{q} i \gamma_5 q) \tag{4.205}$$

$$\mathcal{Q}_5^{(6)} = \frac{\alpha_s}{12\pi}(s^2) G^{\mu\nu,a} G^a_{\mu\nu} \quad \mathcal{Q}_6^{(6)} = \frac{\alpha_s}{8\pi}(s^2) G^{\mu\nu,a} \tilde{G}^a_{\mu\nu} \tag{4.206}$$

where $q = u, d, s$ are the light quarks. Differently from the fermion case, not all the non-relativistic operators contribute to the scattering process for a scalar Dark Matter particle; indeed, since the scalar does not have spin, all those operators involving $\vec{s_X}$ are now absent. For this reason, we will not have contributions from the $\mathcal{O}_4^N$ but only from the $\mathcal{O}_1^N$, so of all the possible relativistic operators, we need to consider only those that, after the hadronization, produce the latter one.

Following the same procedure as for the fermion case, we exploit the equation of motion techniques to match the $SH1$ model onto the Lagrangian 4.173 at tree level to build an effective field theory. The model operator that is relevant to our purpose

$$\mathcal{L} = -\frac{A_H}{2} h S_1 S_1 - \sum_{q=u,d,s} \frac{m_q}{v} h \bar{q} q \tag{4.207}$$

$$+ \frac{1}{2}(\partial_\mu h \partial^\mu h - M_h^2 h^2) \tag{4.208}$$

for simplicity we have defined $A_H = a_H U_{11} U_{21}$. Deriving the equation of motion for the h boson and neglecting the kinetic terms we obtain the effective operators

$$\mathcal{L} = \sum_{q=u,d,s} \frac{A_H m_q}{2 v M_h^2} s^2 \bar{q} q \tag{4.209}$$

$$= \sum_{q=u,d,s} \hat{C}_{3q}^{(6)} m_q s^2 \bar{q} q \tag{4.210}$$

This effective operator correspond to the relativistic operator $\mathcal{Q}_{3,q}^{(6)}$. There is also another contribution from the operator $\mathcal{Q}_5^{(6)}$ that arise at one loop level through the analogous diagram of FIgure 4.17.

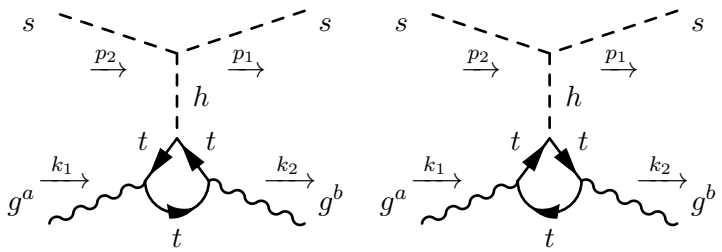

Figure 4.18: The two Feynman diagram responsible for the $\mathcal{Q}_5^{(6)}$ operator.

The corresponding operator is:

$$\mathcal{L} = -\frac{1}{2\pi}\frac{A_H y_t}{v M_h^2}\frac{\alpha_s}{12\pi}(s^2)G^{\mu\nu,a}G^a_{\mu\nu} \tag{4.211}$$

$$= \hat{C}_5^{(6)}\frac{\alpha_s}{12\pi}s^2 G^{\mu\nu,a}G^a_{\mu\nu} \tag{4.212}$$

Given this relativistic operators, we can derive the expression for the non-relativistic Wilson coefficient c_1^N

$$c_1^N = 2m_N\left(\sum_{q=u,d,s} m_N f_{Tq}^{(N)}(2\hat{C}_{3,q}^{(6)}) - \frac{2}{27}m_N f_{TG}^{(N)}(2\hat{C}_5^{(6)})\right) \tag{4.213}$$

$$= 2m_N\tilde{c}_1^N \tag{4.214}$$

The factors of two in front of the relativistic Wilson coefficient appear since the Dark Matter candidate is a real scalar. Also in this case we compute the scattering amplitude in the point like nucleus hypothesis

$$\mathcal{M}_{PLN} = \sum_{N=p,n}\sum_i c_1^N \delta_{ss'}\delta_{MM'} \tag{4.215}$$

computing the amplitude square and then the scattering cross section with 4.189 we get

$$\frac{d\sigma_T}{dE_R} = \frac{1}{8\pi}\frac{m_T}{m_X^2}\frac{1}{v^2}A^2\left(\frac{Z}{A}\tilde{c}_1^p + \frac{A-Z}{A}\tilde{c}_1^n\right)^2 . \tag{4.216}$$

4.6 Numerical analysis

In this section we will show a numerical analysis of the formulas derived in previous section in order better understand the viability of the models we have considered.

4.6.1 Benchmark model $FH1$

The Lagrangian and field content of the model were given in equation 4.23, and, as was previously discussed, the Dark Matter candidate is a Mayorana fermion. In 4.19a, we show the results for an illustrative choice of parameters. The couplings responsible for the interaction between the new physics fields and the muon are taken to be of order one and such that the contribution to the Δa_μ is positive. In particular, we have chosen $-\lambda_1 = \lambda_2 = 1$. As for the Yukawa-like couplings responsible for the interaction of the new physics fermions with the Higgs doublets, they are chosen to be $\lambda_{1H} = -0.2$ and $\lambda_{2H} = 0.3$.

The blue region represents the portion of parameter space for which the Δa_{mu}^{NP} is able to reproduce the experimental deviation found in 2.17. We can clearly see that a sufficiently large contribution to the $(g-2)_\mu$ is obtained in the multi-TeV range; this is a direct consequence of the v/m_μ enhancement stemming from the chirility flip in the 1-loop diagrams. The fact that the new physics particle masses can be of the TeV order allows us to safely evade the colliders exclusion bound. The yellow region represents the parameter space for which a Dark Matter abundance predicted by the model is $\Omega h^2 \leq 0.12$. This relic abundance was calculated considering the Dark Matter fermion decays into gauge bosons and muons. The last one of which is mediated by the scalar doublet, for which a mass of $M_S = 2.5\, TeV$ was taken. Finally, the light green region is excluded by the XENON1T search for Dark Matter. To evaluate this bound, both the spin-independent and spin-dependent interactions of the Dark Matter candidate with the nucleus are considered. As was discussed in the previous section, the cross sections were computed in the Point Like Nucleus hypothesis, so the corresponding exclusion region should be taken as indicative; for this same reason, we have limited ourselves to computing the scattering cross section only with the most abundant Xe isotope relevant for this scenario, which is 129Xe.

In conclusion, the $FH1$ model can account for the Δa_μ anomaly and the correct Dark Matter relic density evading at the same time the constrains stemming from the direct detection searches.

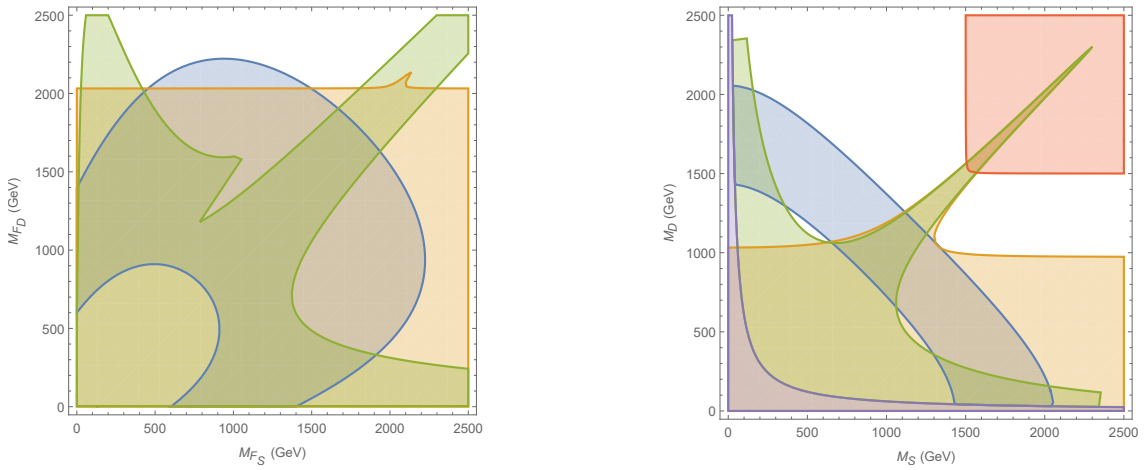

(a) FH1 model

(b) SH1 model

Figure 4.19: Diagrams for the two benchmark models

4.6.2 Benchmark model $SH1$

The Lagrangian and field content of the $SH1$ model are specified in 4.36, and the Dark Matter candidate is the lightest of the real scalars. Also for this model, the new physics couplings have been chosen in such a way that the Δa_μ^{NP} is positive. The values taken are $-\lambda_1 = \lambda_2$. The dimensional

coupling responsible for the interaction of the new physics scalars with the Higgs doublet is taken to be $a_H = v$, where v is the Higgs vev. As for the fermion singlet mass, we have taken the value of $M_F = 1.5\, TeV$.

In 4.19b, the blue region represents the portion of the parameter space for which the Δa_μ^{NP} reproduces the most recent results for the $(g-2)_\mu$ deviation. As can be seen, sufficiently large values are also obtained in the multi-TeV region, analogously to the $FH1$ model case; this is due to the enhancement arising from the chirility flipping Feynman diagrams. The yellow region represents the parameter values for which the Dark Matter candidate is able to reproduce a relic density of $\Omega h^2 \leq 0.12$, through the annihilation into both gauge bosons and muons, the latter one of which is mediated by the scalar fermion. Finally, the green region is excluded by direct detection data taken from the XENON1T experiment. As for the $FH1$ model, the Dark Matter nucleon cross section is evaluated in the Point Like Nucleus limit. For this reason, the bound was computed considering just the most abundant Xenon isotope, 129Xe, and then the exclusion bound should be considered as indicative.

In conclusion, also the $SH1$ model can account for the Δa_μ anomaly and the correct Dark Matter relic density while evading the stringent bounds given by the direct detection searches.

Conclusions

Although the Standard Model provides a very remarkable explanation of a plethora of experimental measurements in particle physics, it is a common belief that it cannot represent the ultimate theory of Nature. In fact, there are a few unanswered fundamental questions, such as the nature and production of Dark Matter, the baryon asymmetry of the universe, the origins of neutrino masses and mixes, excetera. Moreover, there are also a few discrepancies between experimental measurements and theoretical predictions of some observables. A prominent example is given by the muon g-2. This was firstly observed by the experiment E821 at BNL and more recently confirmed by the experiment E898 at FNAL, which found a deviation of 5.0σ. In this thesis, we have studied some possible Standard Model extensions capable of explaining the muon g-2 discrepancy and, at the same time, giving a Dark Matter candidate. We found that this achievement can be obtained at the expenses of introducing at least three new fields coupling both to the muon and to the Higgs boson. They can be divided into two categories based on the nature of the Dark Matter candidate: those which predict a fermionic candidate and those for which the candidate is a scalar particle. We have then specialized our computation on two benchmark models, one for each of the two categories mentioned above, deriving their predictions for the muon g-2. Then, we focused on the Dark Matter candidates, evaluating the corresponding relic density and the relevant cross section for Direct Detection experiments.

Our numerical analysis shows that, assuming $\mathcal{O}(1)$ new physics couplings and new particles at the TeV scale, the proposed benchmark models are capable of explaining both the muon g-2 discrepancy and the correct Dark Matter relic density while respecting all available experimental data.

Appendix A

One-loop computations

A.1 Feynman rules

In this section we will provide the Feynman rule for the Standard Model in the unbroken gauge that have been used in this thesis.

The Lagrangian for the gauge bosons kinetic term is given by:

$$\mathcal{L}_{gauge} = -\frac{1}{4}W^{\mu\nu,a}W^{a}_{\mu\nu} - \frac{1}{4}B^{\mu\nu}B_{\mu\nu} \tag{A.1}$$

Where the $SU(2)_L$ field strength is given by $W^a_{\mu\nu} = \partial_\mu W^a_\nu - \partial_\nu W^a_\mu + g_2 f^{abc} W^b_\mu W^c_\nu$, while the field strength of the $U(1)_Y$ field is $B_{\mu\nu} = \partial_\mu B_\nu - \partial_\nu B_\mu$. These terms are responsible for the gauge boson propagators, Figure A.1 and Figure A.2, and for the $SU(2)_L$ gauge boson trilinear interaction, Figure A.3.

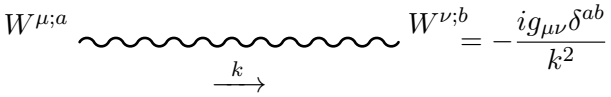

Figure A.1: $SU(2)_L$ gauge boson propagator.

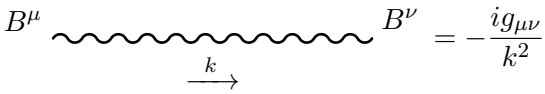

Figure A.2: $U(1)$ gauge boson propagator.

The Higgs doublet Lagrangian in the unbroken phase is:

$$\mathcal{L}_H = D_\mu H^\dagger D^\mu H + \mu^2 H^\dagger H - \frac{\lambda}{4}(H^\dagger H)^2 \tag{A.2}$$

with the covariant derivative given by $D_\mu = \partial_\mu - ig_2 T^a_{ij} W^a_\mu - i\frac{g_Y}{2}B_\mu$, and the $SU(2)_L$ generator are in the fundamental representation. Of all the possible interactions arising from the whole Lagrangian,

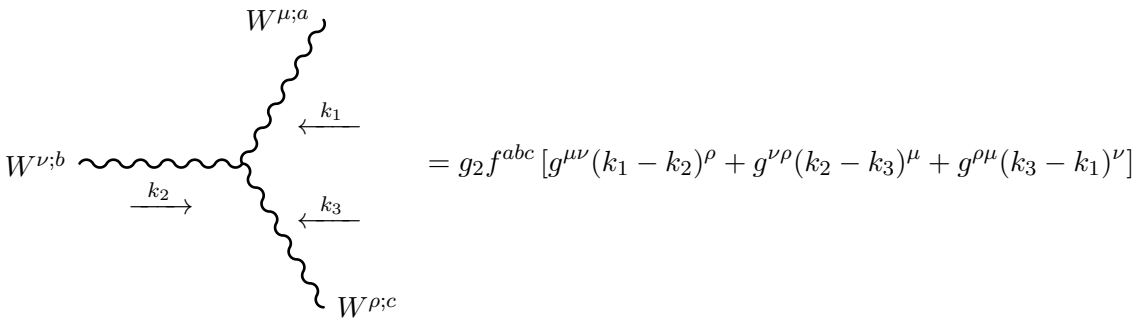

Figure A.3: Feynman rules for the $SU(2)_L$ guage boson self interactions.

we have used just the vertices $H^\dagger HW$ and $H^\dagger HB$, for which the Feynman rules are given in Figure A.4.

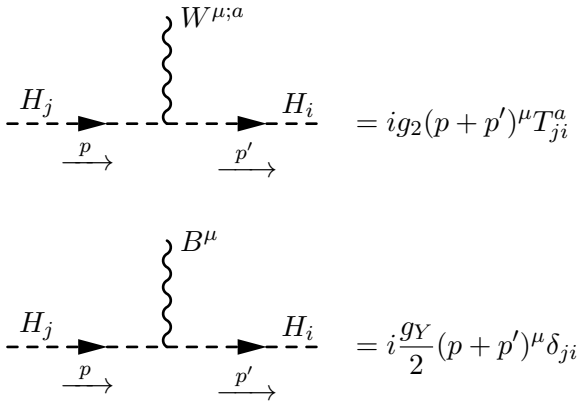

Figure A.4: *Upper row*: Feynman rule for the $H^\dagger HW$ vertex, the i, j indices runs over the component of the Higgs doublet. *Lower row*: Feynman rule for the $H^\dagger HB$ vertex.

The Lagrangian for a fermionic multiplet transforming in the n-dimensional representation of $SU(2)_L$ with hypercharge Y_f is:

$$\mathcal{L}_f = \bar{f}(i\not{D} - M_f)f \tag{A.3}$$

where the covariant derivative is $D_\mu = \partial_\mu - ig_2 T^a_{ij} W^a_\mu - ig_Y Y_f B_\mu$. The fermion propagator and the Feynman rule for the $\bar{f}fW$ and $\bar{f}fB$ interaction are displayed in Figure A.5 and A.6 respectively.

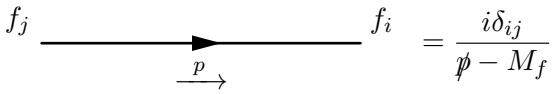

Figure A.5: Fermion propagator. The i, j indices runs over the different components of the multiplet.

The Lagrangian for a scalar multiplet transforming in the n-dimensional representation of $SU(2)_L$ with hypercharge Y_s is:

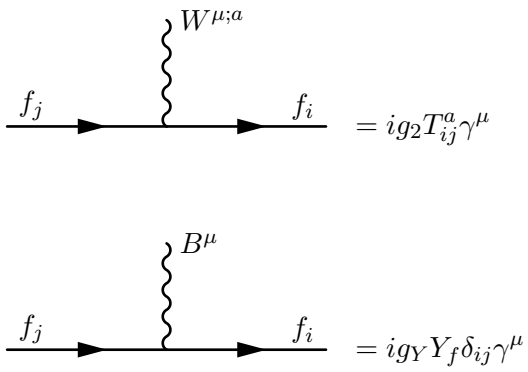

Figure A.6: *Upper row*: Feynman rule for the $\bar{f}fW$ vertex, the i, j indices runs over the different components of the multiplet.. *Lower row*: Feynman rule for the $\bar{f}fB$ vertex.

$$\mathcal{L}_f = D_\mu s^\dagger D^\mu s - M_s^2 s^\dagger s \tag{A.4}$$

where the covariant derivative is $D_\mu = \partial_\mu - ig_2 T^a_{ij} W^a_\mu - ig_Y Y_s B_\mu$. The scalar propagator is given in Figure A.7, the Feynamn rules for the three fields interactions are depicted in Figure A.8 while the Feynamn rules for the four fields vertices are given in Figure A.9.

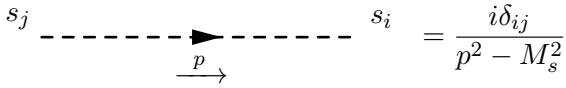

Figure A.7: Scalar propagator. The i, j indices runs over the different components of the multiplet.

The New Physics contribution and their interaction with the muon can be summarize by the $SU(3)_c \times U(1)_{em}$ symmetric Lagrangian:

$$\mathcal{L}_{kin} = (D_\mu s)^* D^\mu s - M_s s^* s + \bar{f}\left(i\not{D} - M_f\right) f + \bar{\mu}\left(i\not{D} - m_\mu\right)\mu \tag{A.5}$$

$$\mathcal{L}_{int} = s^* \bar{\mu}\left(\lambda_2^R P_L + \lambda_2^R P_R\right) f + h.c \tag{A.6}$$

Where the covariant derivative is $D_\mu = \partial_\mu - ieQ$, Q being the charge of the particle.

From this Lagrangian we can derive the following Feynman rules for the vertices involving the new physics particles are in Figure A.10. While the Feynamn rules for the new physics fields interaction with the photon are given in Figure A.11.

A.2 Loop functions

Here we summarize the Master integrals used in the loop computation along with the definition of the loop functions

$$\int \frac{d^d k}{(2\pi)^4} \frac{1}{(k^2 - D)^n} = \frac{(-1)^n i}{(4\pi)^{d/2}} \frac{\Gamma(n - d/2)}{\Gamma(n)} \left(\frac{1}{D}\right)^{n-d/2} \tag{A.7}$$

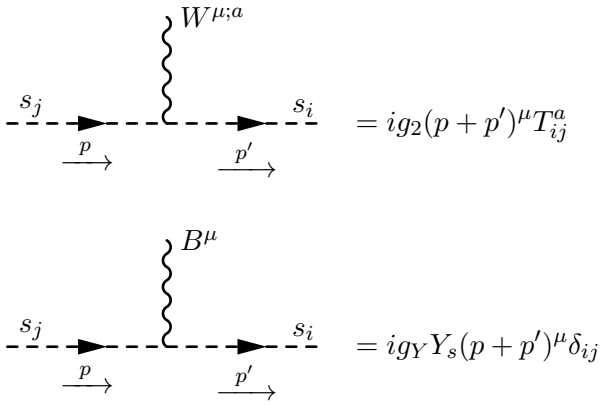

Figure A.8: *Upper row*: Feynman rule for the $s^\dagger sW$ vertex, the i, j indices runs over the different components of the multiplet.. *Lower row*: Feynman rule for the $s^\dagger sB$ vertex.

$$\int \frac{d^dk}{(2\pi)^d}\frac{k^2}{(k^2-D)^n} = \frac{(-1)^{n-1}i}{(4\pi)^{d/2}}\frac{d}{2}\frac{\Gamma(n-1-\frac{d}{2})}{\Gamma(n)}\left(\frac{1}{D}\right)^{n-1-\frac{d}{2}} \tag{A.8}$$

$$2m_f\bar{u}(p')\gamma^\mu u(p) = \bar{p'}\left[(p'+p)^\mu - 2i\sigma^{\mu\nu}(p'-p)_\nu\right]u(p) \tag{A.9}$$

$$\bar{u}(p')\left[(p'+p)^\mu - 2i\sigma^{\mu\nu}(p'-p)_\nu\right]\gamma_5 u(p) = 0 \tag{A.10}$$

$$I^f_{LL}(r) = \int_0^1 dx_3 \frac{(1-x_3)^2x_3}{2\left(x_3+r(1-x_3)\right)} \tag{A.11}$$

$$I^f_{LR}(r) = \int_0^1 dx_3 \frac{(1-x_3)^2}{x_3+r(1-x_3)} \tag{A.12}$$

$$I^s_{LL} = \int_0^1 dx_1 \frac{x_1(1-x_1)^2}{2(1-x_1+rx_1)} \tag{A.13}$$

$$I^s_{LR} = \int_0^1 dx_1 \frac{x_1(1-x_1)}{1-x_1+rx_1} \tag{A.14}$$

$$H^s_{LL} = \int dx_1dx_2dx_3 2\delta(x_1+x_2+x_3-1)\frac{x_3(x_2-x_3)}{1-x_1+rx_1} \tag{A.15}$$

$$K^f_{LL}(r) = \int_0^1 dx_1 \frac{1}{2}\frac{x_1(1-x_1)}{x_1+(1-x_1)r} \tag{A.16}$$

$$H^f_{LL}(r) = \int_0^1 dx_1 \int_0^{1-x_1} dx_2 \frac{x_2(2x_2-2+x_1)}{x_1+(1-x_1)r} \tag{A.17}$$

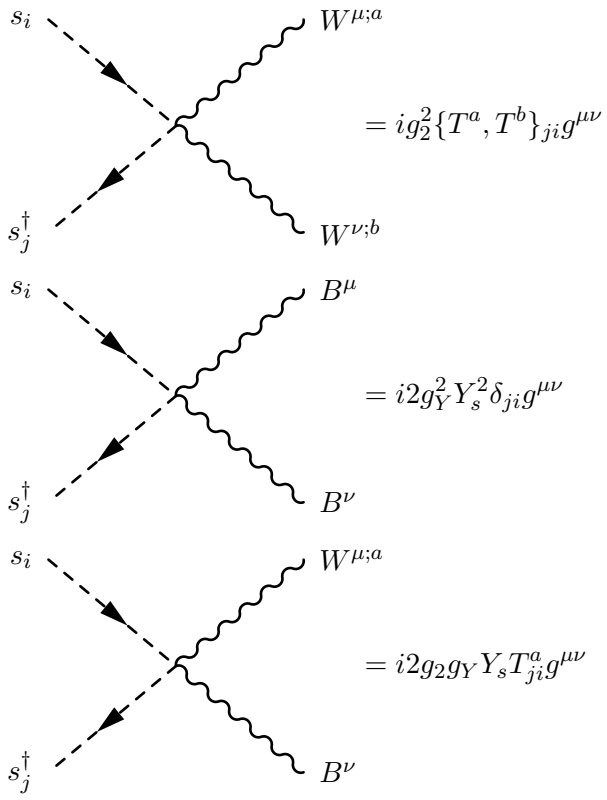

Figure A.9: *Upper row*: Feynman rule for the $s^\dagger sWW$ vertex. *Middle row*: Feynman rule for the $s^\dagger sBB$ vertex. *Upper row*: Feynman rule for the $s^\dagger sWB$ vertex.

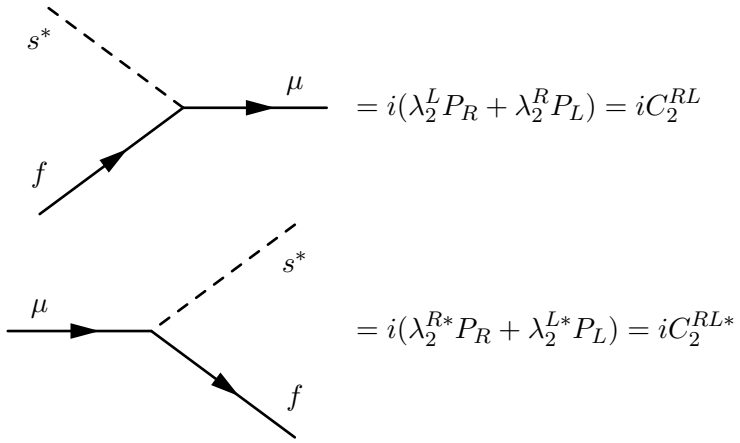

Figure A.10: Feynman rules for the new physics vertices introduced in the Lagrangian 4.44.

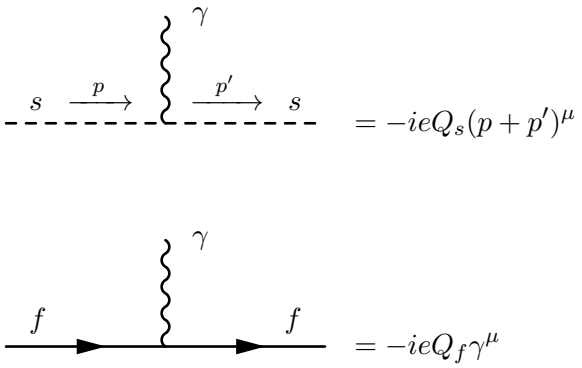

Figure A.11: *Upper row*: Feynman rule for the scalar-photon interaction. *Lower row*: Feynman rule for the fermion-photon interaction.

Bibliografy

[1] José Ignacio Illana and Alejandro Jiménez Cano. *Quantum field theory and the structure of the Standard Model*. 2022. arXiv: 2211.14636 [hep-ph].

[2] Guido Altarelli. *The Higgs and the Excessive Success of the Standard Model*. 2014. arXiv: 1407.2122 [hep-ph].

[3] Juan M. Maldacena. "GRAVITY, PARTICLE PHYSICS AND THEIR UNIFICATION". In: *International Journal of Modern Physics A* 15.supp01b (2000), pp. 840–852. DOI: 10.1142/s0217751x00005449.

[4] Annika H. G. Peter. *Dark Matter: A Brief Review*. 2012. arXiv: 1201.3942 [astro-ph.CO].

[5] Roberto D. Peccei. "The Strong CP Problem and Axions". In: *Lecture Notes in Physics*. Springer Berlin Heidelberg, 2008, pp. 3–17. DOI: 10.1007/978-3-540-73518-2_1.

[6] Andrei D Sakharov. "Violation of CP invariance, C asymmetry, and baryon asymmetry of the universe". In: *Soviet Physics Uspekhi* 34.5 (1991), p. 392. DOI: 10.1070/PU1991v034n05ABEH002497.

[7] David H. Lyth and Antonio Riotto. "Particle physics models of inflation and the cosmological density perturbation". In: *Physics Reports* 314.1-2 (1999), pp. 1–146. DOI: 10.1016/s0370-1573(98)00128-8.

[8] M. C. Gonzalez-Garcia and Yosef Nir. "Neutrino masses and mixing: evidence and implications". In: *Reviews of Modern Physics* 75.2 (2003), pp. 345–402. DOI: 10.1103/revmodphys.75.345.

[9] K. S. Babu. *TASI Lectures on Flavor Physics*. 2009. arXiv: 0910.2948 [hep-ph].

[10] Alex Keshavarzi, Kim Siang Khaw, and Tamaki Yoshioka. "Muon $g-2$: A review". In: *Nuclear Physics B* 975 (2022), p. 115675. DOI: 10.1016/j.nuclphysb.2022.115675.

[11] T. Aoyama et al. "The anomalous magnetic moment of the muon in the Standard Model". In: *Physics Reports* 887 (2020), pp. 1–166. DOI: 10.1016/j.physrep.2020.07.006. URL: https://doi.org/10.1016%2Fj.physrep.2020.07.006.

[12] D. P. Aguillard et al. *Measurement of the Positive Muon Anomalous Magnetic Moment to 0.20 ppm*. 2023. arXiv: 2308.06230 [hep-ex].

[13] Hyun Min Lee. "Lectures on physics beyond the Standard Model". In: *Journal of the Korean Physical Society* 78.11 (2021), pp. 985–1017. DOI: 10.1007/s40042-021-00188-x.

[14] R. D. Peccei. *QCD, Strong CP and Axions*. 1996. arXiv: hep-ph/9606475 [hep-ph].

[15] Sara Celani. *Lepton Flavour Universality tests and Lepton Flavour Violation searches at LHCb*. 2021. arXiv: 2111.11105 [hep-ex].

[16] R.H. Bernstein and Peter S. Cooper. "Charged lepton flavor violation: An experimenter's guide". In: *Physics Reports* 532.2 (2013), pp. 27–64. DOI: 10.1016/j.physrep.2013.07.002.

[17] Tatsumi Aoyama et al. "Complete Tenth-Order QED Contribution to the Muon g-2". In: *Physical Review Letters* 109.11 (2012). DOI: 10.1103/physrevlett.109.111808. URL: https://doi.org/10.1103%2Fphysrevlett.109.111808.

[18] C. Gnendiger, D. Stöckinger, and H. Stöckinger-Kim. "The electroweak contributions to $(g-2)_\mu$ after the Higgs boson mass measurament". In: *Physical Review D* 88.5 (2013). DOI: 10.1103/physrevd.88.053005. URL: https://doi.org/10.1103%2Fphysrevd.88.053005.

[19] Andrzej Czarnecki, William J. Marciano, and Arkady Vainshtein. "Refinements in electroweak contributions to the muon anomalous magnetic moment". In: *Phys. Rev. D* 67 (2003). [Erratum: Phys.Rev.D 73, 119901 (2006)], p. 073006. DOI: 10.1103/PhysRevD.67.073006. arXiv: hep-ph/0212229.

[20] Martin Hoferichter, Bai-Long Hoid, and Bastian Kubis. "Three-pion contribution to hadronic vacuum polarization". In: *Journal of High Energy Physics* 2019.8 (2019). DOI: 10.1007/jhep08(2019)137. URL: https://doi.org/10.1007%2Fjhep08%282019%29137.

[21] M. Davier et al. "A new evaluation of the hadronic vacuum polarisation contributions to the muon anomalous magnetic moment and to $\alpha(m_Z^2)$". In: *The European Physical Journal C* 80.3 (2020). DOI: 10.1140/epjc/s10052-020-7792-2. URL: https://doi.org/10.1140%2Fepjc%2Fs10052-020-7792-2.

[22] Gilberto Colangelo, Martin Hoferichter, and Peter Stoffer. "Two-pion contribution to hadronic vacuum polarization". In: *Journal of High Energy Physics* 2019.2 (2019). DOI: 10.1007/jhep02(2019)006. URL: https://doi.org/10.1007%2Fjhep02%282019%29006.

[23] Fred Jegerlehner. "Leading-order hadronic contribution to the electron and muon $g-2$". In: *EPJ Web of Conferences* 118 (2016). Ed. by G. D'Ambrosio et al., p. 01016. DOI: 10.1051/epjconf/201611801016. URL: https://doi.org/10.1051%2Fepjconf%2F201611801016.

[24] Fred Jegerlehner and Andreas Nyffeler. "The muon $g-2$". In: *Physics Reports* 477.1-3 (2009), pp. 1–110. DOI: 10.1016/j.physrep.2009.04.003. URL: https://doi.org/10.1016%2Fj.physrep.2009.04.003.

[25] G Charpak et al. "The anomalous magnetic moment of the muon". In: *Il Nuovo Cimento (1955-1965)* 37.4 (June 1965), pp. 1241–1363.

[26] F. Combley and E. Picasso. "The muon $g-2$ precession experiments: Past, present and future". In: *Physics Reports* 14.1 (1974), pp. 1–58. ISSN: 0370-1573. DOI: https://doi.org/10.1016/0370-1573(74)90004-0. URL: https://www.sciencedirect.com/science/article/pii/0370157374900040.

[27] J. Bailey et al. "Final report on the CERN muon storage ring including the anomalous magnetic moment and the electric dipole moment of the muon, and a direct test of relativistic time dilation". In: *Nuclear Physics B* 150 (1979), pp. 1–75. ISSN: 0550-3213. DOI: https://doi.org/10.1016/0550-3213(79)90292-X. URL: https://www.sciencedirect.com/science/article/pii/055032137990292X.

[28] G. W. Bennett et al. "Final Report of the Muon E821 Anomalous Magnetic Moment Measurement at BNL". In: *Phys. Rev. D* 73 (2006), p. 072003. DOI: 10.1103/PhysRevD.73.072003. arXiv: hep-ex/0602035.

[29] B. Abi et al. "Measurement of the Positive Muon Anomalous Magnetic Moment to 0.46 ppm". In: *Physical Review Letters* 126.14 (2021). DOI: 10.1103/physrevlett.126.141801. URL: https://doi.org/10.1103%2Fphysrevlett.126.141801.

[30] Louis E. Strigari. "Galactic searches for dark matter". In: *Physics Reports* 531.1 (2013). DOI: 10.1016/j.physrep.2013.05.004.

[31] Gianfranco Bertone, Dan Hooper, and Joseph Silk. "Particle dark matter: evidence, candidates and constraints". In: *Physics Reports* 405.5-6 (2005). DOI: 10.1016/j.physrep.2004.08.031.

[32] Jonathan L. Feng. "Dark Matter Candidates from Particle Physics and Methods of Detection". In: *Annual Review of Astronomy and Astrophysics* 48.1 (2010). DOI: 10.1146/annurev-astro-082708-101659.

[33] N. Aghanim et al. "Planck 2018 results". In: *Astronomy & Astrophysics* 641 (2020), A6. DOI: 10.1051/0004-6361/201833910.

[34] Eugenio Del Nobile. *The Theory of Direct Dark Matter Detection*. Springer International Publishing, 2022. DOI: 10.1007/978-3-030-95228-0.

[35] CMS Collaboration. "Search for dark matter and large extra dimensions in monojet events in pp collisions at $\sqrt{s} = 7\ TeV$". In: *Journal of High Energy Physics* 2012.9 (2012). DOI: 10.1007/jhep09(2012)094.

[36] ATLAS Collaboration. "Search for dark matter candidates and large extra dimensions in events with a jet and missing transverse momentum with the ATLAS detector". In: *Journal of High Energy Physics* 2013.4 (2013). DOI: 10.1007/jhep04(2013)075.

[37] Jure Zupan Lorenzo Calibbi Robert Ziegler. "Minimal models for dark matter and the muon g - 2 anomaly". In: *Journal of High Energy Physics* 2018 (2018). DOI: 10.1007/jhep07(2018)046.

[38] The MEG Collaboration. *Search for the Lepton Flavour Violating Decay $\mu^+ \to e^+\gamma$ with the Full Dataset of the MEG Experiment*. 2016. arXiv: 1605.05081 [hep-ex].

[39] BaBar collaboration. "Searches for Lepton Flavor Violation in the Decays $\tau \to e\gamma$ and $\tau \to \mu\gamma$". In: *Physical Review Letters* 104.2 (2010). DOI: 10.1103/physrevlett.104.021802. URL: https://doi.org/10.1103%2Fphysrevlett.104.021802.

[40] Paolo Gondolo and Graciela Gelmini. "Cosmic abundances of stable particles: Improved analysis". In: *Nuclear Physics B* 360.1 (1991), pp. 145–179. ISSN: 0550-3213. DOI: https://doi.org/10.1016/0550-3213(91)90438-4.

[41] Vladyslav Shtabovenko, Rolf Mertig, and Frederik Orellana. "FeynCalc 9.3: New features and improvements". In: *Computer Physics Communications* 256 (2020), p. 107478. DOI: 10.1016/j.cpc.2020.107478.

[42] Vladyslav Shtabovenko, Rolf Mertig, and Frederik Orellana. "New developments in FeynCalc 9.0". In: *Computer Physics Communications* 207 (2016), pp. 432–444. DOI: 10.1016/j.cpc.2016.06.008.

[43] R. Mertig, M. Böhm, and A. Denner. "Feyn Calc - Computer-algebraic calculation of Feynman amplitudes". In: *Computer Physics Communications* 64.3 (1991), pp. 345–359. ISSN: 0010-4655. DOI: https://doi.org/10.1016/0010-4655(91)90130-D.

[44] Fady Bishara et al. "Chiral effective theory of dark matter direct detection". In: *Journal of Cosmology and Astroparticle Physics* 2017.02 (2017). DOI: 10.1088/1475-7516/2017/02/009.

[45] Fady Bishara et al. "From quarks to nucleons in dark matter direct detection". In: *Journal of High Energy Physics* 2017.11 (2017). DOI: 10.1007/jhep11(2017)059.

[46] E. Aprile et al. "First Dark Matter Search Results from the XENON1T Experiment". In: *Physical Review Letters* 119.18 (2017). DOI: 10.1103/physrevlett.119.181301.

[47] E. Aprile et al. "Constraining the Spin-Dependent WIMP-Nucleon Cross Sections with XENON1T". In: *Physical Review Letters* 122.14 (2019). DOI: 10.1103/physrevlett.122.141301.